



# UNIVERSITÀ DEGLI STUDI DI PADOVA

Dipartimento di Fisica e Astronomia “Galileo Galilei”

Master Degree in Physics (LM-17)

## Final Dissertation

Modelling COVID-19 In a Network

Candidate

Riccardo Milocco

Thesis supervisor

Prof./Dr. Marco Baiesi

Academic Year 2020/2021



# Contents

<b>Contents</b>	<b>ii</b>
<b>Abstract</b>	<b>iv</b>
<b>Motivations</b>	<b>v</b>
<b>1 Introduction</b>	<b>1</b>
1.1 Complexity . . . . .	1
1.1.1 Models Ecosystem . . . . .	1
1.2 A Technical Introduction . . . . .	3
1.3 Network Science . . . . .	4
1.3.1 Graph Theory . . . . .	5
1.3.2 Adjacency Matrix . . . . .	6
1.3.3 Degree . . . . .	6
<b>2 The Network Models</b>	<b>8</b>
2.1 Regular Networks . . . . .	8
2.1.1 Lattice Graph . . . . .	8
2.1.2 Connected Caveman Graph . . . . .	9
2.2 Random Networks . . . . .	9
2.2.1 The Erdős-Rényi Model . . . . .	10
2.2.2 The “Small-World” Property . . . . .	11
2.2.3 The Clustering Coefficient . . . . .	12
2.2.4 Random Graphs are not Real Graphs . . . . .	12
2.2.5 Watts-Strogatz Model . . . . .	13
2.3 Configuration Model . . . . .	14
2.3.1 Poissonian Small-World Network . . . . .	15
2.4 Scale-Free Networks . . . . .	17
2.4.1 Scale-Free Property . . . . .	17
2.4.2 Barabási-Albert Model . . . . .	19
2.4.3 Linearized Chord Diagram . . . . .	20
2.5 Annealed Mean-Field Network . . . . .	20
<b>3 The Epidemiological Models</b>	<b>21</b>
3.1 Homogeneous Mixing . . . . .	23
3.2 Heterogeneous Mixing . . . . .	25
3.3 Order Parameter . . . . .	29
<b>4 Methodology</b>	<b>34</b>
<b>5 Results</b>	<b>39</b>
5.1 The Basic Reproduction Number . . . . .	39
5.2 Watts-Strogatz Model . . . . .	45
5.2.1 Long-Range Watts Strogatz . . . . .	46

5.3	Poissonian Small-World Network . . . . .	47
5.3.1	Overlapping PSW . . . . .	47
5.4	Caveman Model . . . . .	54
5.4.1	Long-Range Caveman model . . . . .	57
5.5	Barabási-Albert Model . . . . .	59
<b>6</b>	<b>Conclusions</b>	<b>63</b>
6.1	Future Developments . . . . .	64
<b>A</b>	<b>Appendix</b>	<b>65</b>
A.1	Scale-Free Distributions Details . . . . .	65
A.2	Recovering Power-Law Distribution . . . . .	68
A.3	The Origins of Preferential Attachment . . . . .	69
A.3.1	Local Mechanisms . . . . .	69
A.3.2	Global Mechanisms . . . . .	69
A.3.3	Optimization Mechanism . . . . .	69
A.4	Error Propagation and recovery time table . . . . .	70
<b>B</b>	<b>Ringraziamenti</b>	<b>72</b>
<b>Bibliography</b>		<b>74</b>

# Abstract

The usual simplified description of epidemic dynamics predicts an exponential growth. This is due to the mean field character of the dynamical equations. However, a recent paper (Thurner S, Klimek P and Hanel R 2020 Proc. Nat. Acad. Sci. 117, 22684) [35] showed that in a network with fixed connectivity, the nodes become infected at a rate that increases linearly rather than exponentially. Experimental data for COVID-19 seem to validate this approach. In this thesis describe the evolution of the COVID-19 pandemic with the SIR model [28], on different network topologies in order to simulate the different containment policies, i.e. “lock-downs”. We will obtain a “sub-exponential” growth of the total cases for a plethora of social networks. This is supported by the presence of a kind of phase transition of the standard deviation of the new cases. In particular, we monitor the effect induced by a significant presence of hubs in the network. Ultimately, we introduce a parameter that we term the epidemic severity to account for the outbreak size of COVID-19.

# Motivations

Last Update: 22-11-2021

“The COVID-19 pandemics has led to a dramatic loss of human life worldwide and presents an unprecedented challenge to public health, food systems and the world of work” [9]. In this scenario, monitoring and forecasting the diffusion of the virus is an essential tool for policymakers to handle the health-care resources and restrictions among individuals. To this purpose, many academics, e.g. [UniPD against COVID-19<sup>1</sup>](#), have been trying to tackle the COVID-19 spreading as well as its side-effects, which have to be considered on the “path to normality”. This drastic shift with respect to the “path to herd immunity” comes from a recent study [17] which shed light on the fact that “herd immunity”, due to delay on vaccinations, could probably not be reached for the end of 2021. On the other hand, due to few practical points [2], it is also probable that the long-term prospects include COVID-19 becoming an endemic disease, much like influenza. Therefore, the recovery of the pre-COVID-19 situation could be slow even in the presence of effective vaccines.

---

<sup>1</sup><https://web.unipd.it/covid19/en/>

# Introduction

## 1.1 Complexity

Since its beginning, Physics has been driven by a “Unification Principle”<sup>1</sup>, which aims at describing the reality as a “reduction” and simplification of its constituents and interactions. Nevertheless, this optimistic gaze, is (amazingly) challenged by the complexity that emerges in the world we are living in. This complexity could have variable origins but also different spatial scales: from ants’ nest to storms, from the markets to human/animal migrations, from the epidemics to ecosystems. Therefore, Nature is capable of obeying simple laws but, on the other hand, to straightforwardly generate complex phenomena. A paradigmatic example is the flocking of birds: the core of the flock assumes different shapes due to a collective interaction among the birds; while an alone bird would proceed in a defined direction. These facts were enough to establish the new branch of *Physics Of the Complex Systems* which ultimate goal is to describe the emergence of the “complex” phenomena from the simple law of physics, e.g. “gravity model” [4]. Having understood that “*More is different*” [1] and its ubiquity, it is natural to demand a formal definition of “Complexity”. Nevertheless, quoting the Nobel Price Murray Gell-Mann [16], “a variety of different measures would be required to capture all our intuitive ideas about what is meant by complexity and by its opposite, simplicity” . In fact, from computational complexity to other information measures, all such quantities are context-dependent and subjective, since they depend on many aspects, such as the detail level (coarse graining) of the entity to describe. Thus, a rough but clear definition could be drawn for the Complex System Society site [31]:

**Definition 1.1.1 (“Complexity”).** Complex systems are systems where the collective behavior of their parts entails emergence of properties that can hardly, if not at all, be inferred from properties of the parts.

In other words, the non-linear interactions among the parts of which a complex system is composed let emerge a behavior which could not be understood simply by applying the fundamental laws to its constituents.

The first representation of this weaved system is by considering entities and connections among them. Thus, a powerful tool to describe it is the Network Science. In particular, the purpose of this thesis is to study the epidemic spreading of the COVID-19 over different network topologies that mimic the underlying social network of contacts. The phenomenon is, thus, regarded as a complex system through the analysis of the SIR model, which grasps the emergent features rather than the microscopic behavior of the disease.

### 1.1.1 Models Ecosystem

Infectious epidemics are responsible for a significant health and economic burden on society. New diseases appear frequently and old diseases persist. Therefore, many mathematical models have been used recently to guide policy makers to mitigate the impact of new infectious diseases (e.g. Polio, H1N1 influenza and Ebola) or established ones (such as HIV, cholera and seasonal influenza). On the other hand, with the phrase *All models are wrong; some models are useful* [7], George Box wanted to highlight that no model, no matter how complicated<sup>2</sup>, is perfect. Thus, a way to evaluate a “successful” model has to be recovered.

---

<sup>1</sup>from Newton with the “gravity”-relationship between an apple and the Moon; passing to Einstein, whom the effects of gravity are equal to the ones of an accelerated rocket for; ending to the *Grand Unified Theory* as an unification of general relativity with the particle physics

<sup>2</sup>Instead, the complexity of a model could challenge its possibility to be predictive in many scenarios. A related topic is the “over-fitted model” in statistical learning or “Occam’s razor” in Philosophy

Inside the “ecosystems” of models, there are the simple models which allow to analytically explain how the primary mechanisms influence important characteristics (e.g. epidemic threshold, epidemic size<sup>3</sup>, how long it will last). To be more accurate, it is also possible to develop models that incorporate much more details about both the disease and individual-level interactions [19].

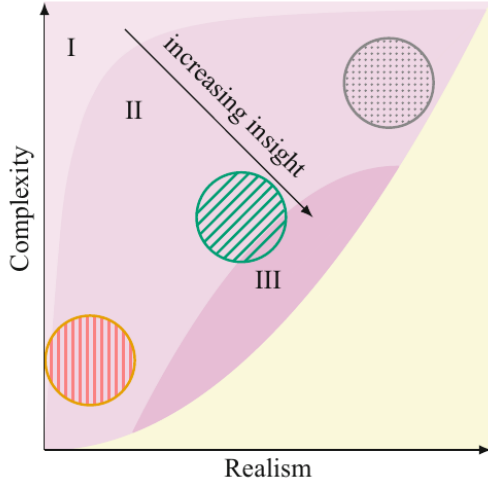


Figure 1.1: A caricature of the relation between model realism, complexity and the insight the model provides [19].

As suggested by the Figure 1.1<sup>4</sup>, models provide maximum insight where the right balance of realism (circle filled with dots, e.g. the Deep Learning for Graph to predict  $R_t$  [11]) and simplicity (circle with vertical lines e.g. on epidemics the deterministic SIR model) is met<sup>5</sup> (central circle with oblique lines).

In this middle region, one could find several works that use network analysis as the underlying structure for a phenomenon( [35] [27] [28]); while other, more involved, that incorporate human mobility data in several hybrid models [33,38] in order to predict its diffusion. For the sake of simplicity, the present thesis is going to deepen the paper of [35]. In particular, Thurner et al. [35], by focusing on the COVID-19 spreading in Austria and in the USA, are able to find a scenario, i.e. a combination of the SIR spreading parameters<sup>6</sup>, such that the outbreak is (quasi-)linear for a value of the average number of contact  $D$ . This behavior of the SIR model is qualitatively comparable with the curves reported by the JHUUniversity reported below. Hence, inspired by [35], the aim of this project is to analyze how the SIR model behaves by changing its epidemic parameters but also the topology of the underlying social network.

<sup>3</sup>how large it will be

<sup>4</sup>“Est modus in rebus” ([19])

<sup>5</sup>The equilibrium point may depend on the specific posed question

<sup>6</sup>the infection rate  $\beta$ , recover rate  $\mu$ , the long-range attachment probability  $p$

## 1.2 A Technical Introduction

At 8 May 2020, none of the affected COVID-19 states have reached “herd immunity” but still they reached the “epidemic peak” due to the containment restrictions on social contacts. One paradigmatic example is the case of Austria, for which the total infected cases at the 08/05/2020 were 0.18% of the total population, remarkably low with respect to the SARS-COV-2 “herd-immunity” level that are supposed to be at 0.8% ([39]) of the entire (susceptible) population.

To qualitatively show the behaviors of Austria, USA and Italy, we produced a graph of the *fraction of total cases* Figure 1.2 (see [18]) from the first available date (25/02/2020) to the beginning of May (08/05/2020). In particular, we obtained the *fraction of total cases* by dividing the total cases for the total population of each state. The purpose of this figure is to show the effect of the policies over the COVID-19 curves. Indeed, the beginning and ending dates where exhibited by the colored big marks on the curves of the total cases. Every state chose to impose the “stay-at-home” order independently on the central government. Hence, we displayed the starting date of the first one (California) and the last ones (Missouri and South Dakota) states; while we report only one ending date as the quoted states ended the stay-at-home restriction at the same time. Nevertheless, we report that some states did not impose the stay-at-home measure: Arkansas, Iowa, Nebraska, North Dakota, South Dakota [26]. Therefore, even if USA has got many more contagions of Austria and Italy, it has the lowest curve due to not restricted lockdowns which did not flatten the fraction of total cases. In the legend, there are reported two important quantities:

- $\max - \min$  is the difference among  $\max$  the total cases at the 08/05/2020 (end of figure) and  $\min$  the total cases at the beginning of the lock down for each state;
- $\max / \text{totp}$  where  $\max$  is defined as before, while “ $\text{totp}$ ” is the total population for each state according to [30].

Starting by the 25/02/2020, the range of the (normalized) total cases are the following: 2-15774 (AUT), 453-217185 (ITA), 16-1295396 (USA) [18]. In turn, this means that Austria could track down the COVID-19 since its early stages; while Italy began already with a considerable amount of cases. Furthermore, we reported in the legend the infected at the beginning of the lockdown (for the USA the stay-at-home-order of the California): 1018 (AUT), 12462 (ITA), 13663 (USA). This means that even if Austria temporally started the lockdown restrictions after Italy, it brought forward the Italian policies. Therefore at 08/05/2020, the total infected were smaller than the Italian ones. The most striking observation is that the (normalized) total cases (Figure 1.2) for USA, after early-stages, exhibits a (quasi-)linear growth for an extended time interval in contrast with the “S-shaped” logistic curve predicted by the standard compartmental models. The extension of the linear regime depends on the onset of the measures; while for early stages, as it was the case for many countries [35] (8 May 2020), an exponential growth dominates the spreading of the disease as in Figure 1.2.

More specifically, an infection may occur for two reasons:

1. interaction between an infected and a susceptible person;
2. contact is “intense” (e.g. long, close,...) enough to lead to a disease transmission.

Hence, the rationale behind the social distancing is that it takes to a reduction of both of these factors. On the other hand, the analytically solvable SIR model assumes that, defined  $N, D$  as the total number of individuals in the population and the average number of contacts respectively, there is the same probability that an individual encounters an infected person (“well-mixed population”) and all the nodes have the same number of neighbors ( $N - 1$  or  $D$ ). This approach allows to recover analytical results for an epidemic spreading but it annihilates the underlying network structure. Therefore, as claimed in [27], there is the need of studying how the network affects the spreading of a disease, but still no focus is put on the spreading below the epidemic threshold [35] as it is the case if nodes were separated through NPIs. In this thesis, we want to (qualitatively) recover the evolutions of Figure 1.2 by taking care of the social network structure. In general, we will focus on the “sub-exponential” behavior of Italy and Austria; meanwhile, we will try to recover the linear growth of the USA. In fact, we chose to study the evolution of a SIR Model in different topologies such as the *standard models* of the graph-theory (“Watts-Strogatz”, “Scale-Free”, “Caveman Model”) but also a new involved topology, i.e. a Poissonian Small-World Network chapter 2. To compare the network evolutions, we will use a “well-mixed” population simulated via an Annealed-Mean-Field Network (see section 2.5). To explain the epidemic onset at early times, we used the *basic reproduction number*, namely  $R_0 := \beta \cdot D / \mu$  where  $\beta, \mu, D$  are the transmission

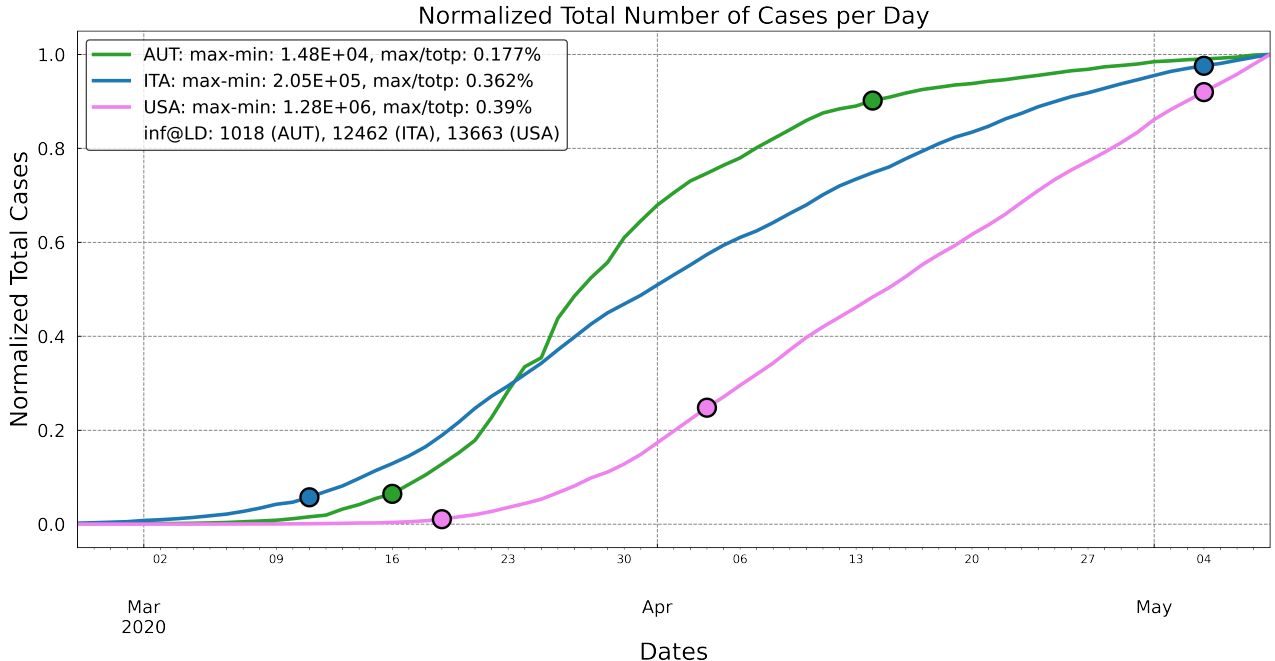


Figure 1.2: The number of total cases normalized to their maximum value in the period 25/02/20 - 08/05/20. The dates of the first lockdown are: 16/03 - 14/04/20 (AUT); 11/03 - 04/05/20 (ITA); California: 19/03 - 04/05; Missouri: 6/04 - 04/05. USA states with no-stay-at-home restrictions: Arkansas, Iowa, Nebraska, North Dakota, South Dakota

and the recovery rates alongside with the average number of neighbors.  $R_0$  is defined as the the average number of new infections caused by an individual in a completely susceptible population<sup>7</sup> [19]. For  $R_0 > 1$  an epidemic spreading is *possible* (not guaranteed); while for  $R_0 < 1$  the disease will die out. Thus, these informations drive naturally to suppose that  $R_0$  could also be a signal of the strength of an epidemic outbreak. Rather, this is not the case, and we will recover different behaviors for an equal  $R_0$  section 5.1. Hence, we introduced the *epidemic severity* measure defined as

$$\Delta R_0(\delta) := \frac{R_0 - R_{c-net}}{\delta} \quad (1.1)$$

where  $\delta := \langle l \rangle$  is the average path length. We will describe it more deeply in Equation 3.2

Finally, we will show the growth of the standard deviation of the daily cases as a function of the average contacts per individual. The rationale is a standard deviation equal to zero implies a linear increase of the fraction of total cases. We will obtain a *critical point* that separates a *sub-exponential* outbreak (less than the 30% of the population), from a stronger one, infecting  $\sim 80\%$  of individuals.

In the following section, we will deepen the area of the Network Science.

### 1.3 Network Science

Two aspects contribute to the popularity of Network Science: its universality nature of networks and the availability of large datasets<sup>8</sup> which map huge networks of the furthest kind, e.g. “food-webs” or the Science of Science. Its roots could be found in the Graph Theory, a mathematical branch devoted to the analysis of the networks (or graphs), and Statistical Mechanics, committed to the formalization of the dynamical processes on networks, such as self-organization and information theory. For our purpose, the Graph Theory allows to formalize a “networky” - complex system such as the social network of the individuals over which a disease

<sup>7</sup>The susceptible individuals are chosen according to “epidemic targets”, e.g. only children for the measles

<sup>8</sup>In reality, also the computational power to analyze them should be remarked.

spreads; while Statistical Mechanics to develop a model focusing on its emergent characteristic, such as a SIR model.

### 1.3.1 Graph Theory

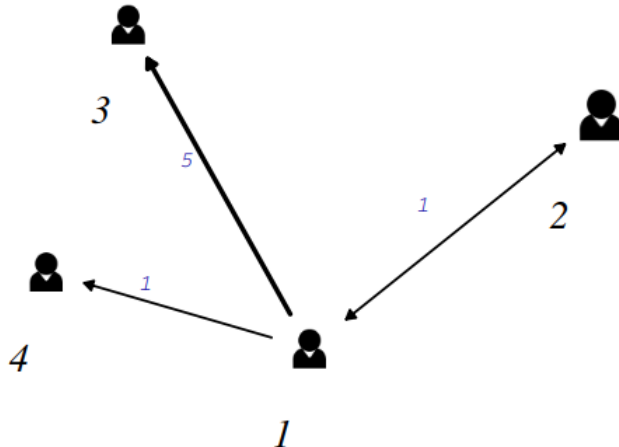


Figure 1.3: Contacts interaction Network. As far as the COVID-19 interaction is concerned, a (risky) contact is defined as the human-droplets that reach one individual. Therefore, a symmetric edge could represent a chat among two persons; where directed edges would be a “one-way” interaction such as in a room with pre-existent droplets. The number above each edge are the weights, which could be the minutes spent in the previous quoted room. Lastly, we will focus on undirected and weight-less graphs.

A graph is a tuple  $(V, E)$  where the “ $V$ ” stands for “vertexes” (1,2,3,4) while “ $E$ ” for “edges” (the links between the vertexes). With the same notation, an edge connecting the node<sup>9</sup>  $i$  to  $j$  is, often, identified by  $(i, j)$ . Formally, the labels of the vertexes are the image of any bijective embedding from the nodes to a chosen set, e.g. integer numbers. The relationship among vertexes are accounted by the edges, which could be unsymmetrical, as for  $(1, 4)$ , and with different strength of the connection, such as  $(1, 4)$  and  $(1, 3)$  which. If all the edges are symmetric, i.e. if  $(A, B)$  implies  $(B, A)$ , the graph is said undirected, e.g. the friendship network; otherwise it is said directed, e.g. the phone contacts network. With the given definitions, it is now clear that roughly everything could be divided in vertexes connected by an arbitrary relation. The simplest example, is the *simple graph*, which is an unweighted, undirected graph containing no graph loops, i.e.  $(i, i)$  edges, or multiple edges such as multiples- $(i, j)$ . It could be represented as the Figure 1.3 forcing all the edges to be weightless and undirected.

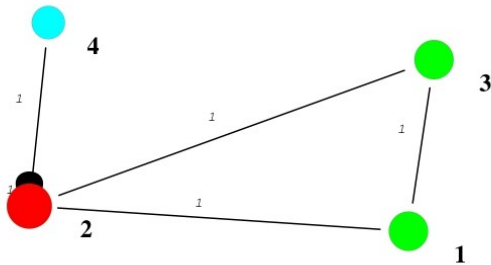


Figure 1.4: We labeled the nodes as 1, 2, 3, 4; while we used the same color for vertexes with the equal number of contacts. Node 2 has a loop (black cupola on top).

<sup>9</sup>In the context of a social network, a vertex represents a person/individual

### 1.3.2 Adjacency Matrix

Typically for real networks, the number of involved nodes is big, e.g. the Google web-graph available at [Stanford University Network Dataset](#) is of the order of the 800k nodes and 5million edges. Thus, despite the clearness of [Figure 1.3](#), the most suitable way of representing a graph is by grouping all its properties in a matrix called the adjacency matrix  $A$ . Starting from the basics, the (symmetric) adjacency matrix for the simple graph above is:

$$A_{ij} := \begin{cases} 1 & \text{if exist an unweighted edge among } i \text{ and } j \\ 0 & \text{otherwise} \end{cases} \Leftrightarrow A = \begin{bmatrix} 0 & 0 & 1 & 0 \\ 0 & 0 & 1 & 1 \\ 1 & 1 & 0 & 1 \\ 0 & 1 & 1 & 0 \end{bmatrix}$$

Hereby,  $A \in M_4(\mathbb{N})$  holds the nature of a simple graph:

- the rows represent the direct connections between the  $i$ -th row and the  $j$ -th column; while, the columns the edge  $(j, i)$ . Thus, there are only 4 nodes;
- unweighted: the value of the elements of  $A$  is binar;
- without loops: the diagonal is 0;
- without multi-edges: the value of the entries of  $A$  are strictly 0 or 1, account for the presence of, at maximum, one edge.

A more involved, adjacency matrix is the one of the rightest graph which present multiples loops<sup>10</sup>. Formally,

$$A = \begin{bmatrix} 0 & 0 & 1 & 0 \\ 0 & 0 & 1 & 1 \\ 1 & 1 & 0 & 1 \\ 0 & 1 & 1 & 2 \end{bmatrix}$$

Furthermore, take into consideration a triangular graph with a tail connected to the upper node. The overall shape is the one of an arrow ( $-\text{latex}$ ) undirected edges and the v is report a (simple) weighted and directed graph with 4 nodes connected by a “central”<sup>11</sup> node 1. In particular,

$$A = \begin{bmatrix} 0 & 1 & 5 & 1 \\ 1 & 0 & 0 & 0 \\ 0 & 0 & 0 & 0 \\ 0 & 0 & 0 & 0 \end{bmatrix}$$

where it is encoded the direct edges since  $A$  is not symmetric. Whether there would be a self-loop, such at  $1 \longleftrightarrow 1$ , there would be a 1 at the first entry (position  $(1, 1)$ ) of the matrix  $A$ .

### 1.3.3 Degree

As quoted before, a (real) network could be very tangled. Thus, the degree distribution, i.e. the normalized number of vertexes with a certain degree, allows to check whether all the nodes have, or not, the same number of contacts even at a plain eye inspection.

Formally, the degree of a vertex, in a (undirected) graph, is the number of edges connected to it. We denote the degree of node  $i$  by  $k_i$  and, by mean of  $A$ ,

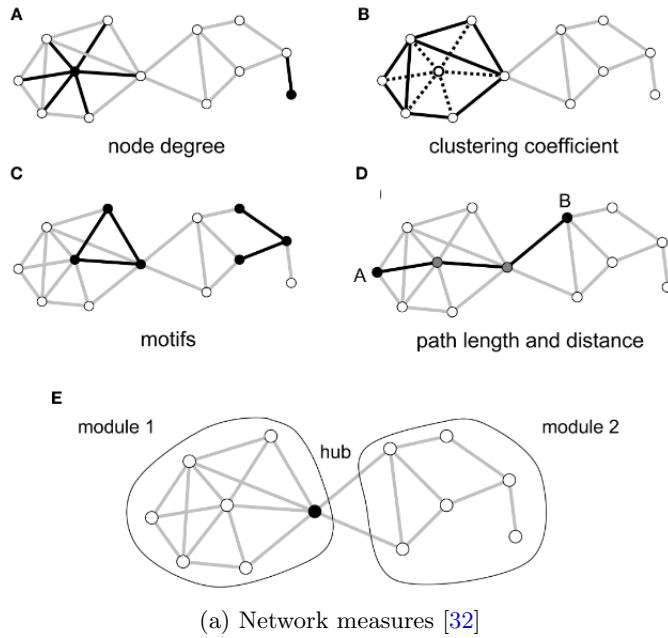
$$k_i := \sum_{j=1}^N A_{ij},$$

where  $N$  is the number of total nodes. For directed graphs, as in [Figure 1.3](#), a distinction between the entering and exiting edges to a node has to be defined. In particular, by a generalization of the previous  $k_i$ ,

$$k_i^{in} := \sum_{j=1}^N A_{ij}, \quad k_j^{out} := \sum_{i=1}^N A_{ij}. \tag{1.2}$$

<sup>10</sup>As far as multi-edges are concerned, the 2 would be off-diagonal

<sup>11</sup>The “centrality” measure of the node is another important quantity which is context-dependent. In this case, the “centrality” refers to a degree centrality for which the most central node is the one with the highest number of contacts



where  $k_i^{in(out)}$  is the number of in-going (out-going) number of edges.

Therefore, by applying the [Equation 1.2<sup>12</sup>](#) to [Figure 1.3](#), it is possible to recover the degree distribution of the vertexes as in the [Figure 1.6](#). Thus, a possible way to build a graph would be to draw the nodes degrees from a fixed distribution and, then, connecting the nodes according to their degree. In fact, this approach, generating a *Configurational Model Network*, is going to be exploited in the further chapters by using a Poissonian degree distribution and connecting the vertexes only to nearest neighbors via an ad-hoc algorithm [subsection 2.3.1](#).

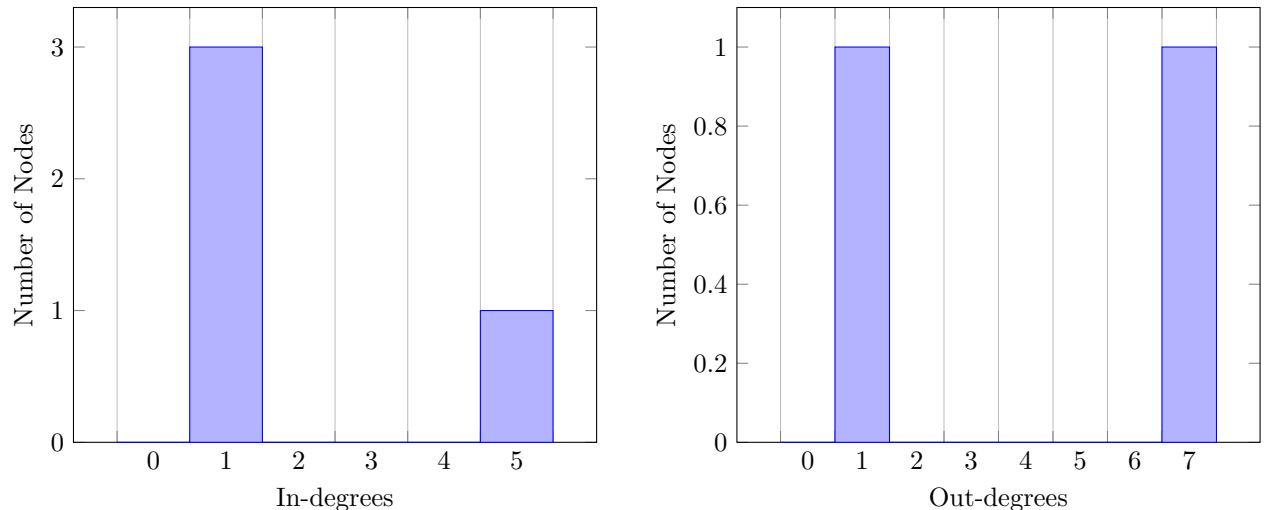


Figure 1.6: Degree Distribution of the [Figure 1.3](#)

<sup>12</sup>A practical check is to count the tails for the out-degree and arrows for the inner-degree. Ultimately, each sum has to equate the number of edges (a undirected edge has to be count doubled)

# The Network Models

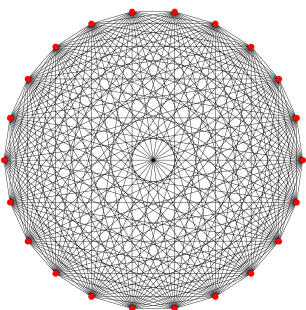
As it could be perceived, modeling a complex (social) phenomenon<sup>1</sup>, as the epidemic spreading on networks, has two main tasks. The first is the identification of the nodes, which is a fairly simple task. The hard one is to pinpoint the emergent correlations in order to connect the vertexes and reproduce the phenomenon. The latter one is the real challenge in network theory.

Many networks are characterized by strong constraints on the node degree which forces a satisfying regularity to be present, e.g. the radial architecture of a spider net or the map of the main streets of Manhattan. Inspired by this, as a first tackle, the pathogen is left to act on a regular society, which individual contacts are differing at most by one: famous examples are the “regular” Watts-Strogatz and the Caveman model.

Most of the real networks, however, do not show a comforting orderliness. Rather, their inner structure seems to be characterized by a certain degree of randomness, e.g. the internet network [6]. Random network theory embraces this feature by constructing network models that are truly random, e.g. Erdős-Rényi. By contrast, they are not able to capture the presence of hubs or, more precisely, the “Scale-Free” property. Thus, new models have to be proposed to generate those highly connected degree nodes, such as the Barabási-Albert models. A review of these is reported in the following sections; alongside with the newly proposed “Poissonian Small World” network (see [35] or subsection 2.3.1).

## 2.1 Regular Networks

### 2.1.1 Lattice Graph



(a) In (a) - fully-connected graph; In (b) -  $D = 4$  regular graph [37]

The “Regular Networks” are characterized by a fixed number of neighbors per node  $D := \langle k \rangle$ . Thus, they are expected as the constituent graphs for the class of systems which constraints  $D$  to a certain value, e.g. solids in

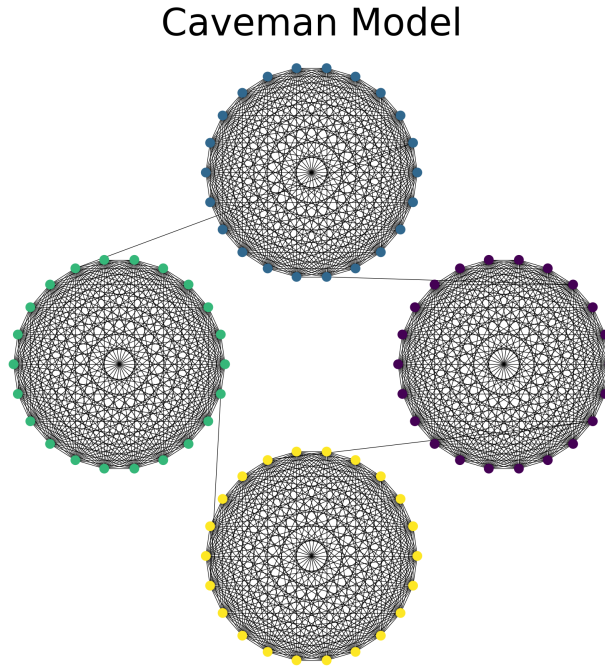
---

<sup>1</sup>The “social” nature has been only evoked for concreteness. Nevertheless, this in-depth presentation of models is interdisciplinary as Network Science itself.

the physics of matter. Ultimately, by trying to study a new phenomenon, it is fundamental to test its behavior on a controlled environment as the one provided by the regular networks.

In subsection 2.2.5, we will introduce the “Watts-Strogatz” model which can interpolate between a regular graph for the parameter  $p = 0$  (Figure 2.1a) and a random network ( $p = 1$ ).

### 2.1.2 Connected Caveman Graph



(a) Connected Caveman Model with one link among consecutive communities.

By analogy with the Non-Pharmaceutical-Interventions (NPIs) which accounts only for the household interactions, we considered the “Caveman Model”.

The rationale is to consider as if one node, of the previously modeled networks, would be a family composed by a fixed number of people. In particular, the Caveman model enables to fix both the number of “caves”/families and the number of individual for each family. This procedure is similar to the one of the “coarse-graining” approach, which aims at simulating the behaviour of a complex system by means of its coarse-grained representation.

In the present thesis, we developed a “locally” connected Caveman model Figure 2.2a, by connecting the consecutive caves with one edge among randomly chosen nodes. Then, we introduced a “rewiring parameter”  $p$  to enable “long-range” connections, resulting in “tunneling cuts” among distant nodes. Furthermore, we added the distant connections over the existing relationships, in order not to spoil the family structures.

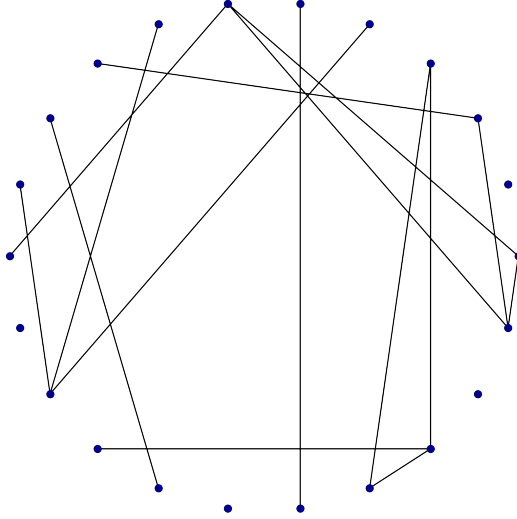
A naive expectation is that the epidemic will spread slower and more stochastically, since the nodes are poorly connected with the rest of the network rather than its inside.

## 2.2 Random Networks

Not all the networks are characterized by hubs as WWW or the airports graphs. In fact, there could be constraints, such as *cost-benefit problem*, which limit the maximum degree of the bigger node. In those cases,

random networks may be the best fit, e.g. national highways network, power grid of generators and switches, ...

### 2.2.1 The Erdős-Rényi Model



(a) Erdős-Rényi Model for  $N = 22, p = 0.1$

The Erdős-Rényi (ER - Figure 2.3a) model was the first attempt to formally describe a random network. In particular, Erdős and Rényi were the fathers of the (random) graph theory, obtained by merging the studies on the networks with the Probability theory.

The primitive hypothesis, for a random wiring, is that the nodes are linked together with a probability  $p$ . Formally,

**Definition 2.2.1** (“Random Network”). A random network  $G(N, p)$  has  $N$  nodes where two nodes are connected with probability  $p$ .

Due to its random nature, this model may have different realizations even with  $N, p$  fixed parameters. Therefore, the number of links and the degree distribution (see subsection 1.3.1) provide a way to differentiate graph with equal  $N, p$ . In particular, a network could exhibit  $L$  links with a probability

$$p_L = p^L \cdot (1-p)^{\binom{N}{2}-L} \cdot \binom{\binom{N}{2}}{L}. \quad (2.1)$$

The Equation 2.1 is the product of 3 terms: the probability to have  $L$  edges; the probability not to have the remaining ones knowing that the total possible node pairs are

$$\binom{N}{2} = \frac{N(N-1)}{2};$$

the total combinations of the  $L$  edges, since one wants to pick  $L$  edges independently on the order. As expected,  $p_L$  could be interpreted as having  $L$  successful results knowing that an edge is chosen with probability  $p$  and the total trials are  $\frac{N(N-1)}{2}$ , i.e. the total edges if  $p = 1$ . Thus, a Binomial distribution with the average number of links equal to

$$\langle L \rangle = \sum_{L=0}^{\frac{N(N-1)}{2}} p_L L = p \frac{N(N-1)}{2}$$

and the average per node contacts

$$\langle k \rangle = \frac{2\langle L \rangle}{N} = p(N-1).$$

The two equations above highlight that  $\langle L \rangle$  and  $D$  could be obtained by multiplying  $p$  by the total number of available links and neighbors resp.<sup>2</sup>. Alongside, as the network becomes denser, i.e. increasing  $p$ , also  $\langle L \rangle$  and  $\langle k \rangle$  would be enhanced. Moreover, by multiplying the expression by  $q := 1 - p$ , it is possible to obtain  $\sigma_{\langle x \rangle}^2 = q \cdot \langle x \rangle$ , where  $x = L$  or  $k$ .

Similarly, the probability of having  $k$  number of contacts is

$$p_k = p^k \cdot (1-p)^{\binom{N-1}{2}-k} \cdot \binom{\binom{N-1}{2}}{k}. \quad (2.2)$$

where  $N - 1$  are the total neighboring nodes differently from  $\binom{N}{2}$ , which were the total node pairs (cf. [Equation 2.1](#)). Another way to recover  $\langle k \rangle$  and  $\sigma_k$  is by means of  $p_k$ .

Real network are sparse. In fact, by defining the “sparsity” of a network as the ratio  $s := \langle k \rangle / N$ , the internet-routers has  $s \simeq 3.0 \cdot 10^{-5}$ , since  $N \simeq 200000$  while  $\langle k \rangle \simeq 6$ . Many others concrete example support this sparsity nature of real networks [6]. Therefore, in the  $\langle k \rangle / N \ll 1$  limit<sup>3</sup>, the [Equation 2.2](#) becomes the Poissonian distribution with average  $\langle k \rangle$

$$p_k = e^{-\langle k \rangle} \frac{\langle k \rangle^k}{k!}. \quad (2.3)$$

Therefore, keeping in mind that the [Equation 2.3](#) is only valid in the sparse regime,

- the explicit expressions of  $\langle k \rangle \simeq p \cdot N$  and  $\sigma_k = \langle k \rangle^{1/2}$  assume a simpler form for a Poissonian distribution. Moreover, as the binomial case,  $\langle k \rangle$  and  $\sigma_k$  increases if  $p$  increases, since the network is becoming denser and, so, more spread in the node degrees than the for low  $p$ .
- it allows the same description for networks with the same  $\langle k \rangle$  but different size  $N$ , since [Equation 2.3](#) does not depend on  $N$ .

## 2.2.2 The “Small-World” Property

A captivating argument, network science allows to study is the “six degrees of separation” or the “Small-World (SW) phenomenon”. The two quoted names comes, respectively, from a theme developed by the Hungarian writer Fridges Karinthy in a play called “Chains” (1978) and an empirical experiment injected by the psychologist S. Milgram in 1967. A famous version of it states that an actor/actress, e.g. Kevin Bacon, is linked to a random actor/actress, e.g. Andrea Scotti, through only few acquaintances: according to [Kevin Bacon Number](#)<sup>4</sup> only by two persons in common. By extending this idea to real networks, it is possible to recover that the distance between two randomly chosen nodes is small [6]. Random networks account for this phenomenon as we will deepen.

On average, the expected number of nodes  $N$  at a certain distance  $d$  is

$$N(d) \approx 1 + \langle k \rangle + \dots + \langle k \rangle^d = \frac{\langle k \rangle^{d+1} - 1}{\langle k \rangle - 1},$$

where we taken advantage of the geometric series, after noting that “1” is the selected nodes,  $\langle k \rangle$  are its neighbors,  $\langle k \rangle^2 \approx \langle k \rangle(\langle k \rangle - 1)$  the next-to-next neighbors and so on. Thus, by considering that for a real network  $\langle k \rangle \ll 1$  and that  $N(d_{max}) \sim N$ ,

$$d_{max} \sim \frac{\ln(N)}{\ln(\langle k \rangle)}$$

On the other hand, the above equation is more suitable in describing  $\langle k \rangle$ , since  $d_{max}$  is dominated by few distant paths from the core giant component. Hence,

$$\langle d \rangle \sim \frac{\ln(N)}{\ln(\langle k \rangle)} \quad (2.4)$$

<sup>2</sup>This is accordance with the formal definition of the “average”

<sup>3</sup>At least for  $\langle k \rangle \simeq 50$  and  $N \simeq 10^3$

<sup>4</sup><https://oracleofbacon.org/movielinks.php>

is the formalization of the Karinthy's "Small-World phenomenon" and it is obtained by considering that most of the nodes are contained within  $\langle d \rangle$ . Indeed, for a real network,  $\ln(N) \ll N$  drives to a "smaller" average path length compared to  $N$ , which is the typical scaling for a regular lattice<sup>5</sup>. Moreover, the denominator of the Equation 2.4 implies that the denser the network becomes, the closer the nodes aggregate. As a sociological example, the average distance of a random person, in the current century, would be derived by applying the Equation 2.4 by fixing  $N \sim 7 \cdot 10^9$  and  $\langle k \rangle \sim 10^3$  yielding  $\langle k \rangle \sim 3.28$  which is a more reliable results than the "six degrees of separation" [6].

### 2.2.3 The Clustering Coefficient

Analyzing a social network, it seems natural to introduce a measure of "community membership" (Figure 1.5a) which capture the possibility to join a local community, e.g. an association or a family (see Figure 1.5a). Indeed, the social structures exhibit the phenomenon of clustering formation: nodes with common characteristics are aggregated into *clusters*.

More precisely, the *local* clustering coefficient  $C_i$  measures the chance of having a link among the neighbors of the  $i$ -th node. As it could be expected,

- $C_i = 0$  as there are no links among neighbors of  $i$ ;
- $C_i = 1$  as there are fully connected neighbors of  $i$ .

In general,

$$C_i := \frac{\text{average links of the } i\text{-th neighbors}}{\text{total links among neighbors}} = \frac{\langle L_i \rangle}{\frac{k_i(k_i-1)}{2}} = p = \frac{\langle k \rangle}{N} = \langle C \rangle \quad (2.5)$$

where  $p$ ,  $k_i$  and  $N$  are the probability of connecting two nodes, the amount of neighboring vertexes of  $i$  and the total nodes respectively,

$$\langle L_i \rangle = p \cdot \frac{k_i(k_i-1)}{2} \quad \text{and} \quad \langle C \rangle := \frac{1}{N} \sum_{i=1}^N C_i.$$

The presence of a link among the two neighbors closes a triangle with the focal node  $i$  ("triadic closure"). Hence,  $C_i$  could also be interpreted as the normalized number of triangles centered in the selected node. In addition,  $C_i = \langle C \rangle$  is independent by the  $i$ -th node degree and, fixing the average degree of a network, it scales with  $1/N$ : for real networks  $p = \langle k \rangle / N$  is small (real networks are sparse) and drives to a smaller  $C$  than the one observed. A model that naturally generates these *triangular* structures, would be a good candidate to enhance the clustering coefficient even for small  $p$ .

### 2.2.4 Random Graphs are not Real Graphs

By looking at a real social network, e.g. at a cocktail party, there is the co-presence of highly connected nodes, called "*hubs*", alongside with the less interacting ones. The Erdős-Rényi (ER) graph does not account for the presence of high-degree nodes [6], since they are strongly damped by the factor term  $1/k!$  in Equation 2.2. Indeed, real networks are sparse but have also strongly heterogeneous degrees, showing a high variance through node degrees.

Secondly, by looking at the evolution of the contact network there could be identified 4 topological regimes starting from isolated individuals for  $\langle k \rangle = 0$  and ending with a fully connected graph for  $\langle k \rangle = N - 1$ , where  $N$  are the total invited persons. The ER model predicts the co-existence of a giant component, containing loops and cycles, alongside with the small ones that aggregate in trees, for  $1 < \langle k \rangle < \ln(N)$  - find a better description below. However, this is clearly at odds with reality since, as a concrete example, in a random electric power-grid some consumers should not get electric power [6]. Many network, as the actor network, are in the connected regime; most are in the supercritical one while still connected. In particular, these regimes characterize the formation of a fully connected network, predicting the emergence of a giant component.

Schematically, recalling  $p$  as the probability of an edge formation,

---

<sup>5</sup>The common notion of physical distance is based on a regular lattice which do not shows the "Small-World" effect. At first glance, this result could be perceived as an uncomfortable.

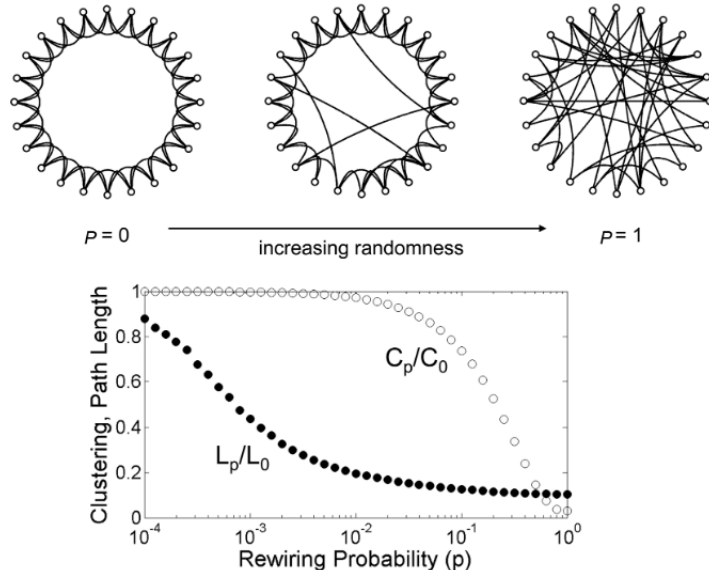
- Sub-critical Regime for  $0 < \langle k \rangle < 1$  ( $p < 1/N$ )
- Critical point for  $\langle k \rangle = 1$  ( $p = 1/N$ )
- Supercritical Regime for  $\langle k \rangle > 1$  ( $p > 1/N$ ): Single giant component formation
- Connected Regime for  $\langle k \rangle > \ln(N)$  ( $p > \ln(N)/N$ )

This is in an one-to-one relation with a First-Order-Phase Transition of Statistical Mechanics. The formation of an ordered giant component could be compared with ice formation: the passage from disordered water molecules to an ordered structure [6].

Thirdly, the real world networks exhibits a “Small-World” phenomenon in disagreement with the [Equation 2.4](#). Hence, a new “Small-World” measure has to be proposed.

Fourthly, fixing  $N$ , the theory suggests that  $C$  is independent on the average number of contacts  $k$ . Nevertheless, this prediction is unsatisfactory, since  $C$  decreases with the increasing of  $k$  for a plethora of the real networks. In particular,  $C/\langle k \rangle \propto N^{-1}$  if  $N \gg 1$ . Thus, a refined model is needed to explain the big *clustering coefficient* for small probability  $p$  (or high  $N$ ).

### 2.2.5 Watts-Strogatz Model



(a) In the top panel, the changing topology from lattice to random-like network; In the bottom panel, the behavior of average path length and clustering coefficient with  $p$  [32]

To face the problem of the “high  $C$  at low edge probability  $p_{ER}$ ” (we redefine here the old  $p$  as  $p_{ER}$ ), while preserving the “Small-World”, Duncan Watts and Steven Strogatz proposed an hybrid model which can interpolated between a regular lattice for  $p = 0$  to a random network model for  $p = 1$ . The new borne model is, thus, called “Watts-Strogatz (WS) model”.

Practically, we started by generating a grid-like network with  $\langle k \rangle$  neighbors for each node. Then, we fixed a node and, for each edge, we rewired its *target* node with a random vertex, according to a probability  $p$ . Lastly, we iterated this rewiring procedure over all the existing edges. Therefore,  $p$  is defined as the probability of having a *distant/long-range* interaction, while  $p_{ER}$  is the probability of having an interaction which could be either *short- or long-range*. Thus, the *distant* vertexes are, on average,  $p \cdot L$  where  $L$  is the total number of links.

We obtained a *degree distribution* that from a peaked histogram of the regular lattice deviated into a Poissonian distribution whenever  $p \neq 0$ . Meanwhile the mean  $D$  remained roughly the same and no *hubs* were generated. A further constraint was that no multiple edges could connect the same pair of vertexes, i.e. no multi-edges. In reality, the presence of multiedges gives a correction of  $1/N$  for big  $N$ , negligible for big  $N$ .

The rationale of WS model is that by a little decrease of clustering (i.e. destroying triangles) corresponds

a significant reduction in the average path length  $\delta := \langle d \rangle$ . Other way around, by connecting nodes in a “long-range” fashion, the overall “triadic closures” are still relevant.

A regular lattice is characterized by a high *clustering coefficient* but an high average path length. In addition, a random network, as seen before, exhibits the “Small-World” property alongside with a low clustering coefficient especially, since triangles are rare for small  $p$ . Therefore, the parameter  $p$  is introduced to fine tune the co-presence of the two kind of networks. Numerical simulation for  $p \in (0.01, 0.1)$  accounts for this fact [23].

Compared to real networks, this model doesn’t explain the presence of the hubs, neglected by the degree distributions, and that  $C(k) \propto 1/k$  where  $k$  is the node degree [6]. In fact, the (four) previous issues will be solved by generating graph with a “scale-free” *degree distribution*. In turn, this implies that *hubs* are naturally present, since  $p \sim k$  as we will report in [Figure 2.4.2](#).

## 2.3 Configuration Model

By means of the *configuration model*, a network can be directly realized starting from a *degree sequence* which either could be drawn from a distribution or a real network of interest [23].

**Definition 2.3.1 (“Degree Sequence”).** The degree sequence is a list of  $N$  numbers  $(k_0, \dots, k_{N-1})$  where  $k_i$  is the degree of node  $i$ .

A degree sequence, thus, determines uniquely a degree distribution but the reverse is not true, since for a particular degree distribution there are  $N!$  possibilities of labeling the nodes, e.g.  $(1, 2, 3)$  has the same degree distribution of  $(3, 2, 1)$ . Moreover, the sum of the degrees has to be *even* in order to build an undirected network. At last, the *configuration model* glues the stubs of different nodes at random until all the degree are saturated. The resulting graph is a “random network with a pre-defined degree sequence”.

Since the number of stubs equals the node degree, each node ends up having the desired degree. In addition, multiple (random) networks may be created from the selected distribution, even displaying some peculiar properties, such as loops or multi-edges. Further constraints has to be imposed to obtain a specific topology, e.g. allow only *short-range* interactions.

The network is characterized by mainly two properties:

- the probability that a fixed node  $i$  may connect to another one  $j$  is

$$p_{ij} = \frac{k_i k_j}{2L - 1}. \quad (2.6)$$

In fact, there are  $k_i$  stubs (or rays) trying to match the  $k_j$  ending of node  $j$ ; while  $2L - 1$  are all the rays available diminished by the chosen one (“ $-1$ ”);

- Since  $p \sim 1/N$  [25], the number of self-loops and multi-links decreases as  $N$  increases. Therefore, it is not needed to exclude them as the network size is large. Nevertheless, arbitrarily rejecting self-loops or multi-links could modify the starting degree distribution, making the analytical calculations difficult.

The purpose of generating an ensemble of networks is to test whether a feature could depend only on the underlying degree distribution  $p_k$ . Indeed, let’s suppose that the presence of the hubs is independent on the other network characteristics rather than  $p_k$ . By exploiting an ensemble of graphs, it would be possible to obtain an average and a standard deviation of that feature. Thus, by comparison with the real value, evaluate if the presence of the hubs depends only on the  $p_k$ .

Another method to generate a network from a fixed degree distribution is the “hidden parameter ( $\eta$ ) method” which do not form multi-edges and loops [6] and allows to tune the average degree  $\langle k \rangle$  modifying the parameter  $\eta$ . On the other hand, the “degree-preserving randomization” provides a method to randomize the connections of a *fixed real network*. In this way, by iteratively swapping the extrema of the edges, it is possible to build a ensemble of networks with the original degree distribution. In the following sections, we will use only the Configuration Model drawing the degrees from a Poissonian distribution [subsection 2.3.1](#).

### 2.3.1 Poissonian Small-World Network

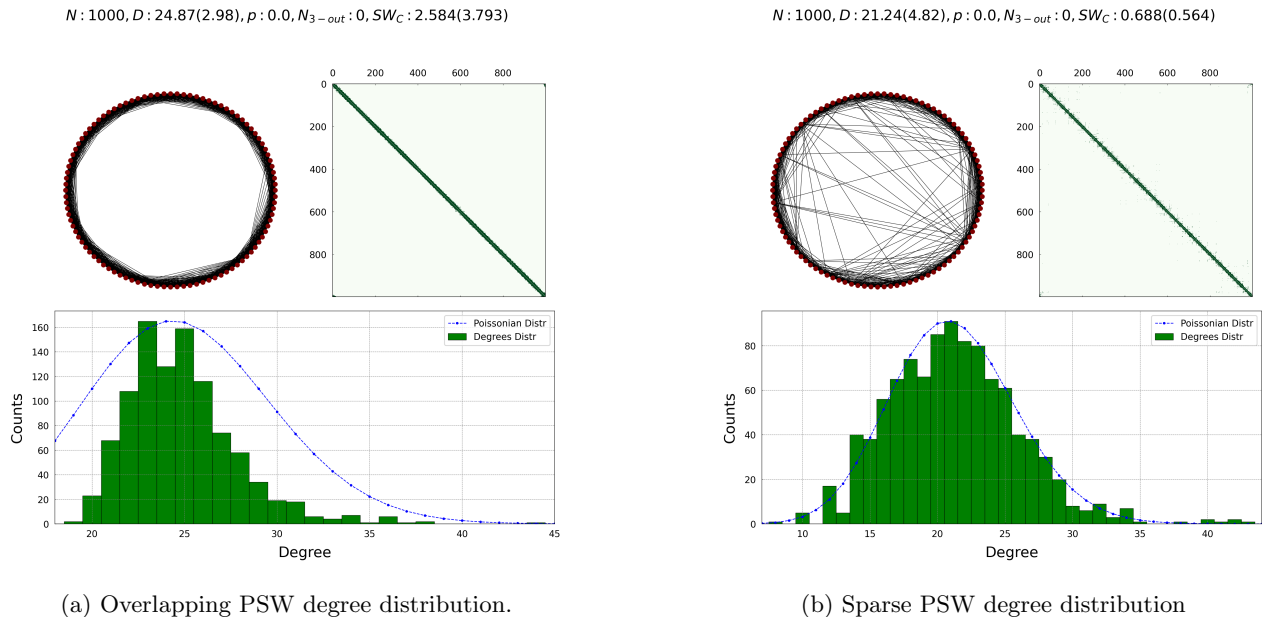


Figure 2.5: Two kind of Poissonian Small-World (PSW) network accounting for the “Overlapping” and the “Sparse” structures. The graph realization (upper left) has  $N = 100$  for a better visualization, we fixed  $N = 1000$  for the adjacency matrix (upper right) and the degree distribution (lower band). We do not report the realizations with  $p = 0.3$ , since it could be straightforwardly obtained by superimposing some long-range links to the current cases as in [Figure 5.1b](#).

A social network is a highly non trivial structure, by including a multilevel organization; weak ties between communities; and temporal aspects that suggest a degree of fluidity with stable social cores [35]. As seen in the [section 1.2](#), however, the lockdown measures prevents the formation of highly connected nodes (hubs), expected in an unconstrained (social) scenario. Thus, a possible approach would be to draw a degree sequence from a Poissonian distribution ( $\langle k \rangle / N \ll 1$ ) and build a graph by connecting the neighboring nodes. This involved structure, called “Poissonian Small-World (PSW) Network” ([35]), enables to capture the heterogeneity in the number of contacts (node degree); the Small-World (SW) phenomenon and the clustering of families alongside with their overlap. Moreover, the WS parameter  $p$  represents the fraction of individuals that are connected at “long-range” through leisure activities whenever  $p \neq 0$ .

Concretely, we generated a PSW using the configuration model with a degree sequence drawn from a Poissonian distribution. To simulate a closed population, we arranged the nodes on a circle: the first and the last nodes of the degree sequence are assumed to be neighbors. Hence, we could capture both the SW property (see [page 11](#)) and the heterogeneity on the node degrees.

With low values of the Poissonian mean  $\mu$ , we took into consideration the lock-down scenario where the average per node degree of contacts is the household size  $D \sim 2.5$  [35]. The configuration model generates a random wiring of the links, producing “long-range” connections which spoil the locality of the community structures (families). Therefore, by an ad-hoc algorithm, we linked the stubs to the nearest nodes on the circle according to their degree. The rewiring procedure arises the choice of whether to preserve *locality* ([Figure 2.5a](#)), obtaining a narrower  $p_k$ , or to fix the *Poissonian distribution* ([Figure 2.5b](#)), introducing some long-range connections. Based on the kind of connections, we address to the former as the “overlapping-PSW” (O-PSW); while the latter as the “sparse-PSW” (S-PSW).

To gain a perceiving understanding of this, we assumed that the nodes were arranged on a circle and we wired them anti-clock wise from the bottom. If the “locality” has to be preserved ([Figure 2.5a](#)), the “actor” node links to its nearest neighboring vertexes even if their degrees have been already saturated by previous wirings. Therefore, the Poissonian distribution was lost. This kind of  $p_k$  resembles the Watts-Strogatz one for  $p_k \neq 0$ . The difference is that  $p \neq 0$  drives to a network with long-range interactions; while here we generated only local connections.

On the other hand, by aiming at *preserving*  $p_k$  (Figure 2.5b), we linked an individual to the nearest contacts, whose degree has not been saturated by the previous re-links. Thus, the target nodes could be distant from the source one. Since in [34], there are reported some intriguing behaviors for a Poissonian Small-World (PSW) but not which of the two kinds. Hence, we decided to examine both the O-PSW and S-PSW networks.

In practice, the “Sparse” wiring algorithm iterates over these steps<sup>6</sup>:

- we choose the lowest degree  $k_l$  node that has not already been saturated;
- we linked an even number of times  $\lfloor k_l/2 \rfloor$  on the clockwise and anti-clockwise nodes, where  $\lfloor *\rfloor$  is the floor function of  $*$ ;
- if the degree of the selected node is odd, we wired one last time ( $k_l - \lfloor k_l/2 \rfloor = k_l \bmod (2) = 1$ ), e.g. anti-clockwise;
- we deleted, among the available nodes, both the chosen node and the target nodes which saturated their degree.

More practically, fixed  $[(1,0), (6,1), (0,2), (2,2), (4,2), (7,2), (8,2), (9,3), (5,3), (3,4)]$ , i.e. a degree sequence composed by (node,degree) tuples. The edges  $(i,j)$  are created by connecting  $i$  to  $j$  and diminishing the degree of  $j$  at each step:

- node 1 is left alone as  $\text{deg}(1) = 0$ ;
- (6,7);
- (0,2) and (0,9)
- (2,0) (already present) and (2,3);
- (4,3) and (4,5);
- (7,6) (already present) and (7,8);
- (8,7) (already present) and (8,9);
- (9,3), (9,8) (already present) and (9,5) - “tunneling” nodes ;
- (5,4), (5,9) (already present) and (5,3);
- node 3 is left with  $\text{deg}(3) = 1$ , but this issue reduces with sparsity  $\langle k \rangle \ll 1$ .

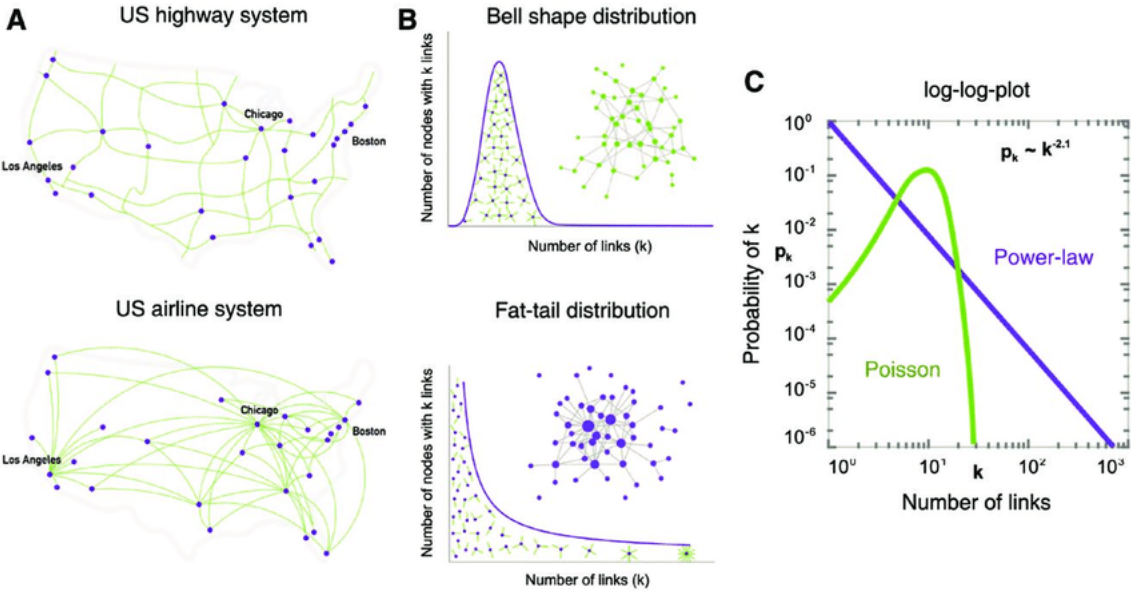
Hence, the algorithm preserves the Poissonian degree distribution, while enhancing the local clustering of the nodes. However, we reported a “long-range” edge  $((9,5))$ , since the nearest available vertexes could be already saturated; therefore, resulting in a distant linking. This “tunneling” nodes are neither “super-spreaders” (or hubs of the infection), since forbidden by the Poissonian degree distribution; nor “super-infectors”, which would be characterized by an higher infectivity rate  $\beta$ .

---

<sup>6</sup>Recall that the degree sequence is already fixed and drawn by a Poissonian distribution

## 2.4 Scale-Free Networks

### 2.4.1 Scale-Free Property



(a) On the left: the comparison of a random network (top panel) and a scale-free one (bottom panel); On the right: their degree distributions on log-log scale) [6]

**Definition 2.4.1** (Scale-Free Network [5]). A scale-free network is a network whose degree distribution follows a power law.

By plotting the degree distribution of the real networks, due to ‘‘hubs’’, a better approximation is obtained via *power-law distributions* (PLDs) of the kind<sup>7</sup>  $p_k \sim k^{-\gamma}$  where  $\gamma$  is called the *degree exponent*.

#### How a scale does (not) emerge

The PLDs are long-tailed functions which describe a phenomenon that has not a reference scale. For example, the heights distribution of a sample population displays a peak at the average height, which is the reference scale for that population. Instead, PLDs do not exhibit a peak but allows also for outliers, e.g. 100ft tall individuals. More precisely, the variance, for a Poissonian distribution, is  $\sigma_k = \langle k \rangle^{1/2}$ , limited as the network grows. Therefore, the  $\langle k \rangle$  scale is trustworthy. At the same time, for a PLDs the variance diverges since [6]

$$\lim_{N \rightarrow \infty} \sigma_k^2 \approx k_{max}^{2-\gamma+1} = \infty. \quad (2.7)$$

since real networks have typically  $\gamma \in (2, 3)$  (WWW has  $\gamma = 2.1$  [6]) and  $k_{max} \sim N$ .

Therefore, a reference scale for PLDs is not naturally present as, extending the Poissonian result, for the *Exponential Bounded Distributions* (EBDs) [6], i.e. when there is an exponential or faster decay for high  $k$ , such as binomial/Poissonian/Gaussian distributions.

#### The maximum degree

In the following, it is developed a quantitative comparison between the maximum degree allowed by EBDs and by PLDs to gain a numerical perception of their difference. In detail,  $k_{max}$  (or the ‘‘natural cutoff’’) is expected to be, roughly speaking, the size of the bigger hub; while  $k_{min}$  approximates the smallest degree. Therefore, for an exponential distribution [6],

$$k_{max} = k_{min} + \frac{\ln(N)}{\lambda}. \quad (2.8)$$

where  $\lambda = 1$  for convenience. The same  $\ln(N)$  dependence would be recovered of any other EBD.

<sup>7</sup>Usually, reported in the log-log scale linear version:  $\ln(p_k) \sim -\gamma \ln(k)$ .

On the other hand, applying the same rationale to a scale-free network,

$$k_{max} = k_{min} N^{\frac{1}{\gamma-1}}. \quad (2.9)$$

The results are somehow expected, since for:

- EBDs:  $k_{max} \sim k_{min}$  since  $\ln(N)$  strongly reduces contribution with  $N$ ;
- PLs: there could be order of magnitude of difference between  $k_{max}$  and  $k_{min}$ .

Indeed, as a simple example, WWW forms a graph of on  $N \sim 10^5$  documents with  $\langle k \rangle \simeq 4.6$  and  $\gamma = 2.1$  [6]. Knowing that  $k_{min} = 1$  for Exponential Bounded Distributions,  $k_{max} \sim 14$ ; while  $k_{max} = 95.000$ . This reinforces the insight that big hubs are naturally arising by increasing  $N$  only for power-law distributions.

### Ultra Small-World

Hubs represent a one-hop bridge for many nodes, since they are connecting the otherwise-distant vertexes. Indeed, the average distance  $\langle d \rangle \sim \ln(\ln(N))$  for  $\gamma \in (2, 3)$ , formally describes the so called “ultra small-world phenomenon”. An heuristic example is the airport lines, which diminish the  $\langle d \rangle$  among (far) cities with respect the national highways.

Surrounding the “Ultra Small-World”, there are three other regimes [10]:

1. Anomalous Regime ( $\gamma = 2$ ) producing a “wheel rim configuration”, a central hub with spoke nodes. In this regime,  $\langle d \rangle = constant$ ;
2. Ultra-Small World Regime ( $2 < \gamma < 3$ ):  $\langle d \rangle \sim \ln(\ln(N))$  gives rise to the “ultra-small world phenomenon” as a slower growth in  $\langle d \rangle$  than random network;
3. Critical Point ( $\gamma = 3$ ) for which  $\langle d \rangle \sim \frac{\ln(N)}{\ln(\ln(N))}$ , marking the passage between the small-world and the ultra-small world;
4. Small World ( $\gamma > 3$ ) random networks are recovered, resulting in  $\langle d \rangle \sim \ln(N)$ .

Thus,  $\langle d \rangle$  is changing with  $\gamma$ , as the smaller it is, the shorter would be the average distance; but also with  $N$ , as it is the “ab ovo” hypothesis for having big hubs.

### Growth and Preferential Attachment

Even with different origins, most real networks display two important features without which it is impossible for hubs to emerge [6]: growth and preferential attachment (see section A.2,section A.3).

In particular, growth is an active process driven by the sequential increasing of the size of the network  $N$  as per the addition of new nodes. Rather, a random network assume  $N$  to be fixed.

Furthermore, new nodes prefer to link to the more connected ones, a process called “preferential attachment”. On the other hand, random networks wire randomly with other nodes.

Ça va sans dire , the model (Figure 2.4.2) has to be dynamical and encode a “preferential” probability which changes every time (“event time”) there is a modification of the topology.

### Final Remarks on Scale-Free

In general, the hosted phenomenon (-a) is complex and affects the graph topology and, in turn, the degree distribution. Rebus sic stantibus , it is sufficient to establish a fair starting point, either EBDs or PLDs class, over which develop gradually ad-hoc features, rather then the meticulous fitting of the degree distribution.

As a final remark, many interesting features of scale-free networks, from their robustness to anomalous spreading phenomena, are linked to the  $\gamma \in (2, 3)$ ; thus, due to the small average distance which strengthen the considered phenomenon. For a more detailed dissertation, see section A.1.

### 2.4.2 Barabási-Albert Model

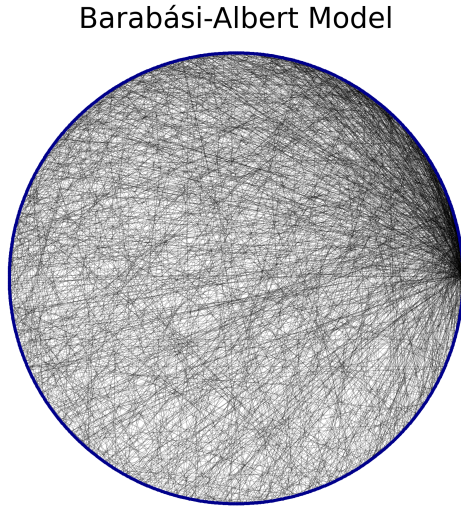


Figure 2.7: Formation of a scale-free network. We can clearly see that the highest part of the network has a darker color than the left side. Indeed, we set the first nodes to be on the right rewired the newer ones according to the preferential attachment, i.e. older nodes are likely to be the hubs of the graph.

To take advantage of growth and preferential attachment, we used the Barabási-Albert model [6]. Indeed, given the total size of the graph  $N$  and the number of edges to attach from a new node to the existing ones  $m \in [1, N]$ ,

- we started with a star-graph with  $m + 1$  nodes;
- **Growth:** at each event time we added a new node with  $m$  stubs which are linked to different nodes;
- **Preferential Attachment:** the probability to wire with a node  $i$  is

$$\Pi(k_i) = \frac{k_i}{\sum_{j=1}^N k_j} \quad (2.10)$$

Therefore, preferential attachment has a stochastic nature not a deterministic one. Moreover, it increases the appeal of the (already) high-degree nodes, alias “rich-gets-richer” phenomenon. As a result, while most of the nodes ends up having few links, a bunch of nodes become highly connected (big hubs). This implies a degree distribution which does not decay exponentially, i.e. a power law with  $\gamma \leq 3$  [6].

Empirical studies on networks, such as actor and scientific collaboration networks, have found that the exponent at the numerator of  $\Pi(k_i) \sim k_i^\alpha$  could differ from 1. Indeed, there are 3 paradigmatic kinds of Preferential Attachments (PAs) by varying the exponent  $\alpha$ : sublinear PAs ( $0 < \alpha < 1$ ), (linear<sup>8</sup>) PAs ( $\alpha = 1$ ), superlinear PAs ( $\alpha > 1$ ). Briefly, the sublinear PAs drives to an “stretched exponential distribution” (see [Equation A.1](#)); the linear to the standard scale-free network; while in the superlinear almost all nodes connects to few super-hubs (winner-takes-all phenomenon). Hence, only for  $\alpha = 1$ , a power-law distribution could be recovered. In addition, after  $t$  event times, the network has gained  $t$  new nodes for a total of  $N = m_0 + t$  nodes and  $m_0 + mt$  links.

---

<sup>8</sup>Commonly, the here-called “linear” PAs is just called “preferential attachment” without further specification.

### 2.4.3 Linearized Chord Diagram

Having in mind the general purpose and results, a more precise description on the building process would clarify two point left open, i.e.

- the arrangement of the initial  $m_0$  nodes;
- whether the next  $m$  links were added simultaneously or one at the time. This could drive to the formation of multi-links, i.e. conflicting edges, due to assumed independent nature of the new stubs.

These problem are solved with the idea of sequentially adding nodes to the graph(s) created at a previous times.

Fixing  $m = 1$  for simplicity, start with the empty graph  $G_m^t = G_1^0$ . At each event time, choose an initial vertex  $v_i$  of  $G_1^{(t-1)}$  and connect it to the new vertex  $v_t$  with probability  $p$  such that

$$p = \begin{cases} \frac{k_i}{2t-1} & \text{if } i \in [1, t-1] \\ \frac{1}{2t-1} & \text{if } i = t \end{cases}. \quad (2.11)$$

Rephrasing it, connect  $v_t$  with  $v_i$  with a probability of  $\frac{k_i}{2t-1}$  if the nodes are different; otherwise,  $\frac{1}{2t-1}$ . This method allows for the formation of multi-edges and loops, but constraints their number to be negligible as the network grows. The present technique referred to  $m = 1$  for an immediate perception. Whether  $m > 1$  stubs are involved, add them one at the time, enabling their contribution to the hubs degree.

## 2.5 Annealed Mean-Field Network

The definition of a AMFN is now given by means of a SIR model spreading over it. Briefly, the SIR model divides the individuals in 3 compartments and accounts for the (direct) infection scheme:  $S - \text{susceptible} \xrightarrow{\beta} I - \text{infected} \xrightarrow{\mu} R - \text{recovered}$ , where  $\beta$  and  $\mu$  are the transmissibility and recovery rate. Thus, we introduced the “annealed-mean-field” network (AMFN) to properly simulate the mean-field SIR model [Equation 3.1](#): a pathogen spreading on a homogeneous mixing of the individuals.

Indeed, we obtained the mean-field SIR model at every time-step  $t$  with the following scheme:

- we selected an individual  $I_1$  over the pool of infected;
- we chose  $\langle k \rangle$  neighbors at random among all the nodes<sup>9</sup>, e.g.  $I_2, I_3$ ;
- we tried to infect them with probability  $\beta$  and to recover  $I_1$  with probability  $\mu$ .

With this procedure, it is highly improbable to re-select the past infector ( $I_1$ ) of a node ( $I_2$  or  $I_3$ ), since the probability goes as  $D/N$ , which typically is much less than one.

Moreover, we fixed the number of neighbors for each node to  $\langle k \rangle$ , giving to this model the “annealed” adjective.

To sum up, we defined an AMFN as a (directed) random network whose  $D$  links are randomly chosen by each node where the agent lays down. With this technique, the individuals are *well mixed*, mimicking a “mean-field” approximation. Therefore, this is used as a benchmark for the SIR spreading on the other networks.

---

<sup>9</sup>A fair spreading should consider as available contacts all the nodes, i.e. the susceptible but also the already infected or recovered ones. Indeed, all nodes are possible count; while only the susceptible ones could be infected.

# The Epidemiological Models

The most studied dynamical process on networks is the spreading of an agent. Rather than its common interpretation as a pathogen, this agent could also be considered as an information (“knowledge spreading”), an ask for collaboration, a mobile/computer virus, a business practice, a rumor or a meme, etc. These phenomena acts on different types of networks; are characterized by peculiar time-scales and follow various microscopic-transmission mechanisms. Despite all of these differences, they obey to a common pattern conveniently captured by analyzing their spreading on a network: the quoted graphs (cf. chapter 2) provides different insights on how links could be created and preserved. Thus, although Satorras and Vespignani started from a diffusion of an epidemic [27], these techniques are used also in many other human-related fields, as the social sciences and digital security.

This thesis is devoted to the infective epidemiology: we will study the behavior of a SIR model, which simulates the COVID-19, on different topologies. In particular, infectious diseases are also called *contagious*, due to their transmission by contacts with a secretion of an ill person, e.g. droplets. They account for 43% of the global burden of diseases alongside with other noninfectious diseases (for example obesity, gambling or smoking) which are equally affected by the graph of contacts [6].

The epidemiological frameworks, in general, find their roots in two fundamental hypotheses:

- Compartmentalization: Each individuals is classified according to a state, or compartment, allowed by the considered model. In particular, the simplest compartments are the following:
  - Susceptible (S): vulnerable people which have not been in contact with the disease;
  - Infectious (I): individuals, which are able to spread the pathogen to their neighbors;
  - Recovered (R): infected individuals which has been removed from the I-state. No difference among deaths or recovered has been settled<sup>1</sup>. Thus, many texts use the fair word “Removed” as a definition of the “R”. On the other hand, we will consider the recovered nodes as present and protecting the remaining susceptible from the infectors.

Driven by some transition probabilities, individuals are able to move among compartments:  $S \rightarrow I$  is a random event regulated by the transmission rate ( $\beta$ ); while  $I \rightarrow R$  by the recovery rate ( $\mu$ ). Therefore, as for COVID-19, in the early stages a large fraction of the population was susceptible, e.g. 99%, called “naive population”. Then, the pathogen drives some nodes into the infectious state; while, at the end, to the “Recovered” compartment.

For convenience, it is also possible to introduce many other compartments to allow for additional states, such as the “asymptomatic” which are able to spread the disease without exhibit symptoms, the first signal of the infection. The epidemiological models are generally called as their constitutive compartments, e.g. “SIR” stands for the node path among the susceptible-infectious-recovered states. The division in compartments has to be considered at a macroscopic scale, since the aim is to improve the prediction of the number of infected; while not caring about the microscopic infection within the host body; all these details, indeed, are encoded in  $\beta$  and  $\mu$ ;

---

<sup>1</sup>In reality, this is not the case since death individuals are no more present in the society and leaves space for new contacts; while immunize nodes shields the more inner nodes, by arranging in a sun-like configuration (a susceptible core and spoken “recovered” nodes)

- Mixing Level: People live and mixes but has a fixed number of total individuals  $N$ , i.e. no death or birth are taken into account (see [25]). Hence, two possible ways, the individuals could get exposed to the disease are:
  - *homogeneous mixing*: this hypothesis assumes that each individual has the same chance of interact with another one, e.g. an infectious. For this reason, it is also called the “fully-mixed”, “mass-action” or “mean-field” approximation. Indeed, the specific degree of a single node is not taken into account; rather, the number of infectious-contacts per node is fixed. In turns, this could be seen as a “field” of mean infectious spikes which attack the susceptible;
  - *heterogeneous (degree-based) mixing*: this approach groups the nodes by their degree of contacts  $k$  and considered them “statistically” equivalent within that class: this is a finer mean-field approximation and could be improved by considering an “individual-based” approximation [19].

It seems natural that the “fully-mixed” hypothesis is false at some extent. In particular, we will show that for small “epidemic strength” ( $R_0$ ) the network structure deeply plays a role, since individuals may transmit a pathogen only to (local) neighbors (see chapter 5). Nevertheless, if a pathogen is “strong” enough the total number of infected are comparable to the one of a “mean-field” approach. Indeed, the spreading on network resembles the mean-field model (AMFN) whenever either  $R_0$  or the long-range connections  $p \cdot N$  are high enough to allow the disease, reaching the epidemic state rapidly.

From the  $S, I, R$  compartments, one finds the following epidemiological model: the  $SI$ , the  $SIS$  and the  $SIR$  (the case of study). In detail, the  $SI$  model accounts for the fact that it would be impossible to recover from the disease, e.g. herpes; the  $SIS$  model for diseases where it would be not possible to waning immunity, thus, returning susceptible, e.g. the HPV, generic flu; the  $SIR$  where the last state is the gained immunity, e.g. the most strain of seasonal influenza or chickenpox. In addition, the  $SIR$  model could be modified with other compartments to better fit the reality. For example, introducing the “quarantined” individuals ( $Q$ ) the  $SIR$  will become a  $SQIR$ , where with a probability  $q$  a susceptible can be isolated from the rest of the population.

By denoting the total number of individuals  $N$ ,  $s(t) := S(t)/N$  is the number of susceptible (healthy) normalized with  $N$ ;  $i(t) := I(t)/N$  is the fraction of already infectious persons; while  $r(t) := R(t)/N$  the recovered one. In this way, the “closed population” translates into  $s(t) + i(t) + r(t) = 1$  at any time  $t$ . Thus, at the initial time ( $t = 0$ ), a seed of infected has to be injected to start the infection, e.g.  $I(0) := 10$ . Therefore,  $s(0) = 1 - i(0)$  since the recovered are  $r(0) = 0$ . Furthermore, let assume that the likelihood of transmitting the disease to a susceptible per unit time is  $\beta$ , i.e. the “transmission rate”; while the “recovery rate” is  $\mu$ . Hence, defining the *basic reproduction number*  $R_0 := \beta \langle k \rangle / \mu$ , this quantity embodies the number of secondary infected in a naive population. Indeed, the probability that a node  $i(t)$  becomes infected during a time interval  $dt$  is  $1 - (1 - \beta dt)^{k_i} \sim \beta k_i dt$ , assuming  $\beta dt \ll 1$  [6]. Similarly, the probability that an infector will infect a susceptible person in the next  $d/dt = \frac{1}{\mu dt}$  times is  $\beta_d := 1 - (1 - \beta \langle k \rangle dt)^{d/dt} \sim \beta \langle k \rangle d = \beta \langle k \rangle / \mu$ , where  $\beta \langle k \rangle dt \ll 1$  and  $k_i \sim \langle k \rangle$ , as it is the case for random networks chapter 2. The latter result could be understood as the complementary probability of not having a “risky” interaction for  $d/dt$  trials [34].

The final goal would be to find the total new daily infected, i.e. a slight modification of  $I(t)$ . Moreover, since the disease-spreading is a stochastic process, it would be the average of the various scenarios (in our case 50 trajectories).

### 3.1 Homogeneous Mixing

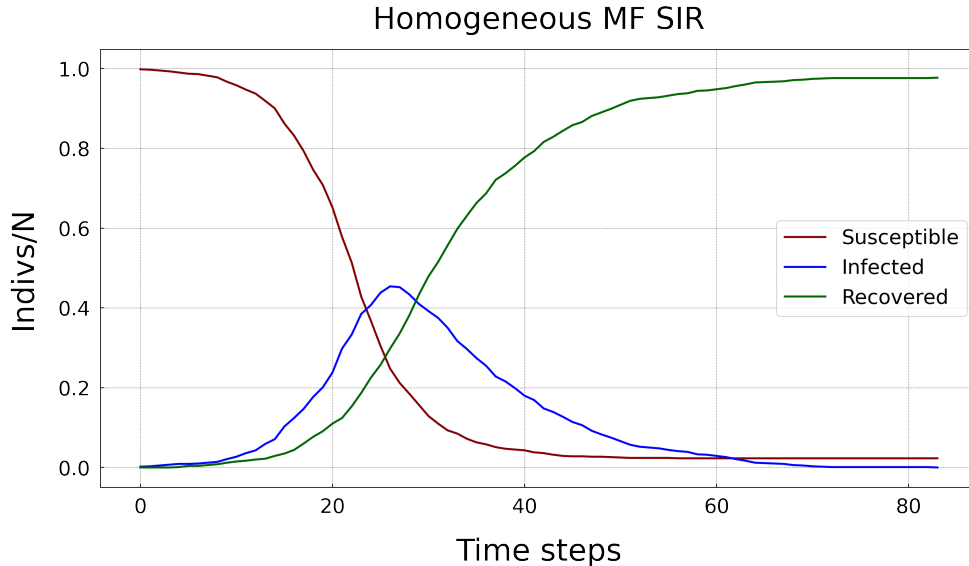


Figure 3.1: Mean-Field SIR with  $N = 10^3$ ,  $\langle k \rangle = 5$ ,  $\beta = 0.2$ ,  $\mu = 0.2$ . As shown, at the end of an epidemic, i.e.  $i(t) = 0$ , a non-zero fraction of susceptible survives which, in turn, accounts for a  $r(t_{end}) = 1 - s(t_{end}) \neq 1$  fraction of recovered nodes.

The “homogeneous approximation” considers the people to mingle and meet completely at random: an infected person can be in contact with  $\frac{\langle k \rangle S(t)}{N}$  susceptible individuals. Taking into account that at a time  $t$  there are  $I(t)$  infected which spread the disease at a rate  $\beta^2$  and recovers at a rate  $\mu$ , the SIR equations are the following [25]

$$\begin{cases} \frac{ds}{dt} = -\beta \langle k \rangle s i \\ \frac{di}{dt} = \beta \langle k \rangle s i - \mu i = \beta \langle k \rangle (1 - i - r) i - \mu i = \mu (R_0 s - 1) i \\ \frac{dr}{dt} = +\mu i \end{cases} \quad (3.1)$$

where it has been exploited the fact that the population is closed, i.e. no death/births are considered. This translates into  $s + i + r = 1 \quad \forall t$  or even  $ds/dt + di/dt + dr/dt = 0 \quad \forall t$ . In addition, the right most equality shows how the definition of *basic reproduction number*  $R_0$  could be recovered directly from the equations. Finally, note the removal of the time dependence since  $s(t), i(t), r(t)$  is understood.

To solve Equation 3.1, by integrating “division” of the third equation and the first equation

$$s(r) = s_0 e^{-\beta \langle k \rangle r / \mu} \quad (3.2)$$

where it has been required that  $s(t = 0) = s_0$  arbitrarily. Then, substituting  $s(r)$  into the second equation [25],

$$\frac{dr}{dt} = \mu (1 - r - s_0 e^{-\beta \langle k \rangle r / \mu}). \quad (3.3)$$

Now, solving this equation for  $r$  gives, in turn, the possibility to find  $s$  and, thus,  $i$ . In principle,

$$t = \frac{1}{\mu} \int_0^r \frac{du}{1 - u - s_0 e^{-\beta \langle k \rangle u / \mu}}.$$

The initial conditions can be chosen arbitrarily but the most suited is to fix a small number  $c \ll N$  of infected individuals such that  $s_0 = 1 - c/N \approx 1$ ,  $i_0 := i(0) = c/N \approx 0$  and  $r_0 \approx 0$ .

<sup>2</sup>In many text books, e.g. [25], the  $\beta \langle k \rangle$  total rate considered in the following is just  $\beta$ .

Unfortunately, this equations have no closed form, but special insights could be reached by looking at the plot of the numerical solutions of [Equation 3.1](#).

The case where  $R_0 < 1$  represents the scenario when the pathogen will die out fast from the population, i.e. a limited spreading occurs.

Indeed, at early times  $t \approx 0 \implies i(0) \sim 0, r(0) \sim 0$ .

Therefore, [6]

$$i(t \approx 0) \sim i_0 e^{(\mu(R_0 - 1)t)}.$$

On the other hand, the SIR features are more involved if  $R_0 > 1$ :

1.  $s(t)$  is monotonically decreasing; while  $r(t)$  is always increasing;
2.  $i(t)$  increases depending on the availability of susceptible: at early times the increasing is exponential; then, deflect and decreases on the way to the end of the epidemic, i.e.  $i(t_{max}) = 0$ ;
3.  $s(t_{max}) > 0$  since when  $i \rightarrow 0$  there are no infected individuals left to infect the remaining susceptible. Formally,  $r(\infty) := \lim_{t \rightarrow \infty} r(t)$  is the total size of the outbreak, i.e. the total number of individuals who ever catch the disease.

Setting  $dr/dt \stackrel{!}{=} 0$ ,  $s_0 \simeq 1$  (“naive population”) and using [Equation 3.3](#), the solution of

$$r = 1 - e^{-\beta\langle k \rangle r / \mu} \quad (3.4)$$

is precisely  $r(\infty)$ . Therefore, whenever  $r(\infty) \neq 1$  is a sign that “herd-immunity” is reached, alongside with  $1 - r(\infty)$  susceptible left;

4. the characteristic time

$$\tau = \frac{1}{\mu(R_0 - 1)}$$

is the time needed to reach about the 36% of the population and it is the inverse of “disease velocity”, which further depends both on the possibility to infect and the average nearest neighbors. With this new measure of epidemics, it would be possible to recover the previous result observing that there is a spread iff  $\tau > 0$ , i.e.  $R_0 > 1$ .

Interestingly, it would be possible to recognize  $S \leftrightarrow r$  and  $D := \langle k \rangle \leftrightarrow \beta\langle k \rangle / \mu$  ([Equation 3.4](#)) where the “left” quantities are describing the percolation phenomenon and the “right” ones the SIR spreading describes. In this way, the equation [Equation 3.4](#) regulates the size  $S$  of the giant component of a Poisson random graph. In particular, the SIR infection of neighboring nodes could be seen as a bond percolation process of an agent, e.g. water, which propagates according to the same probability distribution [25], [6]. This analogy allows to double the interpretations of the results of [Equation 3.4](#). Indeed, in percolation theory, the giant component size  $S$  depends on the  $D$  average degree of links per node when  $N \rightarrow \infty$ .

Therefore, the final outbreak size  $r(\infty)$  depends on  $\beta\langle k \rangle / \mu$  and the *basic reproduction number* is, conveniently, defined as  $R_0 := \beta\langle k \rangle / \mu$ .

Moreover,  $r(\infty)$  goes continuously to  $I(0)/N \sim 0$  as  $1^+ \leftarrow R_0$ ; while it is constantly  $I(0)/N$  for  $R_0 \rightarrow 1^-$ . Analogously of the appearance of the giant component, the point where (first-order) phase transition occurs, i.e.  $R_{0c} = 1$ , is called epidemic transition. Thus,  $R_{0c}$  separates the “epidemic” ( $R_0 > R_{0c}$ ) from the “non-epidemic” ( $R_0 < R_{0c}$ ) regime. The  $R_0$  dependence of  $r(\infty)$  has to be somehow expected since if an infection has less transmissibility than recovery ( $R_0 < 1$ ), the pathogen would die out fast. On the way to  $R_{0c}$ , an increasing of the  $\beta/\mu$  ratio would describe a less strong epidemic, which consecutively provide a minor  $r(\infty)$ .

To be precise,  $R_0$  is the number of second infections in a naive population, i.e. at early times  $t \approx 0$ :  $\beta/\mu = \beta\tau$  is the probability to infect over a time-interval of  $\tau$ . Thus,  $R_0$  is an estimate of the slope of the curve describing the infection at the start of the epidemic. Furthermore, it is a rough marker of an exponential growth<sup>3</sup>. (for  $R_0 > 1$ ) or vanishing of the pathogen (for  $R_0 < 1$ ) since  $I(t) \approx R_0^{t/d}$ . On the other hand,  $R_0 = 1$  is not indicative of whether this slope is going to increase until  $r = 1$  (pandemic scenario), decreases fast guiding into  $r(\infty) \ll 1$ , or both resulting in  $r(\infty) < 1$ . Indeed, for a more precise signal on the spreading behavior depending only by the initial conditions, higher-order features of the underlying network should be taken into account. A new reproduction number is going to be proposed in the next section.

<sup>3</sup>For SI model,  $\lim_{\mu \rightarrow 0} R(t) = \infty$  since every infected could arbitrarily infect all the other nodes. In a real scenario,  $R_0 (\leq N')$  is finite, as the size  $N'$  of a population is finite.

## 3.2 Heterogeneous Mixing

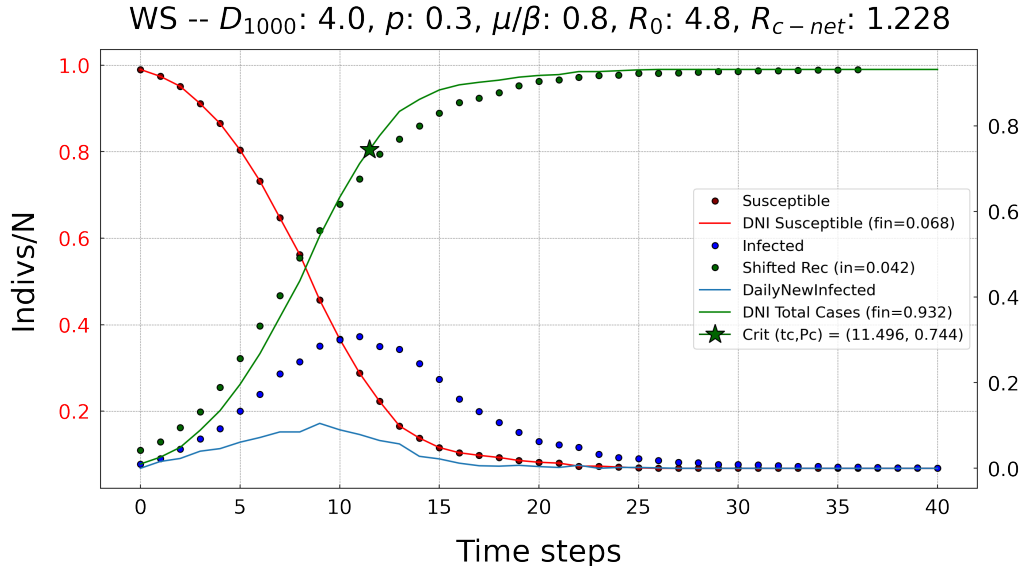


Figure 3.2: Degree-Based SIR using Erdős-Rényi Graph with  $N = 10^3, p = 0, \langle k \rangle = 4, \beta = 0.3, \mu = 0.25$ .  $R_0 \sim 4.8 > R_{c-\text{net}} \sim 1.2$  where  $R_{c-\text{net}}$  is defined in Equation 3.13. Thus, the pathogen could evolve in the network. The dotted evolution are obtained by solving the Equation 3.1 for the standard compartments S-I-R; while the continuum line accounts for the daily new infected  $C(t)$ , the total cases  $\pi(t) = P(t)$  and the susceptible as  $\tilde{s}(t) = 1 - \pi(t)$ . Eventually, the recovered nodes shifted by the average recovered time  $d = 1/\mu$  are similar but not the same of the total cases (solid green line). Lastly, by means of the Equation 4.5, the green star ( $\text{Crit}(t_c, P_c)$ ) is a good estimate of the maximum of  $i(t)$ , as it predicts the critical time  $t_c$  and the value of  $P_c$  correctly.

As described in the previous chapter, within a well-mixed population, every node could infect, at any time,  $\langle k \rangle$  susceptible neighbors. This is not the case for a plethora of real networks, e.g. Barabási-Albert model as they are “scale-free”, namely  $\langle k^2 \rangle$  typically diverges for the *degree exponent*  $\gamma \leq 3$ . Thus, imposing that each individual must have  $\langle k \rangle$  contacts, it drives to a model that underestimate the number of infected. This, in turn, could have worse effect than overestimating it.

An improvement would be to consider that if a pathogen spreads on a network, the individuals with more links are more likely to be infected. Therefore, the nodes are further classified according to their degree and assumed statistically equivalent within their class. This approximation is, thus, called degree-based mean-field (DBMF) approach [6]. Indeed, choosing the same compartments as in Equation 3.1 (S,I,R), one finds  $3 \cdot k_{\max}$  classes, i.e. 3 compartments for each degree, but there are no further differences among nodes with the same degree  $k$ .

Formally, the total fraction of infected is  $i(t) = \sum_{k=0}^{k_{\max}} p_k i_k(t)$ . Iterating the same decomposition on the susceptible  $s(t)$ , recovered  $r(t)$  and substituting them into the Equation 3.1,

$$\begin{cases} \frac{ds_k}{dt} = -\beta k s_k \Theta_k \\ \frac{di_k}{dt} = \beta k s_k \Theta_k - \mu i_k = \beta k (1 - i_k - r_k) \Theta_k - \mu i_k \\ \frac{dr_k}{dt} = +\mu i_k \end{cases} \quad (3.5)$$

here  $\beta$  is defined as the transmission rate and  $\mu$  the recovery rate. Note, in addition, that these equations are valid for  $k = 0, \dots, k_{\max}$  and that we suppressed the  $t$  dependence for easiness of notation. Furthermore, in Equation 3.5, the *density function* at  $t \approx 0$  is defined

$$\Theta_k(t) = i_0 \frac{\langle k \rangle - 1}{\langle k \rangle} e^{t/\tau}. \quad (3.6)$$

Namely, it represents the fraction of infected nodes surrounding a susceptible individual with degree  $k$  at early times. Its explicit expression would be recovered shortly but note that, a priori, it can depend both on  $k$  and  $t$ .

Lastly, the [Equation 3.5](#) depend, by construction, on  $k$  but the  $\langle k \rangle$  dependence is no more present. In turn, the network structure is encoded into the  $\Theta_k(t)$  factor, which in the homogeneous case was  $i(t)$ . Before tackling the problem of solving them, it is necessary to explicitly recover the  $\Theta_k(t)$  factor.

## The Density Function

The density function, as reported before, provides the fraction of infected nodes neighboring a susceptible node of degree  $k$ . In fact, as we are going to prove, this estimate accounts for all the infectors connected with an arbitrary number of hops, since it has no upper-limit.

To start with, assume that the underlying topology has no degree correlation among nodes, i.e. vertexes are connected at random, thus an hub could equally connect with another hub or a lower-degree node. These network are called *neutral networks*. Hence, the probability of a vertex to point to a degree  $k'$  node is the excess degree

$$q_{k'} = \frac{k' p_{k'}}{\langle k \rangle}. \quad (3.7)$$

Indeed, the probability of choosing a degree- $k'$  node is  $p_{k'}$  times  $k'$ , since it owns  $k'$  stubs to connect with. As  $q_{k'}$  should be a probability, the denominator comes to match the  $\sum_k q_k \stackrel{!}{=} 1$  constraint. The [Equation 3.7](#) is local, random and linear in the “bias term”  $k$ . Therefore, as reported in the [subsection A.3.1](#), it is the starting point to build the (linear) preferential attachment.

For a disease to spread, it is assumed that at least one of the spokes of the infected node is connected to the its infector node: only  $k' - 1$  links would be available for the contagion. Therefore,

$$\Theta_k(t) = \frac{\sum_{k'} (k' - 1) p_{k'} i_{k'}(t)}{\langle k \rangle} = \Theta(t) \quad (3.8)$$

where the rightmost equation explicitly display the independence on  $k$ .

In order to capture the time-dependence of  $\Theta(t)$ , it would be taken advantage of the SIR model, following these steps: differentiate the [Equation 3.8](#), insert [Equation 3.5](#) and consider  $1 - i_k - r_k \approx 1$ , which it is the case at early times. This procedure yields [6]

$$\begin{cases} \frac{d\Theta}{dt} = \left( \beta \frac{\langle k^2 \rangle - \langle k \rangle}{\langle k \rangle} - \mu \right) \Theta \\ \Theta(0) \stackrel{!}{=} i_0 \frac{\langle k \rangle - 1}{\langle k \rangle} \quad \text{I.C.} \end{cases} \quad (3.9)$$

which solving by  $\Theta$  yields

$$\Theta(t) = C e^{t/\tau} \quad (3.10)$$

where

$$C := i_0 \frac{\langle k \rangle - 1}{\langle k \rangle} \quad \text{and} \quad \frac{1}{\tau} := \beta \left( \frac{\langle k^2 \rangle}{\langle k \rangle} - 1 \right) - \mu. \quad (3.11)$$

The onset at  $t \approx 0$  of an epidemic is possible if, and only if,  $\tau > 0$ . This, further, implies that the number of infected nodes grows exponentially with time (cf. [Equation 3.10](#)). This threshold depends on the ratio  $\beta/\mu$  defined the *biological factor*  $\lambda := \beta/\mu$ , since it depends only on the epidemic parameters. Indeed, separating the *biological factor*  $\lambda$  from the network features,

$$\lambda > \lambda_c \Rightarrow R_0 > R_{c-net} \geq 0 \quad (3.12)$$

where we have defined the *critical reproduction number*  $R_{c-net}$  as

$$R_{c-net} := \frac{\langle k \rangle^2}{\langle k^2 \rangle - \langle k \rangle} \quad (3.13)$$

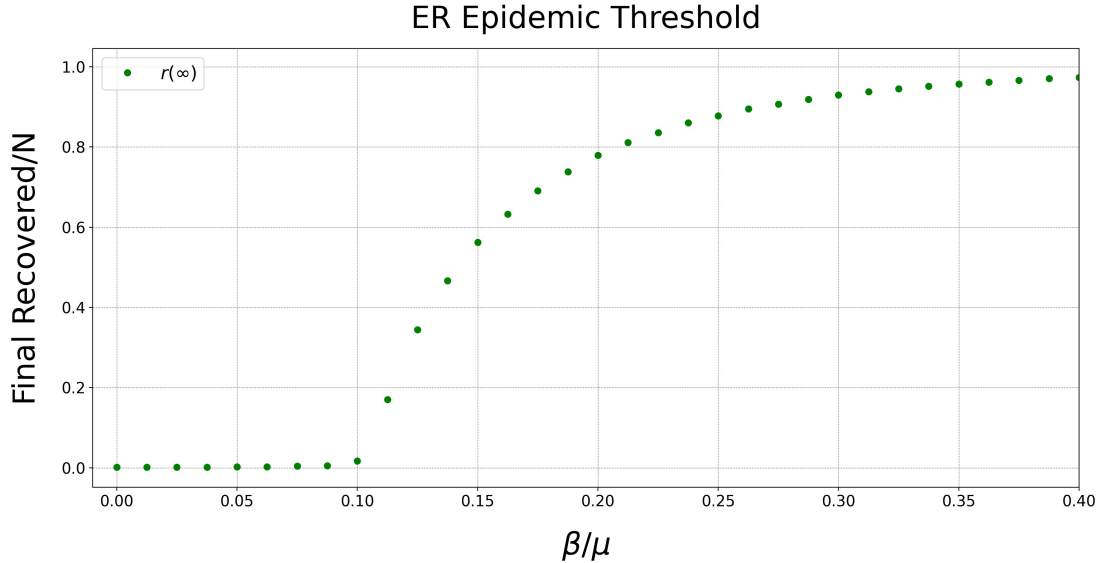


Figure 3.3: Epidemic Threshold  $\lambda_c := \beta_c/\mu$  of a ER Graph with  $N = 10^4$ ,  $\beta \in [0, 0.4]$ ,  $\langle k \rangle \sim 10$ ,  $\mu = 0.8$ . Using  $R_0 = \lambda \cdot \langle k \rangle \stackrel{!}{=} 1$ , the departure from zero happens near  $\lambda_c = 0.1$ , due to finite size effects. Thus,  $\lambda < \lambda_c = 0.1$  implies a fast-decaying pathogen.

and the “epidemic threshold”  $\lambda_c$  as

$$\lambda_c := \left[ \frac{\langle k^2 \rangle}{\langle k \rangle} - 1 \right]^{-1}. \quad (3.14)$$

The left-most side of [Equation 3.12](#) underlines that the natural decay of a pathogen, i.e. fixed  $\beta$ , depends on the degree-heterogeneity ( $\langle k^2 \rangle$ ),  $\mu$  and  $\langle k \rangle$ .

As  $\lambda_c$  is defined as a “threshold”, the final outbreak size, namely the total recovered  $r(\infty)$ , is not linear by increasing the spreading rate; rather, it goes under a phase-transition exceeding  $\lambda_c$ . This behavior is shown in [Figure 3.3](#) for a (random) Erdös-Rényi model.

For a *Poissonian network*  $\langle k^2 \rangle = \langle k \rangle (\langle k \rangle + 1)$ <sup>4</sup>, resulting in the *epidemic threshold*  $\lambda$  of a random network [6]

$$\lambda_c = \frac{1}{\langle k \rangle} \Rightarrow R_{c-net} = 1.$$

where a general definition of the *critical reproduction number*  $R_{c-net}$  could be find in [Equation 3.13](#). Since the average number of contacts  $\langle k \rangle$  is finite,  $\lambda_c$  plays the role of a true threshold, which separates the epidemic regime to the non-endemic regime according to [Equation 3.12](#).

For a *scale-free network*, the second moment  $\langle k^2 \rangle \xrightarrow{N \rightarrow \infty} N^{3-\gamma} \rightarrow \infty$  diverges for large networks, namely  $N \rightarrow \infty$ , since  $\gamma < 3$  (see [Equation A.1](#)). In this limit,  $\lambda_c, \tau \rightarrow 0$  showing, respectevely, the fact that even low-transmissibility disease are successfully spreading in the population and are instantaneous. In reality, the finite size of the network forces  $\lambda_c$  and  $\tau$  to be small but finite. Moreover, the average path length  $\langle d \rangle \rightarrow 0$  in the same limit, since the hubs become bigger as the number of nodes grows. Hence, the hubs play the role of the super-infectors that enable the pathogen to persist and diffuse within the population.

The exposed examples are at the extrema of the plethora of graph models. For many other networks exhibiting an enhancement of the second moment  $\langle k^2 \rangle > \langle k \rangle (\langle k \rangle + 1)$ , there is a reduction both of the epidemic threshold and the characteristic time of the disease. More specifically, the *critical epidemic threshold* can be rewritten as

$$\lambda_c = \left[ \lambda_{c-MF}^{-1} + \left( \frac{\sigma}{D} \right)^2 \right] \quad (3.15)$$

where  $\lambda_{c-MF} := (D - 1)^{-1}$ . Therefore, whenever  $\sigma \neq 0$ ,  $\lambda_c < \lambda_{c-MF}$  and produces an enhancement on the fraction of the fraction of total cases  $\pi(t)$ . Note that  $\lambda_{c-MF}$  has the same expression also for a Regular Lattice since  $\langle k^2 \rangle = \langle k \rangle^2 + \sigma^2 = \langle k \rangle^2$ .

<sup>4</sup>As a comparison, for a Poisson-distributed random variable  $k$  holds  $\sigma_k^2 = \langle k^2 \rangle - \langle k \rangle^2 = \langle k \rangle$ . Thus,  $\langle k^2 \rangle = \langle k \rangle^2 + \langle k \rangle$

In conclusion, in contrast with the “mean-field” predictions, which drives to  $\lambda_c = 1/\langle k \rangle$ , in a heterogeneous SIR model the same quantity depends according to [Equation 3.14](#). Thus, it varies, by changing the underlying topology.

To sum up, for  $\lambda > \lambda_c$  the total epidemic outbreak size  $i(t \rightarrow \infty) \neq 0$ ; while for  $\lambda < \lambda_c$ ,  $i(t \rightarrow \infty) = 0$ , since the pathogen is not strong enough to reach an endemic state. Moreover,  $\lambda_c = 0$  for a “typical” ( $\gamma < 3$ ) large scale-free network; while  $\lambda_c \neq 0$  for the random networks.

## About the SIR equations

No analytic solution exists for the equations of the SIR model. Furthermore, even the early times analysis exhibits some technical difficulties which demands for the numerical simulations of the ODEs of [Equation 3.5](#).

### Early Times

At early times ( $t \approx 0$ ) the recovered and the susceptible individuals are negligible, namely  $r_k, s_k \approx 0$ . Therefore, according to [Equation 3.5](#) and [Equation 3.10](#), the fraction of infected is

$$\begin{cases} \frac{di_k}{dt} = -\mu i_k + i_0 \beta k \frac{\langle k \rangle - 1}{\langle k \rangle} e^{t/\tau} \\ i(0) \stackrel{!}{=} i_0 \quad \text{I.C.} \end{cases} \quad (3.16)$$

whose, first equation, could be straightforwardly rewritten as

$$\frac{di_k}{dt} + \mu i_k - i_0 B e^{t/\tau} = 0 \quad (3.17)$$

where  $i_0 B(k) := i_0 \beta k \frac{\langle k \rangle - 1}{\langle k \rangle}$ .

Hence, the solution of the last equation assumes the form

$$i_k(t) = i_0 \left[ C_1(k) e^{t/\tau} + C_2(k) e^{-\mu t} \right] \quad (3.18)$$

where we defined as

$$\begin{cases} C_1(k) := \frac{B(k)\tau}{1+\mu\tau} = \lambda \cdot \left[ k \left( \frac{\langle k \rangle - 1}{\langle k \rangle} \right) \right] \cdot \frac{1}{\tau} \\ C_2(k) := 1 - C_1(k) \end{cases}$$

Note how  $C_1(k)$  is determined by the contribution of the pathogen ( $\lambda := \frac{\beta}{\mu}$ ), the network and the interaction among the two ( $\tau^{-1}$ ).

In this way, the initial exponential-phase has two contribution: the first, which grows in time, due to an interplay among the disease and the underlying network; the second is diminishing the number of infected according to the recovery of infected individuals.

For *scale-free networks*, the “degree exponent”  $\gamma < 3$  accounts for  $k$  and  $\tau^{-1}$  to diverge as the network grows. This, in turns, gives birth to a peculiar limit of  $C_1(k)$ :

$$C_1(k) \propto \tau k \propto \frac{1}{\int k^2 p_k dk} k \rightarrow 0 \cdot \infty. \quad (3.19)$$

The underlying probability degree distribution  $p_k$  has to be exploited in order to solve the limit [Equation 3.19](#) and gain epidemiological insights.

On the other hand, the networks, such that  $k \sim \langle k \rangle$ , e.g. Poissonian ones, find a good approximation in the random limit, i.e. when the individual contacts are limited by a cost-benefit constraint as the power-grids. Therefore, also  $\langle k^2 \rangle$  is bounded and

$$i_k(t) \approx i(0) + (C - C_2(\langle k \rangle) \mu) t \quad (3.20)$$

where  $C := \frac{\beta(\langle k \rangle - 1)}{\tau}$  since  $\langle k \rangle \approx k$  and  $e^{at} \approx 1 + at$  as either  $t \approx 0$  or  $a \approx 0$ .

Summarizing, the degree-block approximation is itself a “mean-field” framework, since all the nodes with degree  $k$  are equivalent. However, this approach, although simplifying the calculations, it is not completely correct. Indeed, for the SIS model (with reinfection), the formal mathematical calculations drive to a vanishing epidemic threshold even for  $\gamma > 3$  [6].

**A new quantity for the epidemic severity** As quoted previously,  $R_0$  should be modified as it represents only the initial “strength” of the pathogen without considering the underlying topology, e.g. the “long-range” contacts  $pN$ . Indeed, the *degree-based mean-field* provides an average behavior of the pathogen for a plethora of networks since we accounted for  $D, \langle k^2 \rangle$  and not for  $p$  or other more involved measures. Concretely, it drives to completely different scenarios where the epidemic either brutally invade the population or is limited to a small percentage (Figure 5.3). Thus, we introduce a new quantity called *epidemic severity* defined as

$$\Delta R_0(\delta) := \frac{R_0 - R_{c-net}}{\delta} \quad (3.21)$$

where  $\delta := \langle l \rangle$  is the average path length.

In particular, the dependence on the “network effectiveness”  $\frac{1}{\delta}$  captures the fact that as long-range nodes increase the epidemic is favored, since there are allowed the “jumps” into new pools of susceptible.

### 3.3 Order Parameter

According to Equation 3.12, a disease spreads at early times if the average number of contacts  $D := \langle k \rangle$  exceed the *critical average degree*  $D_c$  defined by imposing  $R_0 = \lambda \cdot D = 1$ .

Formally,

$$D_c := \frac{R_{c-net}}{\lambda} \quad (3.22)$$

where the *critical reproduction number*  $R_{c-net}$  is defined in the Equation 3.12. Thus, the exponential growth of the number of cases is recovered for  $D > D_c$ . Moreover, whether the network is not so heterogeneous,  $R_{c-net} \sim 1$ , which becomes exact ( $= 1$ ) for a Poissonian distribution (see Equation 3.2). In general, as for the reported networks (chapter 5), Equation 3.22 yields  $D_c \sim \frac{R_{c-net}\mu}{\beta}$  for  $t \approx 0$ . The Barabási-Albert model is the only exception where  $D_c$  is smaller, due to the high heterogeneity of its underlying degree distribution.

A rough estimate of the daily new cases is  $C(t) \propto R_0^{t/d}$  where  $d$  is the average time an individual remains infected, namely  $d := 1/\mu$ . Generally, since the transmission rate  $\beta$  and the recovery rate  $\mu$  are fixed, the exponential growth occurs for  $D > D_c$ . For  $D \sim D_c$ , the number of total infected  $\pi(t)$  will behave critically, i.e.  $\pi(t) \propto t^\alpha$ , where  $\alpha \in (1, 2)$  for a simply connected (no multiedges or loops) short-range network embedded in dimension 2. More in detail,  $\alpha \sim 2$  for a network resembling a regular lattice in 2 dimensions, since  $C(t) \propto t^2$  is proportional to the covered area of the infection front; while  $\alpha \sim 1$  for a tree or a collection of 1-dimensional chains, as the front spreads linearly as a flame along a fuse, i.e.  $C(t) \propto t$ . For this reason, we would refer to the “fuse-model” as a 1D-grid with  $D$  neighbors per node. Thus, the Overlapping Poissonian small-world network (alias OPSW) of Figure 2.5a is an extension of this model since it allows for a Poissonian distribution of the number of contacts per person [35]. In between these regimes, the specific  $\alpha$  is influenced and shaped by non-pharmaceutical interventions (NPPIs).

Schematically, for a fixed pathogen with  $\lambda = \beta d$  and the rewiring probability  $p$ ,  $R_0 \propto D$  and  $D_c$  characterizes the nature of the epidemics as [35]

- for average number of contacts  $D > D_c$ , the situation starts to resemble a mean-field with the fraction of total cases  $\pi(t) = R(t + d)$ , where the shift in time is due to the fact that the average time of one infected to recover is  $d$  days. In addition, the number of infected assumes a typical bump in the immediate days after the beginning and it is an evident mark of an exponential growth both in the daily new cases  $C(t)$  and the total cases  $\pi(t)$  Figure 5.8b.
- for  $D < D_c$ , the sub-exponential behavior is recovered with the consequence that the final outbreak size is lower than the mean-field one Figure 5.8a.

A proper way to characterize this transition is per the definition of the order parameter [35] as the standard deviation (SD) of the new daily cases  $C(t)$ , after excluding all the days without new cases.

Formally,

$$O := SD(C) = \begin{cases} 0 & \text{if } C(t) = \text{constant} \\ \neq 0 & \text{otherwise.} \end{cases} \quad (3.23)$$

In other words, a linear growth of the total cases  $\pi(t)$  is possible only when the new daily cases are constants, since  $\pi(t) \propto t$ . In most of the curves present in chapter 5, the exponent  $\alpha < 1$ , but still the epidemic develops a “sub-exponential growth” (green curve) which is comparably interesting since it deviates from the mean-field solution (orange curve) (Figure 5.3). For  $D > D_c$ ,  $C(t)$  develops a defined peak which, in turn, produces an enhancement of the SD alongside with an exponential growth of the total cases, similarly as in the mean-field case. The evolution of the epidemic curves at different  $D$  is reported in Figure 5.3. Hence, a strong deviation of SD from zero signals the presence of a nonlinear increase of  $\pi(t)$ .

### Analytical critical degree

In Statistical Mechanics, the dimensionality of a system is crucial to legitimate the mean-field approximation: the Ising Model is well modeled by a mean-field in a dimension  $d \geq 4$  as it captures its phase transition. Similarly, on networks with non-regular topologies, the average degree (if the network is not “scale-free”)  $D$  can set a threshold/scale above which the mean-field solution will be a good approximation of the phenomenon. Moreover, the Equation 3.22 is valid only for early times. Hence, to account for the time evolution, it should be considered  $R(t)$  as defined in Equation 3.24. In turn, this will allow to account for an estimate of the average infected neighbors  $n(t)$ <sup>5</sup> and, therefore, obtain a different  $D_c$  for a Erdős-Rényi and a “fuse” models: as  $n(t)$  increases, also  $D_c$  has to be larger for an exponential growth.

In particular, as the epidemic grows an infected person would have at least one infected neighbor, that is its infector. Hence, we will call *effective reproduction number* the  $R(t)$  defined as [34]

$$R(t) := (D - n(t))\lambda, \quad (3.24)$$

where  $n(t)$  is the average number of not-susceptible neighbors. Other way around, the fraction of susceptible is defined as  $\nu(t) := 1 - n(t)/D$ .

Since the “fuse-model” accounts only for local interactions,  $n(t)$  represents the fraction of susceptible individuals in the neighborhood of the infection front; while for the ER model,  $n(t)$  is the fraction of the entire population. Therefore, a low infectivity ( $\nu(t) \sim 1$ ) implies that for an Erdős-Rényi model,  $n(t) \sim 1$ , since an infected is surely infected to its infector. Still, for a “fuse-model”  $n(t) = (1 - \nu(t))/D$  where  $\nu(t) \sim 1/2$  as, intuitively, only the individuals over the epidemic front remain susceptible and on average are half of the network.

Hence, whenever  $n(t)$  is known, the critical degree  $D_c$  assumes the form

$$D_c = n(t) + \lambda^{-1}. \quad (3.25)$$

In the following section, it is going to be derived  $n(t)$  and, in turn,  $D_c$  for the ER model (see chapter 2) and the tree- or chain-like “fuse model” [35].

### Erdős-Rényi Graph

For a Erdős-Rényi random graph with “rewiring probability”  $p$ , the average degree of contacts is  $D = Np$ . Hence, the number of not susceptible nodes near an infected vertex is

$$n(t) \sim 1 + (D - 1)(1 - \nu(t)) \quad (3.26)$$

where 1 is the past infector of the chosen node added with the remaining neighbors which are infected or recovered [34]. This expression yields  $n(t) \sim 1$  for a low infective epidemic as  $\nu \sim 1$ .

---

<sup>5</sup>This quantity considers both the current and the past infected, i.e. infected and recovered or, with a twisted lettering, the “non-susceptible” individuals.

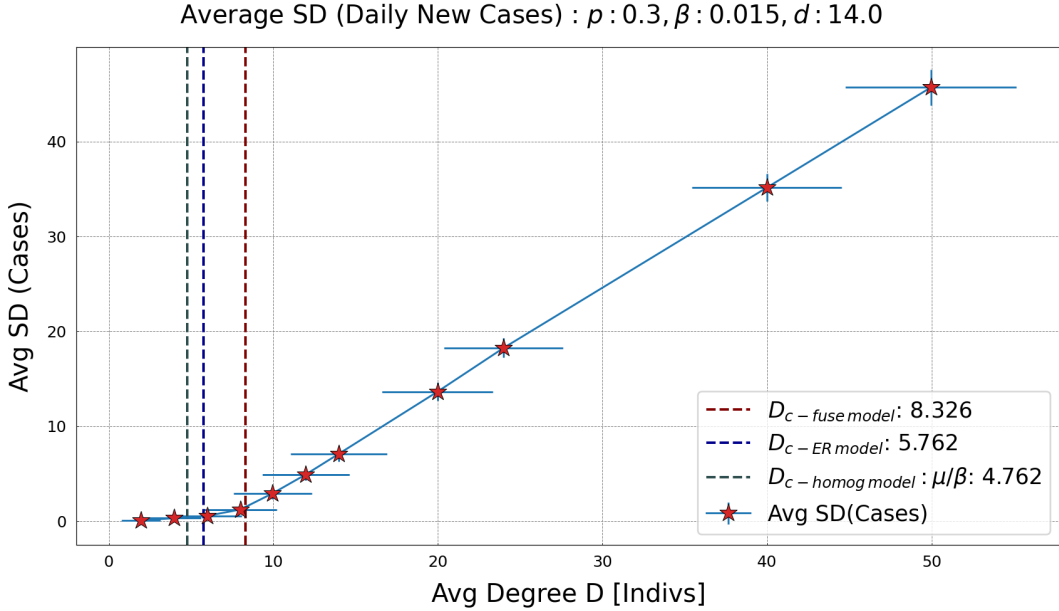


Figure 3.4: In the figure, it is reported the order parameter defined in Equation 3.23 as a function of the average number of contacts. More specifically, it is the average over the simulated 50 trajectories of the standard deviations of the daily new cases. It displays a transition from linear to exponential regimes of a Poissonian-SW Network. Using Equation 3.31,  $D_c \sim 8.3$  is a fair estimate of the average number of contacts for which a burdening outbreak, barely infecting half of the population. We plotted both the order parameter and  $D$  with errorbars.

Inserting the obtained  $n$  in Equation 3.25,

$$D_c^{ER} = 1 + \frac{\lambda^{-1}}{\nu(t)}. \quad (3.27)$$

In this manner,  $D_c^{ER}$  increases as  $\nu(t)$  drops: more contacts are needed to spread a disease if there are less susceptible available. However, for low infection or at the starting of the epidemics  $\nu(t) \sim 1$  and the  $D_c$  is fixed by choosing the biological factor  $\lambda$ .

### The fuse model

A “fuse-model” is a one-dimensional chain of individuals with  $D$  neighbors per node. Therefore, similarly to the Erdős-Rényi case,

$$n(t) \sim 1 + (D - 1)(1 - \nu(t))(1 - p) \quad (3.28)$$

where the fraction of long-range nodes  $p$  has been introduced since the fuse model accounts only for local interactions. Hence, inserting the derived  $n(t)$ ,

$$D_c = 1 + \frac{2\lambda^{-1}}{(1 + p)}. \quad (3.29)$$

where the fraction of susceptible  $\nu(t) \sim 1/2$  on average. Formally, averaging the initial and the final fraction of susceptible,

$$\nu(t_{max}) \sim 1 - \frac{vt_{max} + 0}{2} = 1/2 \quad (3.30)$$

where  $1 = N$  is the (normalized) total population;  $t_{max} := N/v = 1/v$  is the maximum time of the infection;  $v$  the velocity of propagation of the epidemic front. Indeed, the infection roughly propagates as a wave at constant velocity  $v$ . Thus, the “right-part” of the “fuse” is composed by susceptible nodes ( $\nu(t) \sim 1/2$ ), while the “left-part” by the infected or recovered vertexes.

This equation provides the average number of contact below which the mean-field approximation fails, as a function of  $p, \beta, \mu = 1/d$ . On the other hand, a “fuse model” account for a spreading over a segment of  $N$  nodes; while the considered network models are characterized by a circular structure. Hence, even if exploiting the local interactions, the “fuse-model” does provide a good estimate of  $D_c$  only for some networks, e.g. [Figure 5.12a](#). In the other cases, it is expected to overestimate the critical degree since the epidemic is more constrained than in the studied network.

### Mathematical Derivation of the Critical Degree for the *Fuse Model*

In this section, it is going to be obtained the critical degree  $D_c$  [35] for a “fuse-model”: a one-dimensional chain of individuals with  $D$  neighbors per node.

In particular,

$$D_c = 1 + \frac{2\lambda^{-1}}{1+p}. \quad (3.31)$$

The same result may be used for the Overlapping Poissonian Small-World network.

The first step is to introduce an invariant probability function  $\rho(x, t) = f(x - vt)$  that grasps the dynamics of the infection front:  $\rho(x, t)$  is the probability, a node in the  $x$  location is infected at time  $t$ . In particular,  $x$  is the network distance, as the number of in-between nodes from the initial infected node;  $t$  is the time passed in days after disease started infecting and  $v$  is the traveling velocity of the spreading along the  $x$  axis. A pedagogical representation of  $\rho$  could be find in [34]: roughly speaking, it has the shape of a  $\arctan(x - vt)$  where, on the  $x$ -axis, there is the 1d-chain on nodes; while, on the ordinates, the probability  $\rho(x, t) \in [0, 1]$  interval<sup>6</sup>. Furthermore, the center of  $\rho$  coincides with an arbitrary node ( $q$ ), which has  $\rho(q) = 1/2$ .

To estimate  $v$  and  $\rho(x, t)$ , it is taken advantage on  $\rho(x, t+1)$  assuming that  $v$  is such that all the “non-susceptible nodes” are indeed infected, not recovered. Hence, the probability of being infected at a following time  $t+1$  is

$$\rho(x, t+1) = \rho(x, t) + (1 - \nu(t))2D\beta\langle\rho\rangle(x, t)(1 - \rho(x, t)) \quad (3.32)$$

where  $\langle\rho\rangle(x, t)$  is the (local) average probability of being infected at  $(x, t)$  over the adjacent neighbors. In other words, the [Equation 3.32](#) considers the probability of already being infect; alongside with 2 terms:

- $1 - \nu(t)$  and  $1 - \rho$  which are the fraction of infected nodes and the probability of being susceptible;
- $\delta := 2(1 - \nu(t))D\beta$  is the total probability rate of having (at least) a contagion over the  $2(1 - \nu(t))D$  infected neighbors.

For a one-dimensional front, its radius proceed at a  $x = vt$  pace and, defining  $\tau$  as the next infection time, the a ratio of the non-susceptible/susceptible nodes may be approximated as

$$\frac{1 - \nu(t)}{\nu(t)} = \frac{t + \tau}{t} = 1 + \frac{\tau}{t} = 1 + v\tau\mathcal{K}.$$

Moreover, defining  $\tau$  as the time one single node is infected  $v \cdot \tau = 1$  implying that

$$\nu(t) = \frac{1}{2 + \mathcal{K}} = \frac{1}{2}$$

since for a flat “fuse model”  $\mathcal{K} = 0$ .

Similar to the Ricci curvature of a Riemannian manifold, the *discrete graph curvature* measures how the geometry of a pair of neighborhoods deviates from a “flat” case of a grid graph. Such information is related to how information propagates in the neighborhood [36]. The formal definition of *curvature of the front* is  $\mathcal{K} := \pm 1/\mathcal{R}_{front}$  where  $\mathcal{R}_{front}$  is the radius of the fitting circle of the front:  $\mathcal{K} > 0$  for concave case; while  $\mathcal{K} < 0$  if the front surrounds an island of susceptible. For the poissonian small-world network,  $\mathcal{K} = 0$ , since the front is flat. The analogy with the Ricci curvature is a sphere, an iperboloid and a flat plane.

Lastly, the naive expectation is recovered since  $\nu(t) \sim 1/2$ .

<sup>6</sup>The “past” nodes have higher  $\rho$  while the future nodes have diminishing probability of being infected.

Inserting the [Equation 3.32](#) on the invariance condition

$$\frac{\partial \rho}{\partial t} = -\frac{\partial x}{\partial t} \frac{\partial \rho}{\partial x} = -v \frac{\partial \rho}{\partial x}, \quad (3.33)$$

with the further approximation that  $\langle \rho \rangle(x, t) \sim \rho(x, t)$ ,

$$\rho(x, t) = \frac{1}{1 + e^{\delta(\tau x - t)}} \quad (3.34)$$

with  $\delta := 2(1 - \nu(t))D\beta$ . For this solution,  $\rho(vt, t) = \rho(0, 0) = 1/2$  marks the infection front [\[34\]](#).

The average probability of the nodes on the left of the front being infected is

$$\hat{\rho} \sim \frac{1}{\nu(t)D} \int_{-\nu(t)D}^0 dx \rho(x, 0) = 1 + \frac{1}{\delta'} \log\left(\frac{1 + e^{-\delta'}}{2}\right) \sim \frac{1}{2} + \frac{1}{8}\delta' + O(\tau^3) \quad (3.35)$$

where it has been exploited that  $\delta' := \tau\delta\nu(t)D$  and the last expansion as  $\tau \ll 1$  [\[34\]](#). Thus,  $\hat{\rho}$  could also interpreted as the probability of the past infected nodes.

Moreover,  $n$  could be obtained considering the situation where a  $\nu(t)$  nodes are susceptible but the “past” nodes are not and viceversa:  $\nu(t)\hat{\rho}$  or  $(1 - \nu(t))(1 - \hat{\rho})$ .

Formally,

$$n \sim 1 + (D - 1)(\nu(t)\hat{\rho} + (1 - \nu(t))(1 - \hat{\rho})) \sim 1 + (D - 1)\left(\frac{1}{2} - (1 - 2\nu(t))\frac{1}{8}\delta'\right) \quad (3.36)$$

which for a flat infection, where  $\nu(t) \sim 1/2$ , reduces to

$$n = 1 + \frac{1}{2}(D - 1). \quad (3.37)$$

Ultimately, introducing the  $pD$  long-range (“lr”) neighbors; while keeping the infection low,  $n_{lr} \sim 1$ . Since  $n$  is a local estimate, removing the  $n_{lr}$  contribution,

$$n = 1 + \frac{1-p}{2}(D - 1) \quad (3.38)$$

and, therefore,

$$D_c = 1 + \frac{2\lambda^{-1}}{1+p}. \quad (3.39)$$

This estimate express the critical degree, i.e. the average number of contact under which the mean-field approximation fails, as a function of  $p, \beta, \mu = 1/d$ . As a second order approximation in  $\tau$  as been exploited in [Equation 3.35](#), overestimates the number of infected which, in turn, drives to an overestimation of  $D_c$ . Other sources of divergence from the simulated critical degree may be the finite size effects or deviation from  $= 0$ .

# Methodology

$$R_0 : 2.76(0.078) > 1.081(0.094), D_{994} : 13.14(0.37), \text{OnRing} : 1, p : 0.0, \beta : 0.015, d : 14.0$$

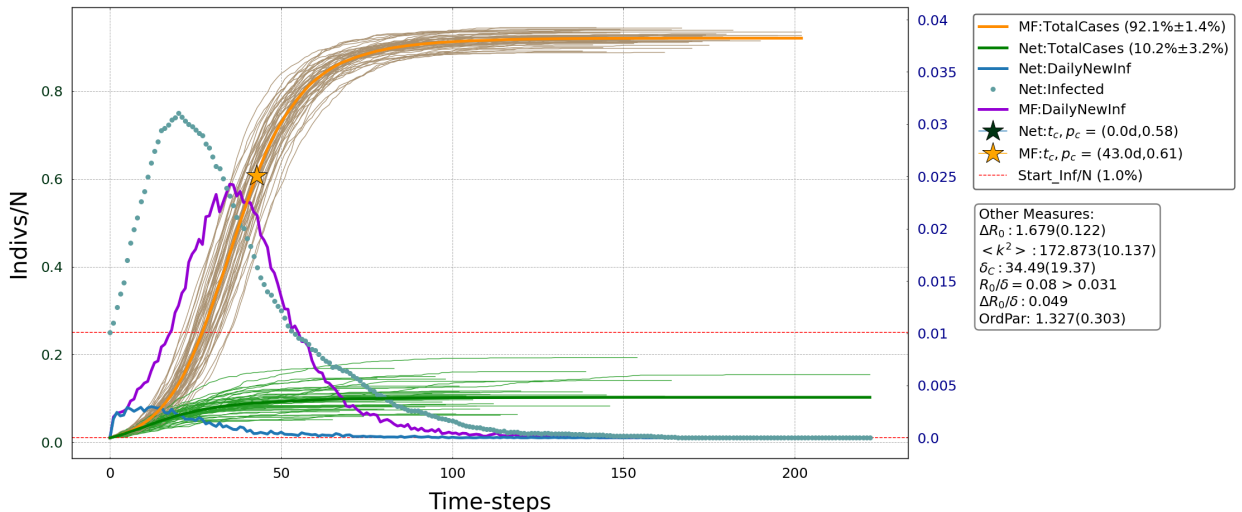


Figure 4.1: A pathogen spreading on a Caveman model with  $D = 14$ . The plot shows some curves for a network spreading: the total cases  $\pi(t)$  (green), the daily new cases  $C(t)$  (blue) and the infected  $i(t)$  (cyan dots). Following the same order, but for a Annealed-Mean-Field Network,  $\pi(t)$  (orange) and  $C(t)$  (violet). Moreover,  $\pi(t)$  are plotted on the left axis; while  $C(t)$  and  $i(t)$  on the right. The two dashed red lines are marking the number of starting infected at the beginning of infection. Every pale-green trajectory could be thought as a realization of the COVID-19 in different parts of the world, as if evolving with these parameters. The big stars mark the estimated maximum for the mean-field approximation as a yellow star (cf. Equation 4.3) and the heterogeneous SIR in green (cf. Equation 4.5). If the level of  $\pi(t_{critical})$  is not reached by the simulated total cases, the star is not shown, as in this case. Still, we reported the estimated  $\pi(t_{critical})$  in the legend.

As reported in section 1.2, the goal of this thesis is to study of the “(quasi-)linear formation” <sup>1</sup> of the total cases  $\pi(t)$  for a SIR evolution on networks, e.g. Figure 4.1. Indeed, as NPIs measures prune the social contacts to avoid the presence of highly connected nodes (super-spreaders or hubs), the “well-mixed assumption” drives to diverging results from the real ones. To appreciate this difference, the evolution on a network and on a “Annealed Mean-Field Network” (see section 2.5) will be reported in the same figure (cf. chapter 2). Moreover, there will be reported the number of infected  $i(t)$  of the SIR ODEs (see Equation 3.5) only for the network spreading, in order to validate whether the epidemic has started, namely  $di/dt > 0$ .

**Infection Scheme** As in [35], we initialized the  $N = 1000$  total individuals as susceptible and we randomly chose  $i(0) = 10$  vertexes as the starting infectors. Moreover, we select an “epidemic”, i.e. by fixing the transmission rate  $\beta$ , and the recovery rate  $\mu$ , alongside with the average number of contacts  $D := \langle k \rangle$  and the fraction of long-range contacts  $p$  in the underlying network.

<sup>1</sup>The “(pseudo)-linear” is recovered for an epidemic where  $C(t) = \text{constant}$  for a reasonable amount of time, e.g. 20 time-steps. In turns, this implies a linear growth of the total cases.

The infection scheme, equal for both the mean-field, via Annealed-Mean-Field Network (AMFN), and the network models, is the following. At every time-step  $t$ , we find all the infected nodes and we infect the susceptible neighbors with probability  $\beta$  per unit time (transmissibility or microscopic spreading rate). After this “infectious” phase, at the same time-step  $t$ , we simulate their recovery with probability rate  $\mu = 1/d$  (recovery rate), where  $d$  are the average days, an individual stays infected.

To implement the stochasticity nature of an epidemic, generate a random number between  $q \in [0, 1]$  and infect the chose susceptible neighbors as  $q \leq \beta$ . Similarly, for the recovery transition with  $\mu$ .

For every  $t$ , collect the infected  $i(t)$ , the “new daily cases”  $C(t)$ <sup>2</sup> alongside with their (normalized) “cumulative sum”  $\pi(t) := \sum_{t' \leq t} C(t')/N$ , as shown in the panels in [section 1.2](#) reporting the real collected data. Proceed iterating the infection chain, until the dynamic comes to a halt, i.e.  $i(\infty) = 0$ , while  $s(\infty) \neq 0, r(\infty) \neq 0$ .

After having collected the daily new cases  $C(t)$  and the total cases  $\pi(t)$  also for the AMFN (see [section 2.5](#)), we produced a plot with the joined  $C(t)$  and  $\pi(t)$  from a specific network, e.g. Watts-Strogatz, and the AMFN. Moreover, there would be a series of plots for each model, since  $D, p, \beta, \mu$  are the free parameters to be chosen. Referring to [Figure 4.1](#), one finds one scale for  $\pi(t)$  (left ordinate axis) and another on the right axis for  $C(t)$  and  $i(t)$ . For the network evolution there are  $\pi(t)$  (solid green line),  $C(t)$  (solid blue line) and  $i(t)$  (azure dots); while, for the AMFN,  $\pi(t)$  (solid orange line) and  $C(t)$  (solid violet line). The starting infected seeds are reported as a straight red dashed horizontal line in the two different scales. Thanks to this method, one gains more insight on the departure of the network spread from the mean-field SIR.

Finally, since [Equation 3.5](#) are not linear, there is a strong dependence on the initial conditions: an epidemic reaching 150 individuals starting with 10 infected could have a different trend than the one that diffuses in 15 nodes with 1 initial contagion.

**Relevant Quantities on Adjacency Matrix Plots** In [Figure 4.2](#), we show the panel devoted to the network properties. Specifically, in the title one finds the number of nodes ( $N$ ), the average degree  $D$ , the fraction of distant nodes  $p$ , the “outsider” nodes  $N_{3-out}$  whose degree  $k > 3D$  and the small-world coefficient defined as

$$SW_c := \frac{\delta}{\ln(N)} \quad (4.1)$$

where the  $\delta = \langle l \rangle$  is the average path length and the  $C$  stands for the fact that the network is connected. For a Barabási-Albert model, we will display the “Ultra Small-World” coefficient:

$$USW_c := \frac{\delta}{\ln(\ln(N))} \quad (4.2)$$

Moreover, we reported a visual representation of the graph (upper left), the contact matrix (upper right) and the degree distribution (lower band). In particular, we will generate it for every studied graph (see [chapter 5](#)).

### Relevant Quantities on SIR Plots.

In the SIR plots, e.g. [Figure 4.3](#), there are reported different quantities which is better to highlight. Hence, from left to right:  $R_0$  and  $R_{c-net}$ ; the average degree  $D$  with at the subscript the overall individuals  $N = 1000$ <sup>3</sup>; the “OnRingLinks”<sup>4</sup> if a Caveman Model is considered; the rewiring probability  $p$  and the epidemic parameters  $\beta, \mu$ . In the legend, there are present the fraction of total cases  $P(t)$  or  $\pi(t)$  of the mean-field and the network evolutions; the daily new cases  $C(t)$  of both the AMFN and the studied network; the estimated maximum ( $\star$ ) for both of the mean-field and the network epidemics; the percentage of the starting infected nodes. Furthermore, the difference  $\Delta R_0 := R_0 - R_{c-net}$ ; the  $\langle k^2 \rangle$ ; the average path length  $\delta_C$ ; the division by the average path length of the previous quantities and the Order Parameter  $SD(C)$ . All the quantities in the rounded brackets are the errors obtained by using the propagation formula (see [section A.4](#)).

<sup>2</sup> $C(t) = N(i(t) - i(t-1) + r(t) - r(t-1))$ . A clear example is the following:  
 $(I(t-1), S(t-1)) \rightarrow (R(t), I(t))$ ,  $C(t) = 1$  as  $i(t) - i(t-1) = 0$  but  $r(t) - r(t-1) = 1/N$ .

<sup>3</sup> $N$  would not be always fixed to  $N = 1000$ . In fact, for a Caveman Model of clique size equal to 33,  $N = 999$ .

<sup>4</sup>We introduced a parameter which accounts for how many links departs from a clique to the next one on a circle, since the cliques are not connected locally in a Caveman Model. Thus,  $OnRingLinks = 1$  means that one family is connected clockwise and anti-clockwise.

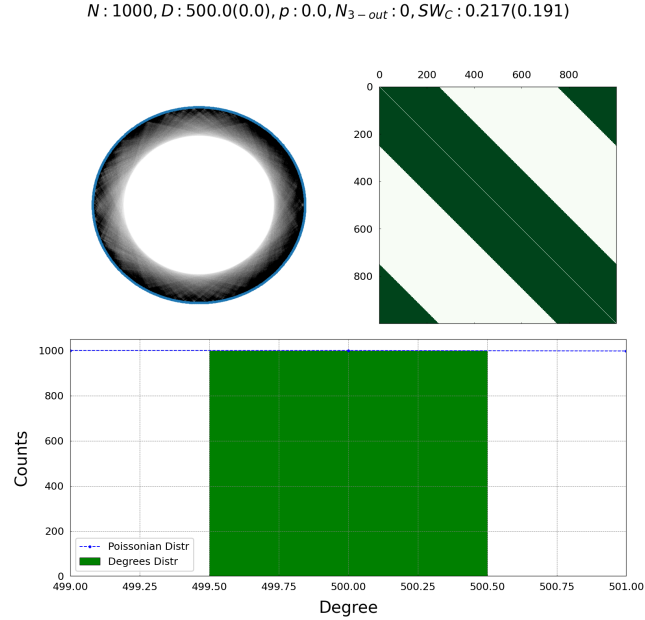


Figure 4.2: Lattice Graph panel for  $D = 500$ . On the upper left, there is the graphical realization of the network, characterized by a  $\vee$  structure of connections for each node. On the upper right, the adjacency matrix; while, on the bottom, the probability distribution  $p_k \cdot N_{3-out}$  and  $SW_C$  are, respectively the number of nodes whose degree is  $k > 3D$  and the coefficient of small-worldliness  $SW_C := \delta / \ln(N)$  where  $\delta$  is the average path length and  $C$  display whether the network is connected. Instead, the size of the largest component is going to be returned.

Formally, we estimated the maximum of the cases  $C(t)$  ( $\star$ ) in two ways. The first, according to [Equation 3.1](#), yields

$$R_0 \cdot s(t) \stackrel{!}{=} 1 \implies \pi(t_{critical}) = 1 - \frac{1}{R_0} \quad (4.3)$$

where the fraction of susceptible  $s(t) = 1 - \pi(t)$ . Since  $\pi(t_{critical})$  is obtained using the mean-field equations, it is valid at every time and only for the AMFN (orange curve). On the other hand, by substituting  $R_0$  with  $R(t)$  into the [Equation 3.12](#),

$$R(t) = (D - n(t))\lambda \stackrel{!}{=} R_{c-net} \quad (4.4)$$

which yields

$$\pi(t_{critical}) = \frac{1}{1-p} \left[ 1 - \frac{R_{c-net}\lambda^{-1}}{D-1} \right] \quad (4.5)$$

where the average number of infected  $n(t) \sim 1 + (D-1)\pi(t)(1-p)$  (cf. [Equation 3.28](#)) with  $p \neq 0$ . By contrast, this estimate is valid only at early times and, as it will be seen, produces a better estimate not in all the scenarios but whenever the diffusion is similar to a mean-field one. Recovered  $\pi(t_{critical})$ , by interpolation with the two nearest total cases  $\pi(t)$ , it could be obtained the intermediate time  $(t_{critical})$ . Hence, the tuple  $(t_{critical}, p_{critical})$  is estimated.

The rationale behind is that after  $t_{critical}$ , the number of cases are going to decrease since  $R_0 \cdot s(t) < R_{c-net}$ , as the susceptible are no more feeding the pathogen which is going to die out.

#### Non trivial dependence of $t_{max}$ and $\sigma(t_{max})$ .

The duration of an average of different epidemics  $t_{max}$  seems to increase as an interplay among the network and the pathogen strength. Indeed,  $t_{max}$  is higher as the pathogen posses a “balanced” diffusion for which a plethora of many trajectory could last more. By contrast, for a weak diffusion, many scenarios accounts for a fast decaying pathogen; while for a stronger one, the outbreak will reach all the population in a short time. See [subsection 5.3.1](#).

$$R_0 : 2.76(0.078) > 1.081(0.094), D_{994} : 13.14(0.37), \text{OnRing} : 1, p : 0.0, \beta : 0.015, d : 14.0$$

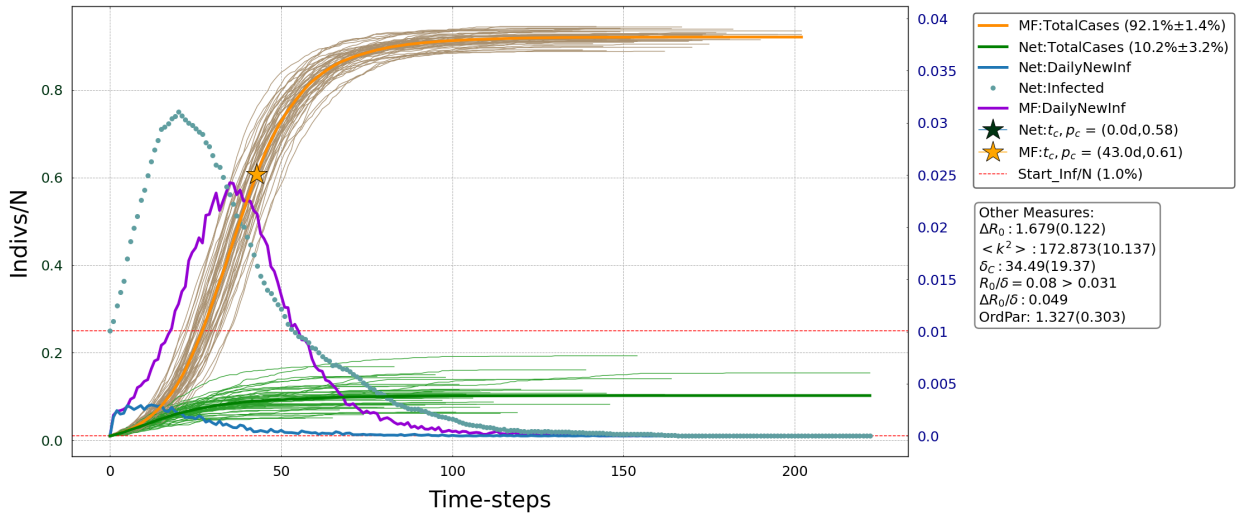


Figure 4.3: A pathogen spreading on a Caveman model with  $D = 14$ . The plot shows some curves for a network: total cases  $\pi(t)$  (green), the daily new cases  $C(t)$  (blue) and the infected  $i(t)$  (cyan dots). Following the same order, but for a Annealed-Mean-Field Network,  $\pi(t)$  (orange) and  $C(t)$  (violet). Moreover,  $\pi(t)$  are plotted on the left axis; while  $C(t)$  and  $i(t)$  on the right. The two dashed red lines are marking the number of starting infected at the beginning of infection. Every pale-green trajectory could be thought as a realization of the COVID-19 in different parts of the world, as if evolving with these parameters.

The variance  $\sigma(t_{max})$  embodies the “degree of randomness” of the trajectories displayed in pale green (network-based) and brown (mean-field): we reported them after the  $\pm$  sign in the legend. Its behavior is similar to the one of  $t_{max}$ . For a in-depth analysis, see subsection 5.3.1 or section 5.1.

### Order Parameter at work

The theoretically estimated average critical degree of contacts  $D_c$  have been obtained by means of three models: homogeneous mean-field approximation, ER-model, fuse-model (cf. Equation 3.25). Note that  $D_{c\text{-homogmodel}} < D_{c\text{-ERmodel}} < D_{c\text{-fusemode}}$ , since it is easier for the epidemic to exponentially grow in a random network than following local paths (fuse model). In addition, the fuse model, in many cases, overestimates  $D_c$ , since it considers an epidemic which is strongly suppressed by moving in a fuse (see Equation 3.3). Other sources of divergence could be the average number of susceptible  $\nu \sim 1/2$  which it is not the case at early times. Thus, instead of an exact prediction, the estimated  $D_c$ s allow to put an upper and a lower bound on the real  $D_c$  of the studied networks. Indeed, the ER case provides a good comparison with an homogeneous approximation, as for networks with a large fraction  $p$  of distant nodes; while the “fuse model” is on the other extrema where the nodes strongly overlaps only locally, i.e. the regular lattice case reported in section 5.1.

Ultimately, the difference of the Figure 3.4 with Figure 3.3 is that, even if similar in shape, the former represents the evolution of the order parameter  $SD(C)$  driven by the average number of contact  $D$ . Meanwhile, the second the final infected size  $i(t_{max})$  as guided by the transmissibility  $\beta$ . A possible improvement should be to consider a plot  $i(t_{max})$  dependent by  $D$ , which is expected to behave as Figure 3.3.

### Parameters Discussion

According to [21] (2021), the most relevant studies <sup>5</sup> on social contact patterns report 2 – 5 average contacts per day during the lockdown, i.e. nearly the household size. This estimate is, roughly, lower than the pre-COVID-19 ones of 7 – 29 average contacts per day. On the other hand, Mossong et Al. ([24]) (2008), based on 8 European states, reported a pre-COVID-19 average of 13 contacts per day, while Leung et Al. [20] (2017) find an average per day contacts of 8 individuals for the habitants of Hong Kong. The purpose of this thesis is to be grounded on real estimates. Thus, the main plots are going to be focused on the  $D < 30$  regime, especially on  $D = 6, 11, 14, 24$ . Little room is going to be left for  $D > 30$  as it can be the case for leisure activities, e.g. exhibitions or discotheques. Since COVID-19 spreads over face-to-face interactions, the latter case is crucial for

<sup>5</sup>These works are extracted from PubMed, Medline, Embase and Google Scholar

the re-opening of the crowded activities.

For the Watts-Strogatz model, the fraction  $p$  is defined as the fraction of edges that connects two nodes at random, i.e. distant. In addition, these far connections are obtained by “rewiring” the existing local edge. Therefore the node degree is preserved. As a concrete example, for a network with  $D = 3, p = 0.3, N = 1000$ , the number of long-range interactions are  $N_{lr} = 900$ . We generated the networks according to this rewiring scheme. On the other hand, right after the severe lock-down only some classes of individuals could connect to distant nodes, e.g. industrial worker. This choice was made upon the need of their services, rather than its contacts. Thus,  $p'$  would be defined as the fraction of *distant nodes*, which an individual interacts with. A concrete implication is that, primary, the long-range interactions will be smaller, e.g.  $0.3 * 100 = 300$  distant contacts. Secondly, for any topology of social network, the 300 edges will be rewired into short-cuts of the graph. The relationship among  $p$  and  $p'$  is,  $p = p' \cdot D$ . Therefore, the epidemic curves for  $p$  are higher than the one for  $p'$ , although one case could be recovered from the other by a rescaling.

For the Caveman Model, we chose families of household size 3 according to [15] and the average number of contacts  $D = 8$  for the comparison with the minimum  $D$  for all the reported networks.

The epidemic parameters we choose as the transmissibility  $\beta = 0.015$  ([35]) and the average days of recovery  $d = 14 \text{ days}$  ([14]). Then, in order to capture different scenarios,  $\beta = 0.1$  or  $d = 4 \text{ days}$  while preserving the other parameters, e.g.  $D, \dots$ . In particular,  $\beta = 0.1$  embodies a stronger epidemic; while  $d = 4 \text{ days}$  the introduction of Pharmaceutical Measures, e.g. vaccines. In particular,  $d = 4 \text{ days}$  days are comparable with the recovery time of a generic flu. Hopefully, this could be the case after a strong vaccination campaign. Since the SIR model does not distinguish among asymptomatic or symptomatic,  $d = 4 \text{ days}$  would characterize both an asymptomatic and an hospitalized infected.

Lastly,  $\beta$  and  $\mu = d^{-1}$  (see Equation A.4 for measure units) depends on many factor and especially on the studied population. Therefore, to have a broad inspection of the capabilities of a network topology it is worth considering different combinations of  $\beta$  and  $\mu$ .

# Results

In the following sections, after a discussion on the *basic reproduction number*  $R_0$ , we will analyze the *epidemic severity* to account for the burdening of a pathogen within a population. Subsequently, we will display the evolution of a disease (see [section 3.2](#)) on different graphs (see [chapter 2](#)). In particular, we generated one version of each network with local connections, namely with  $p = 0$ , and a second one with long-range interactions, i.e.  $p = 0.3$ . Thus, we simulated the COVID-19 spreading, by fixing  $\beta = 0.015$  and  $d = 14$  [35]. In addition, we will obtain two scenarios by choosing, one at a time, the transmissibility  $\beta = 0.1$  and the recovery days  $d = 4$ . The average contacts  $D$  and the distant fraction of nodes  $p$  will be drawn from the COVID-19 curves. Furthermore, we will analyze the behavior of the order parameter  $SD(C)$  (see [section 3.3](#)) for a Poissonian Small-World network and the Barabási-Albert model. Ultimately, we will compare the different evolutions of the pathogens, in order to understand the interplay among the disease and the underlying social network.

The main result will be that the Caveman model is the best suited topology in constraining the diffusion among the studied graphs. By contrast, for a pathogen with more transmissibility ( $\beta = 0.1$ ) a large fraction of the population will still be infected. Thus, only major restrictions could be effective, e.g. forced quarantines. The other networks have less control on the disease since they are not made of clusters. More precisely, we organized the nodes on a circle and we wire them with a defined scheme. In turn, the latter procedure generate a  $\vee$  structure which strongly overlaps as  $D$  increases and, thus, enhances the epidemic severity. In addition, we will order the networks based on the final outbreak size  $\pi_{max}$  at  $p = 0$ : regular Watts-Strogatz ([section 5.1](#)), Overlapping Poissonian Small-World (O-PSW) model ([subsection 5.3.1](#)) and a Barabási-Albert model ([section 5.5](#)). For  $p = 0.3$ , the result remains the same.

For a practical implementation, we generated the networks with  $N = 1000$  nodes, 10 starting infected individuals ( $i(t = 0) = 10$ ) while zero daily new infected ( $C(t = 0) = 0$ ). Then, we performed the simulation over the Google Colab CPUs of [22]. Lastly, before facing the following parts, we suggest to firstly dive into [chapter 4](#) for a more general discussion on the introduced quantities and behaviors.

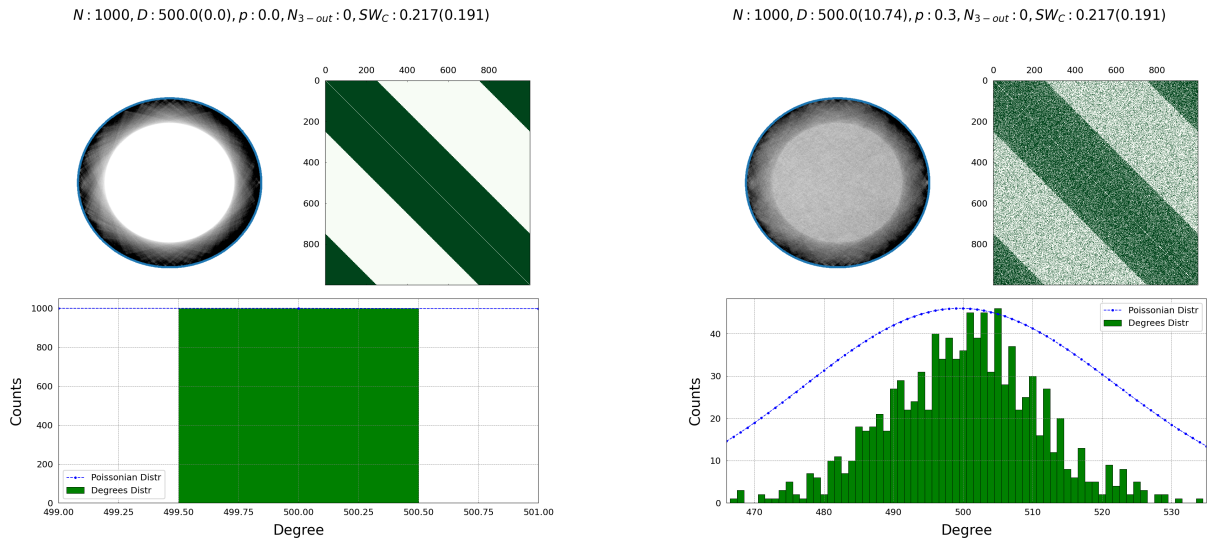
## 5.1 The Basic Reproduction Number

The *basic reproduction number*  $R_0$  is defined as the number of secondary cases at the beginning of the epidemic. Thus, the goal of this section is to test whether  $R_0$  can account also for the “epidemic strength”, i.e. the total cases  $\pi_{max}$ , among different network models. We will recover that it is not suited for this scope, since different evolutions share the same  $R_0$ . Rather,  $\pi_{max}$  is better described by the *epidemic severity*

$$\Delta R_0(\delta) := \frac{R_0 - R_{c-net}}{\delta} \tag{5.1}$$

where  $1/\delta$  is a kind of “network efficiency”: a low value of the average path length  $\delta$  drives to a higher spreading of a pathogen.

The work-flow is the following. We generated a fully-connected graph using a “Watts-Strogatz” (WS) algorithm with  $D = 999, p = 0$ . This model is, thus, called “Regular Lattice Graph”. Then, the core idea was to fix  $R_0$  and visualize how the epidemic curves changed by varying the transmissibility  $\beta$  and  $D$ . In particular, we fixed



(a) Lattice Graph panel for  $D = 500$ : a realization of the graph (upper left), adjacency matrix (upper right), degree distribution (lower band). The node (thin azure border) are connected among the neighbors via  $D = 500$  edges (black annulus). The white inner circle represent to missing of short-cut connections.

(b) Regular graph with an average number of contacts  $D = 500$  and  $p = 0.3$ . The shadowed center of the graphical representation (upper left) signals the presence of shortcuts connecting distant nodes.

Figure 5.1: Regular Lattice Network for average contacts  $D = 500$ . We show on the upper left the graphical representation of the network; on the upper right its adjacency matrix and on the lower part the degree distribution (see chapter 4)

the recovery rate  $\mu = 1/d$  and, then, we divided the average number of contacts  $D$  while doubling  $\beta$ . Formally,

$$R_0 = \text{constant} = \frac{D}{q} \cdot \frac{\beta q}{\mu} \quad (5.2)$$

where  $q$  goes from 1 to the maximum power of 2 s.t.  $D/q > 1$ . Hence,  $\mu$  fixes the value of the *basic reproduction number*  $R_0$  since  $R_0 = \text{constant}/\mu$ . The resulting progression is

$D \in [999, 500, 124, 62, 30, 14, 6, 2]$  where, since the WS algorithm works only with even  $D$ , we, arbitrarily, rounded all the odd  $D$  to the lowest (even) integer. Furthermore, we also simulated the epidemics on a Watts-Strogatz graph with short-cut probability  $p = 0.3$  (called “Long-Range WS”) in Figure 5.1. The network panel in Figure 5.1 shows a WS network with  $D = 500$  for both  $p = 0$  and  $p = 0.3$ .

For a rough representation, every node connects with its neighboring vertexes producing a  $\vee$  structure of edges. The overlap among the  $\vee$ 's increases as  $D$  is enhanced (see Figure 5.1). In this way, the pathogen is constrained to move locally, yielding a limited number of new daily cases  $C(t)$  (blue curve) and, in turn, total cases  $\pi(t)$  (green one).

Finally, since the transmissibility  $\beta$  and the average number of contacts  $D$  are arranged in a peculiar way, we do not report the Order Parameter  $SD(C)$ .

## SIR spreading over a Regular Lattice Graph

In this subsection, we will display the SIR curves for a local ( $p = 0$ ) lattice graph.

As a starting point, the Figure 5.2 displays a scenario where the pathogen could spread on the network, namely the *basic reproduction number*  $R_0 > R_{c-\text{net}}$ . Nevertheless, its diffusion remains limited to a much smaller fraction of the population (4.3% of the total population) than in the Annealed-Mean-Field Network (AMFN) case. In fact, the epidemic is just spreading on a 1D lattice, since  $D = 2$ , where only nearest neighbors are connected as in a fuse with the identified extrema. On the other hand, the mean-field SIR infects random nodes on the fuse. Thus, the stochasticity of an epidemic of an AMFN is *slightly* larger than the network one, since

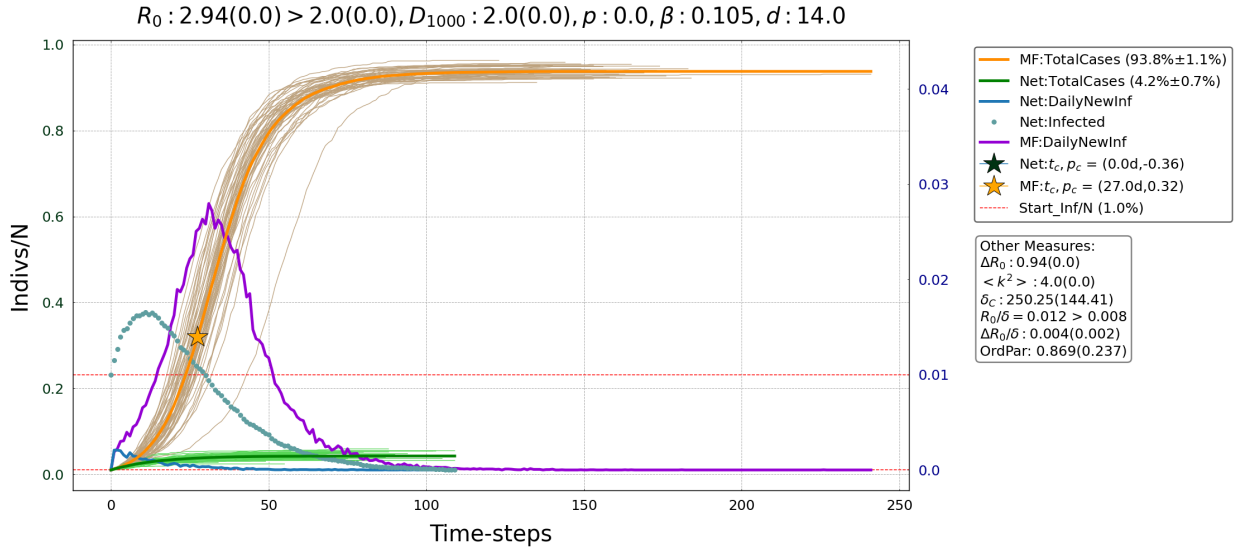


Figure 5.2: Network SIR model (green) benchmarked with the Annealed-Mean-Field Network (orange). Since  $R_0 > R_{c\text{-net}}$  (Equation 4.4) the pathogen could increase the fraction of infected  $i(t)$  (azure dots). On the other hand, since the network is weakly connected, the total cases  $\pi(t)$  remains limited.

$D$  is low. Thus, the increasing value of the infected  $i(t)$  (azure dots) implies that the epidemic has started but the fuse model is strongly containing the pathogen.

Secondly, it is worths defining the final fraction of total cases as

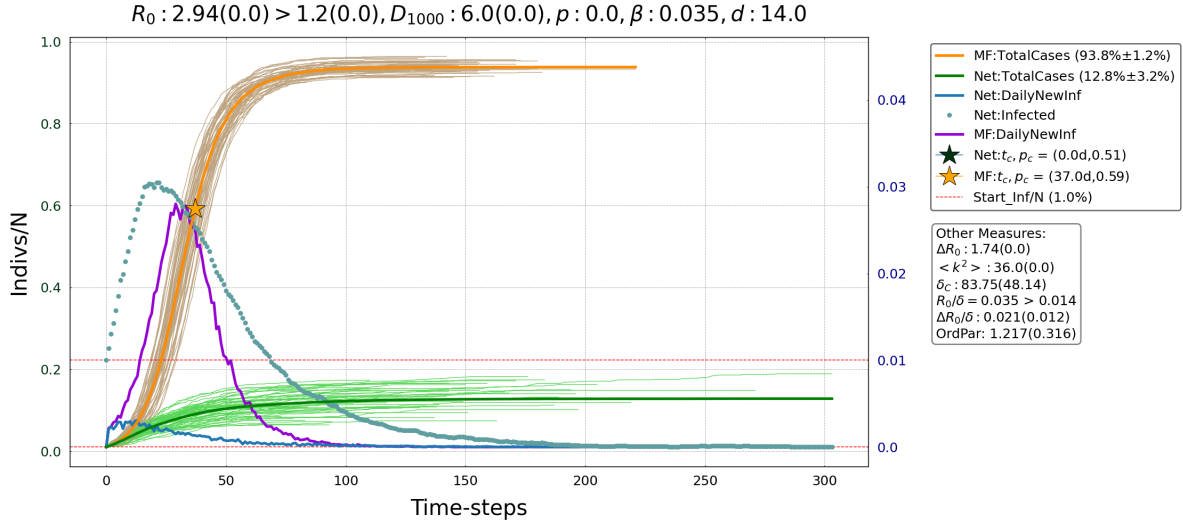
$$\pi_{max} := \pi(t_{max}) \quad (5.3)$$

where  $t_{max}$  is time at the end of the infection, i.e. when the fraction of infected individuals vanishes ( $i(t) = 0$ ). Therefore, by fixing  $R_0 \sim 2.94$  as in Figure 5.3, the  $\pi_{max}$  grows as  $D$  increases. In addition, Equation 3.12 implies that the *critical reproduction number*  $R_{c\text{-net}} = (1 - D^{-1})^{-1}$  decreases when  $D$  increases. As expected,  $R_{c\text{-net}}$  is more likely to be overtaken when a regular lattice has more neighbors.

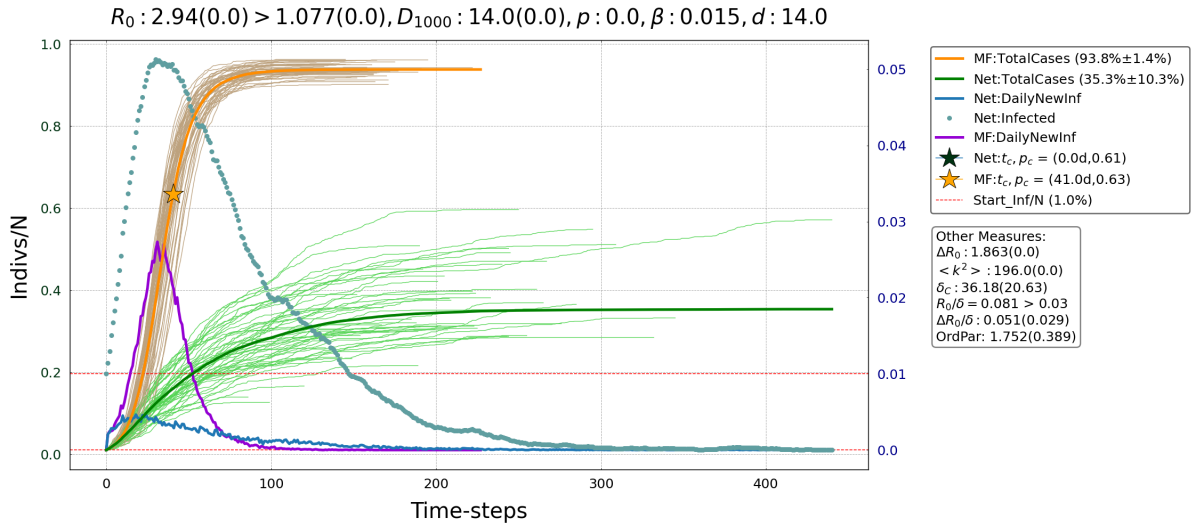
Moreover, Figure 5.3 displays a the (pseudo-)linearity regime for  $D = 6$ . As expected, the final outbreak size is increased:  $\pi_{max}$  is around 3 times higher than the  $D = 2$  case. In addition  $D = 6$ , is slightly above the upper bound of 2 – 5 lockdown contacts per person [21]. Hence, this could be the evolution of a small village with light stay-at-home orders.

By continuing enhancing  $D$ , the network becomes more tangled, due to the increasing overlapping among the neighborhoods. Thus, the epidemic diffuses more rapidly showing that the  $R_0$  is informative only to early times. Rather,  $\Delta R_0(\delta)$  seems a more precise quantity to account for the epidemic severity, since it augments as  $D$  increases (cf. Figure 5.3b).

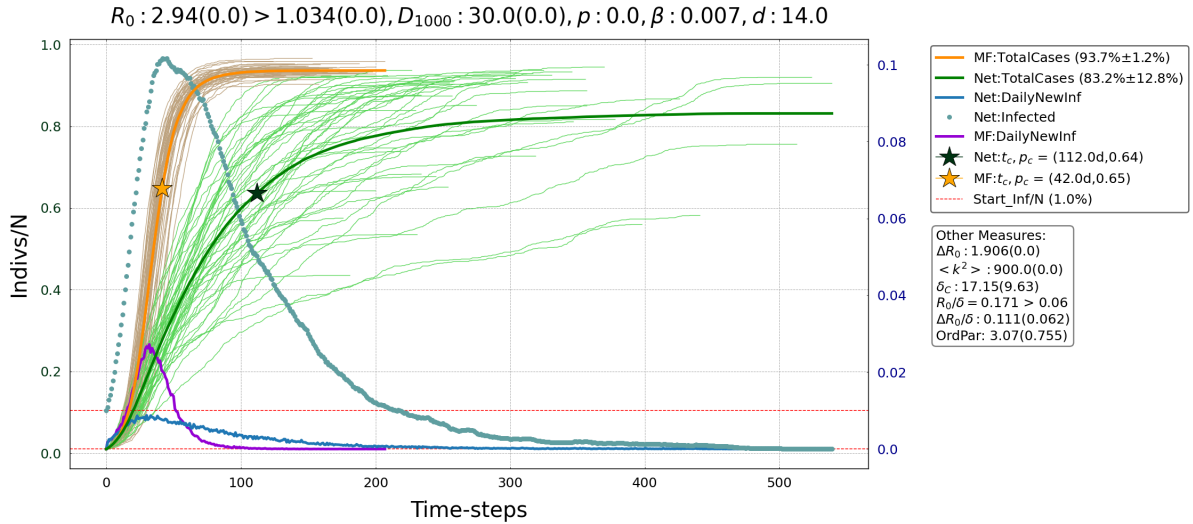
Finally, using Equation 4.5, the estimated maximum of the infected nodes  $i(t)$  (green star) overestimates the real maximum of the heterogeneous SIR evolution (cf. Figure 5.3c). To obtain the Equation 4.5, we made the assumptions that the Equation 4.4 and Equation 3.28 hold at every time. The former takes into consideration only quantities at early times. Thus, this deviation was somehow to be expected. The latter seems a fair approximation at every time. A possible solution could be to refine the *critical reproduction number*  $R_{c\text{-net}}$ . In fact, if  $R_{c\text{-net}}$  increases, then, the  $\pi(t_{critical})$  diminishes. The prediction worsens even more when the long-range wiring probability  $p$  is different from zero (see Figure 5.1). Instead, the maximum value predicted for every mean-field evolution (orange curve) is correct as it was obtained directly from the ODEs Equation 3.1 (see chapter 4).



(a) Regular Lattice with  $D = 6$  and  $\beta = 0.036$ . This evolution displays a remarkable (pseudo-)linearity in the total cases  $\pi(t)$  (green curve) and a total outbreak size nearly 3 times higher than the one reported in Figure 5.2. Ultimately,  $D = 6$ , [15], could represent the evolution of a small village with light stay-at-home orders.



(b) Regular Lattice with  $D = 14$ . Linearity is lost.  $\Delta R_0(\delta)$  increases while  $R_0$  remains the same. The introduction of  $1/\delta$  enforces that for a network with low average path length the pathogen can spread more easily than in graph with higher path length.



(c) Regular Lattice with  $D = 30$ . The estimated maximum of  $i(t)$  (green star) is overestimated; while the maximum for a mean-field is correct (yellow star).

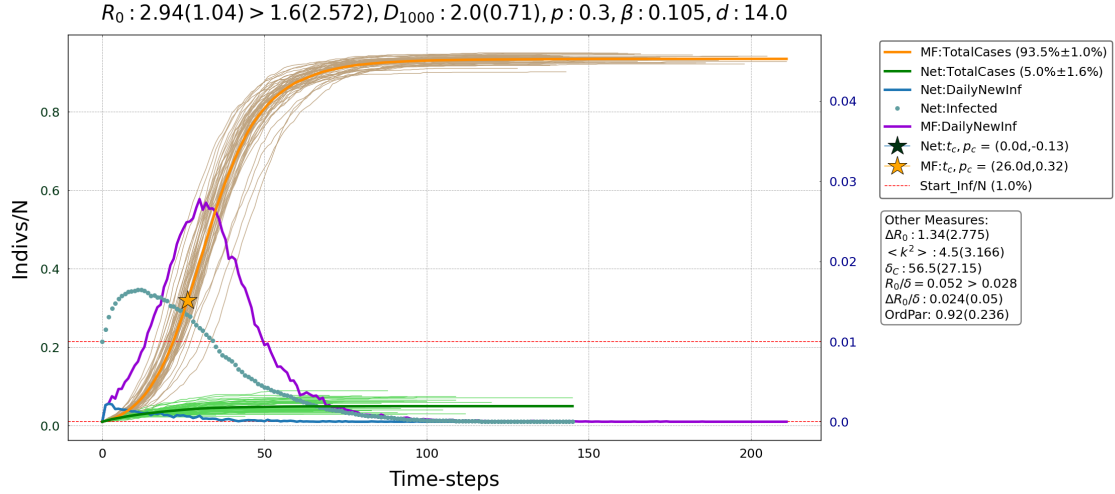
Figure 5.3: The spreading curves over a regular lattice as  $D$  increases. The classical  $R_0$  remains constant, while the *epidemic severity*  $\Delta R_0(\delta)$  (cf. Equation 3.2) varies.

### Long-Range Watts-Strogatz model

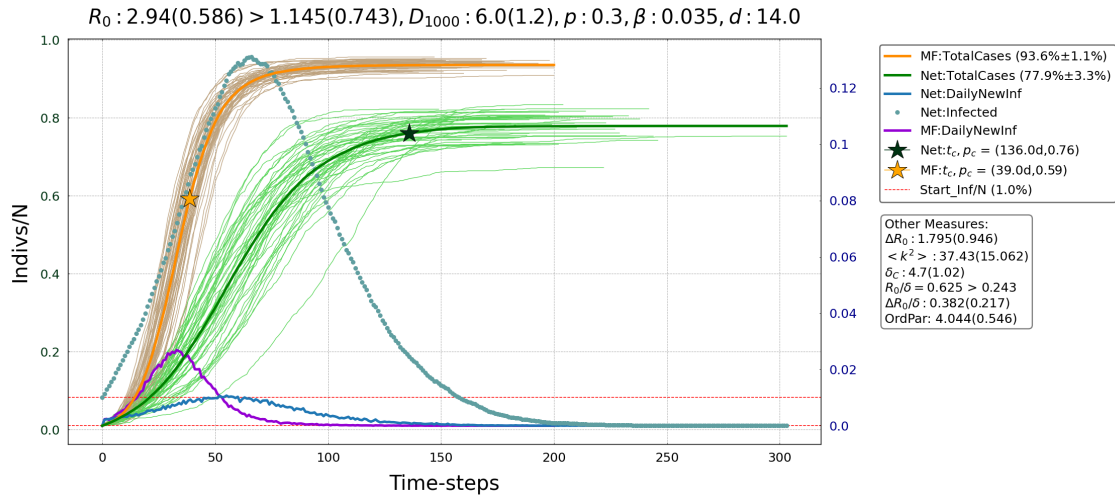
As the probability of connecting to distant nodes is increased, i.e.  $p = 0.3$ , the “Long-Range” Watts-Strogatz model starts to resemble a mean-field network where all the nodes are connected at random (see [Figure 5.1b](#)). Therefore, the total cases at the end of the epidemic will grow. The SIR spreading for  $D = 6$  ([Figure 5.4b](#)) shows an increasing final fraction of total cases  $\pi_{max}|_{p=0.3} \sim 72\%$  against the  $\pi_{max}|_{p=0} \sim 12\%$  of the regular case in [Figure 5.3a](#). This is, somehow, the aim from the [section 1.2](#): the network really plays a role in constraining the disease, yielding a linear growth of the total infected even for big  $R_0$  ( $R_0 = 2.94$ ) but a small  $D = 6$  comparable with the number of contacts in a light lockdown [[21](#)].

In [chapter 4](#), we briefly indicated that  $t_{max}$  and the variance  $\sigma(t_{max})$  increase as the pathogen has a “balanced diffusion”. In particular, in [Figure 5.4](#), the  $\pi_{max}$  of the  $D = 6$  evolution displays an intermediate value between the  $D = 14$  and  $D = 2$  cases. Hence,  $t_{max}$  and  $\sigma(t_{max})$  are higher for the  $D = 6$  than in the other evolutions. A rough explanation comes from the upper bound of population size  $N$  and the lower one as an epidemic ends whenever  $i(t) = 0$ . In fact, those constraints seems to even out the trajectories, producing a lower  $t_{max}$  and  $\sigma(t_{max})$ .

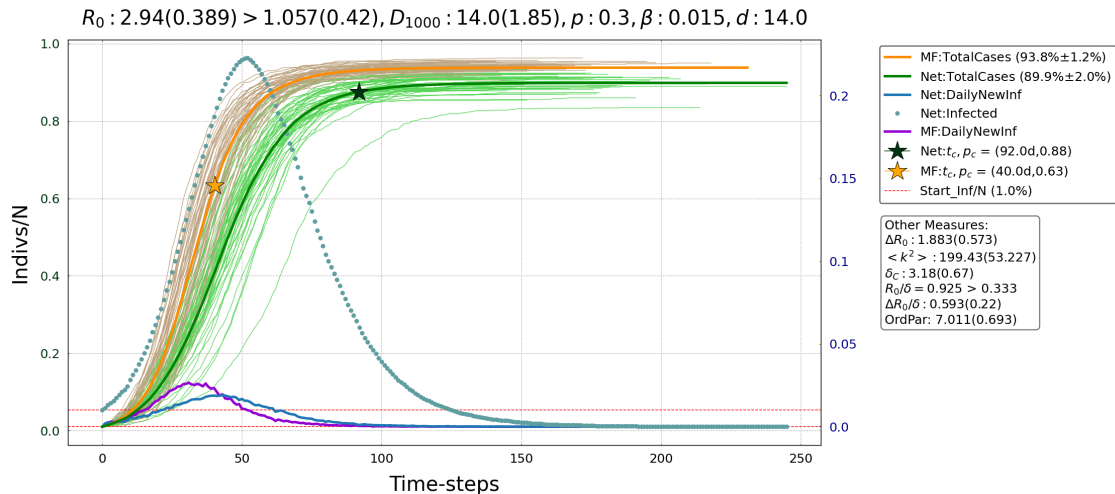
Since for Long-Range WS the spreading is enhanced, the take home message is that local wiring, and eventually social distancing, is effective. In turn, this could drive to a remarkable suppression of fraction of total cases  $\pi(t)$  if  $D$  is small enough as seen in [Figure 5.2](#) or [Figure 5.3a](#).



(a) Remarkably linear regime over barely the entire evolution. As the network accounts for small  $D = 2$  and low rewiring  $p$ , the epidemic is flatten similarly to the  $p = 0$  case: [Figure 5.2](#)



(b) The (quasi-)linearity is lost and the exponential growth is recovered. By contrast to the  $D = 2$  case, here the enhancement with respect to [Figure 5.3a](#) is more pronounced: the total cases are barely 6 times the “regular” ones. As quoted before, the estimated maximum (green star) worsens as  $p \neq 0$ . Moreover, only  $\Delta R_0(\delta)$  grasps the epidemic severity with respect [Figure 5.3a](#). Indeed, the two  $R_0$ ’s are equals; while the differences  $R_0 - R_{c\text{-net}}$  could suggest that the  $p = 0$  case would be stronger than the current case. Nevertheless, it is the opposite as captured by  $\Delta R_0(\delta)$ . Finally,  $t_{max}$  and  $\sigma(t_{max})$  are higher than the  $D = 2$  and  $D = 14$  scenarios.



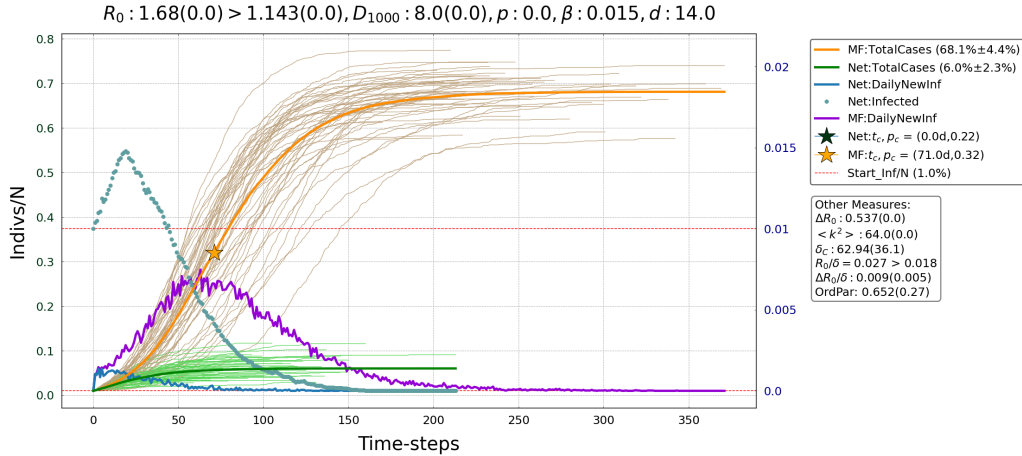
(c) Watts-Strogatz model for  $D = 14$  and  $p = 0.3$ . As quoted before, the estimated maximum (green star) from [Equation 4.5](#) worsens as  $p = 0.3$ .

Figure 5.4: Watts-Strogatz model spreading curves for  $D = 6$  and  $D = 14$  and  $p = 0.3$ .

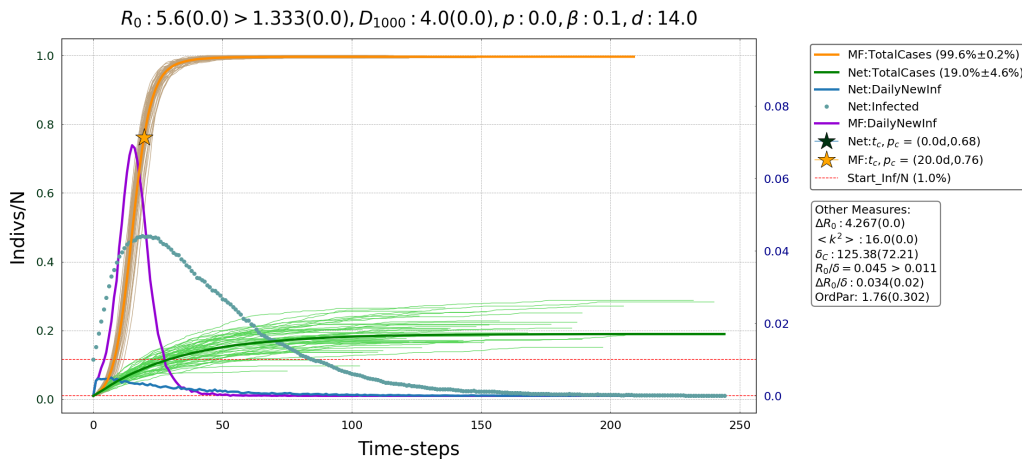
## 5.2 Watts-Strogatz Model

In the following section, we will report the epidemic curves for the COVID-19 epidemic parameters ( $\beta = 0.015, d = 14$ ); alongside with the evolution of a new pathogen, namely  $\beta = 0.1$  and the COVID-19 treated with pharmaceutical interventions for  $\beta = 0.015, d = 4$ . We will pick the same Regular Lattice ( $p = 0.0$ ) of the previous section. Then, we will add the fraction of distant nodes via  $p = 0.3$ . These curves will be used as a benchmark for the future models.

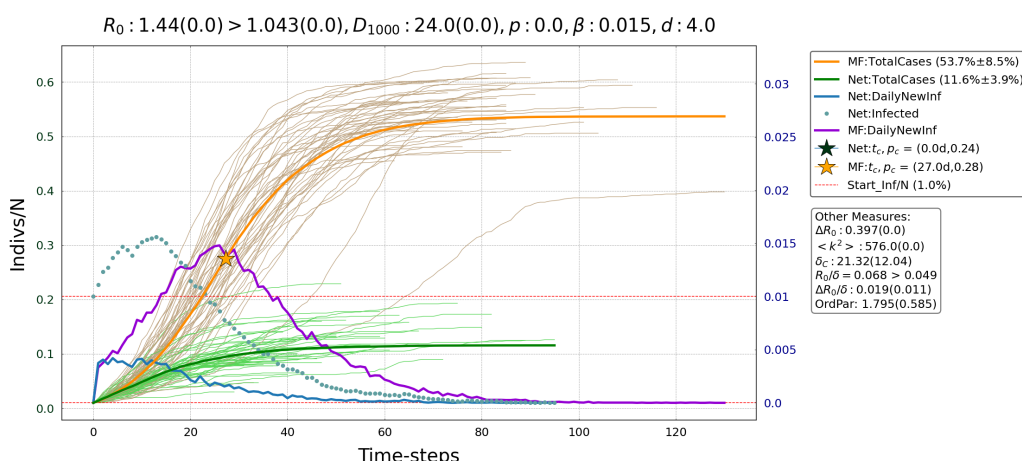
In the following figures, we will recover that the fraction of total cases  $\pi(t)$  will be enhanced as  $D$ , the transmissibility  $\beta$  or the fraction of the distant interactions  $p$  increase (Figure 5.5a, Figure 5.5b, Figure 5.6a). By contrast, we will report that  $\pi(t)$  decreases when the pharmaceutical interventions drives to a faster recovery of the infected, namely  $d = 4$  (Figure 5.5c).



(a) SIR diffusion for  $D = 8$ . As expected, the total cases  $\pi(t)$  for  $D = 14$  (Figure 5.3b) are higher than the current ones. On the other hand, for  $D < 8$ , the epidemic curves shows less contagious while they shares the same shape of this evolution, e.g. Figure 5.2.



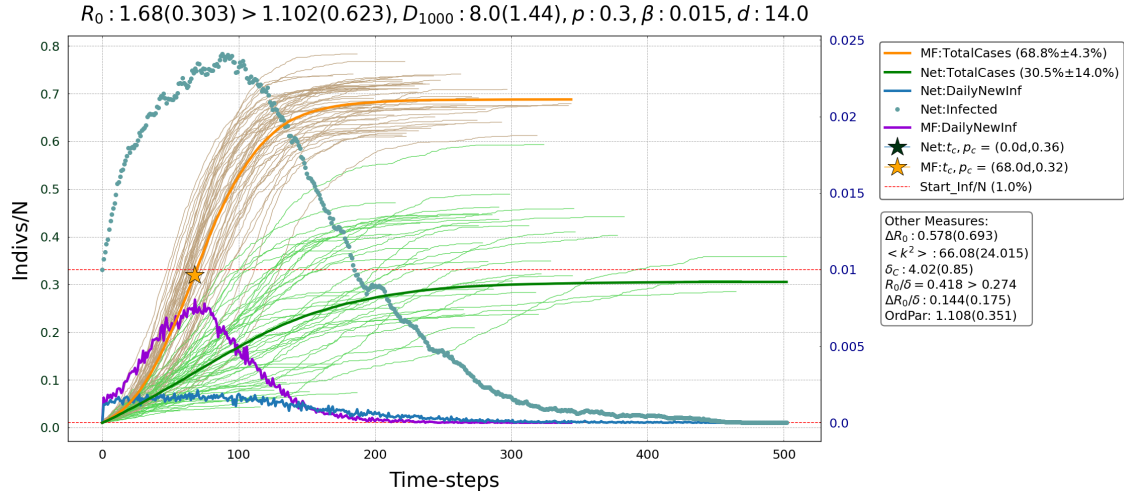
(b) A new pathogen with a higher transmissibility  $\beta = 0.1$  than COVID-19. Indeed, the final outbreak size  $\pi_{max}$  is higher than the COVID-19 one of Figure 5.5a even if the average contacts are halved.



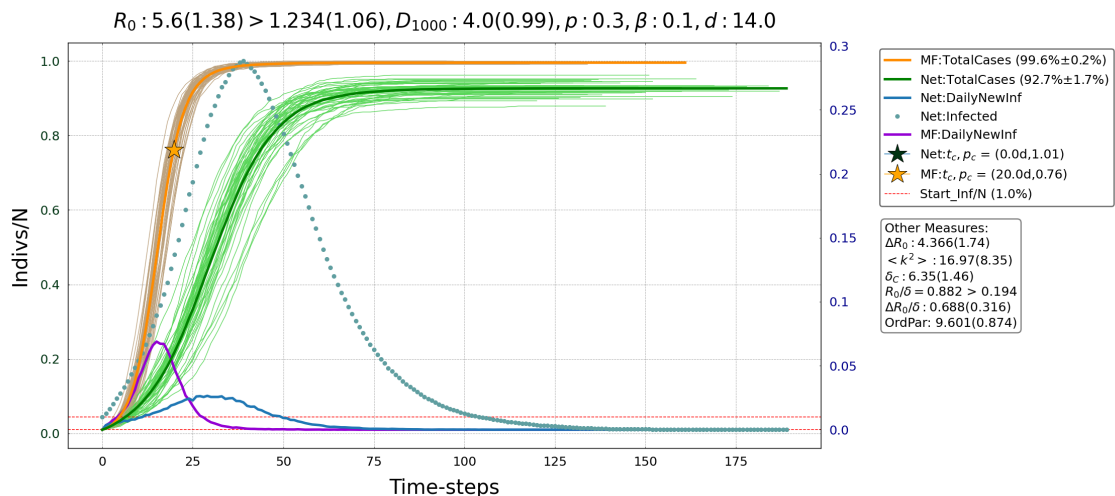
(c) Regular Lattice graph evolution of COVID-19 with pharmaceutical interventions, namely the recovery time is  $d = 4$ . We noted a remarkable control on the pathogen, since the total outbreak size remains small even though  $D = 24$ .

Figure 5.5: Regular Watts-Strogatz model spreading curves for  $D = 4, 8, 24$  while, once at a time,  $\beta = 0.1, d = 4$ . The  $D = 14$  case was reported in Figure 5.3b.

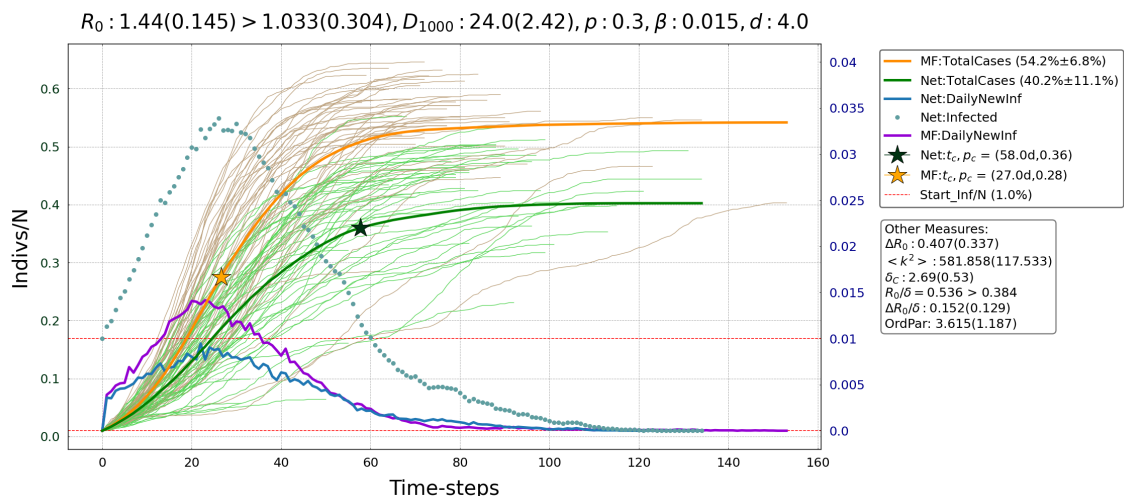
### 5.2.1 Long-Range Watts Strogatz



(a) SIR diffusion for  $D = 8$  with long-range interactions. Ultimately, the  $\pi_{max}$  is higher than the Figure 5.5a but lower than the  $D = 14$  case.



(b) A new pathogen with a higher transmissibility  $\beta = 0.1$  than COVID-19. Indeed, the final outbreak size  $\pi_{max}$  is higher than the COVID-19 one of Figure 5.6a. The spreading on network resembles the mean-field model (AMFN) since the disease is sustained either by  $R_0 \sim 5.6$  and by the long-range connections ( $p \cdot N \sim 300$ ).



(c) Regular Lattice graph evolution of COVID-19 with pharmaceutical interventions.

Figure 5.6: Long-Range Watts-Strogatz model with  $p = 0.3$ . We reported the spreading curves for  $D = 8, 4, 24$  while, once at a time,  $\beta = 0.015, 0.1$  and  $d = 14, 4$ . The case where  $D = 14$  was reported in Figure 5.4c. By means of Equation 4.5, the estimated maximum of  $i(t)$  (green star) is overestimated; while the maximum for a mean-field is correct (yellow star). In addition, the former worsens as  $p = 0.3$ .

### 5.3 Poissonian Small-World Network

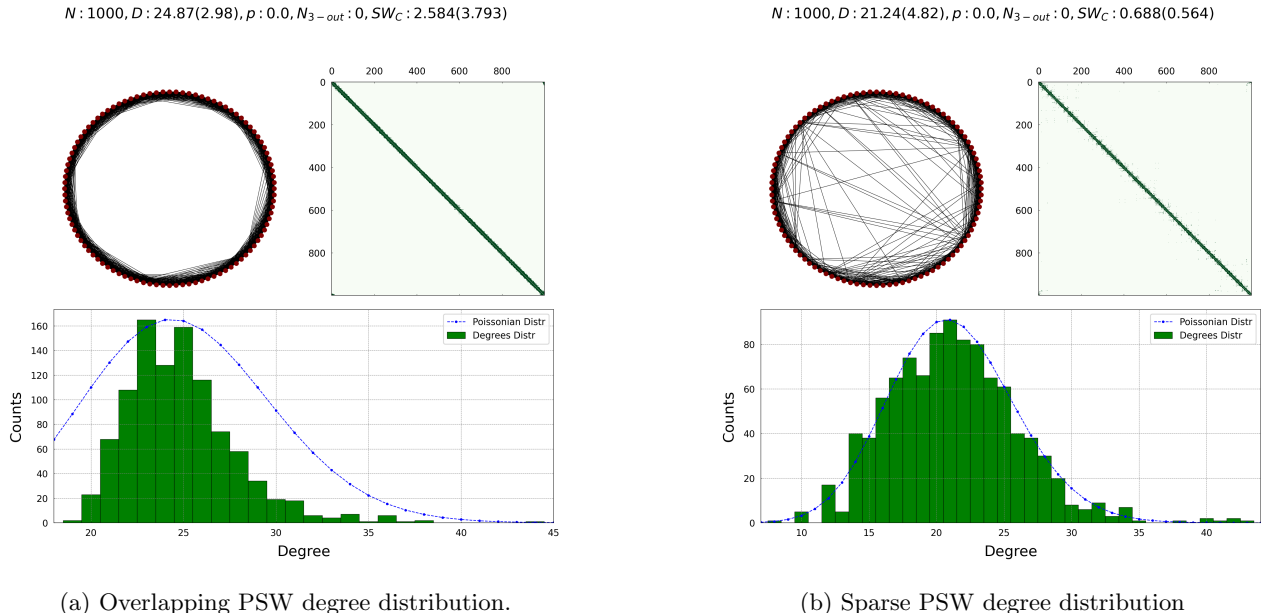


Figure 5.7: Two realization of PSW network: “Overlapping” and “Sparse” models. The graph realizations (upper left) have  $N = 100$  for a better visualization, while we fixed  $N = 1000$  the adjacency matrix (upper right) and the degree distribution (lower band). We do not report the realizations with  $p = 0.3$ , since it could be straightforwardly obtained by the superimposing some long-range links to the current cases as in Figure 5.1b.

The NPIs measures have forced the individuals to lower their number of contacts, i.e. 2 – 5 contacts [21], in order to avoid the hubs formation, whose role is to produce a vanishing epidemic threshold (see chapter 3). Therefore, to capture the absence of hubs while retaining the heterogeneity on the number of contacts, we introduced a Poissonian small-world (PSW) network. As introduced in chapter 2, we will use the Overlapping Poissonian Small-World (O-PSW) model. The Sparse Poissonian Small-World (S-PSW) model preserves the underlying Poissonian distribution but enables some long-range nodes even at  $p = 0$  (chapter 4). Hence, we will not review the results: it is enough to note that the SPSW implies an enhancement of  $\pi(t)$  with respect to the OPSW. The latter is a “local” PSW since we connected the neighboring nodes according to their degrees, drawn from a poissonian distribution of average  $D$ . Thus, it is more suited to mimic a local structure as for a “light” lockdown scenario.

Our goal will be to test if this configurations enhance or diminish the total cases  $\pi(t)$  with respect the Watts-Strogatz model (see section 5.1). In particular, we simulated the COVID-19 pandemic, by fixing the transmissibility  $\beta = 0.015$  ([35]) and the incubation period  $d = 14$  ( $\mu \sim 0.07$ ) (see Equation A.4) from [14]. As before, we analyze also the  $d = 4$  case, choosing  $\beta = 0.015$  and enhancing  $D = 24$ . In addition, we report the scenario where  $\beta = 0.1$  (a stronger epidemic) (see Figure 5.9a). The final result will be that the SPSW produces a higher fraction of total cases  $\pi(t)$  than the OPSW, which, in turn, displays a more elevated  $\pi(t)$  than the Watts-Strogatz model. Indeed as seen in subsection 2.3.1, the Sparse Poissonian Small-World (S-PSW) network accounts for long-range edges even if not directly introduced, namely for  $p = 0$ . Thus, we will not report its results but it is enough to underline that it produces an enhancement on  $\pi(t)$  due to the distant connections.

#### 5.3.1 Overlapping PSW

In this section, we will display the typical behaviors of a SIR model on a Overlapping Poissonian Small-World (O-PSW) network for both  $p = 0.0$  and  $p = 0.3$ . For brevity, we will refer to the one with  $p = 0$  as the “regular” OPSW (R-OPSW), while the latter as the “long range” OPSW (LR-OPSW). As said, we will recover that the OPSW model provides less control on the pathogen spreading with respect to the Watts-Strogatz model.

Finally, we will show the change of the order parameter, namely the standard deviation of the daily cases  $SD(C)$ ,

as a function of  $D$ . This will highlight the separation among a sub-exponential regime and an exponential growth of the fraction of total cases  $\pi(t)$ . The total cases will grow exponentially for  $D = 14$ .

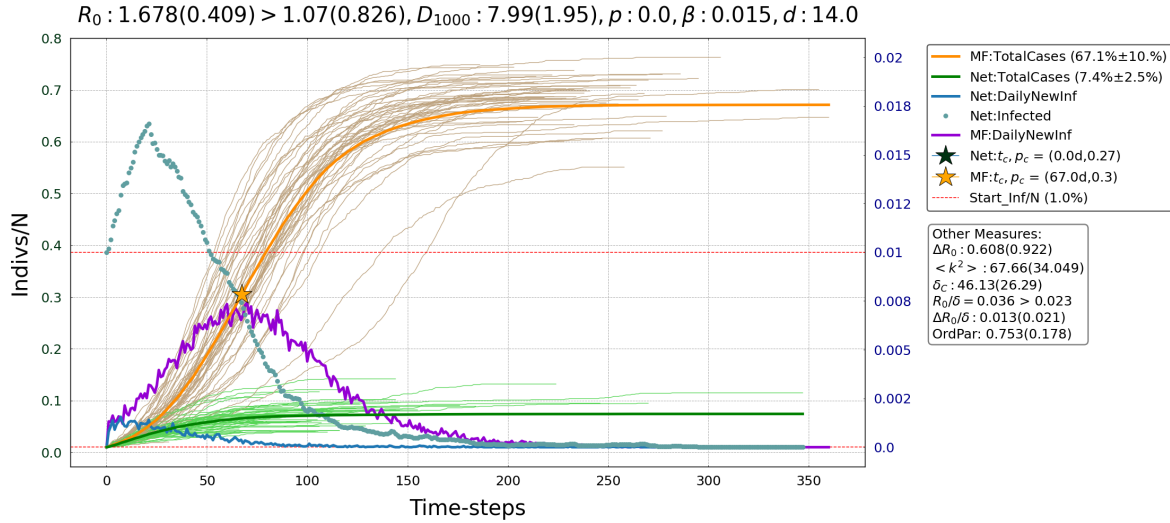
### SIR on Regular O-PSW

The [Figure 5.8](#) displays the emergence of the exponential growth of the final fraction of total cases  $\pi_{max}$ , defined in the [section 5.1](#), as  $D$  increases. For  $D = 8$  there is not an exponential growth, even at early times where there is a big pool of susceptible. Rather, this is the case for the Annealed-Mean-Field Network (orange curve) representing a mean-field approximation.

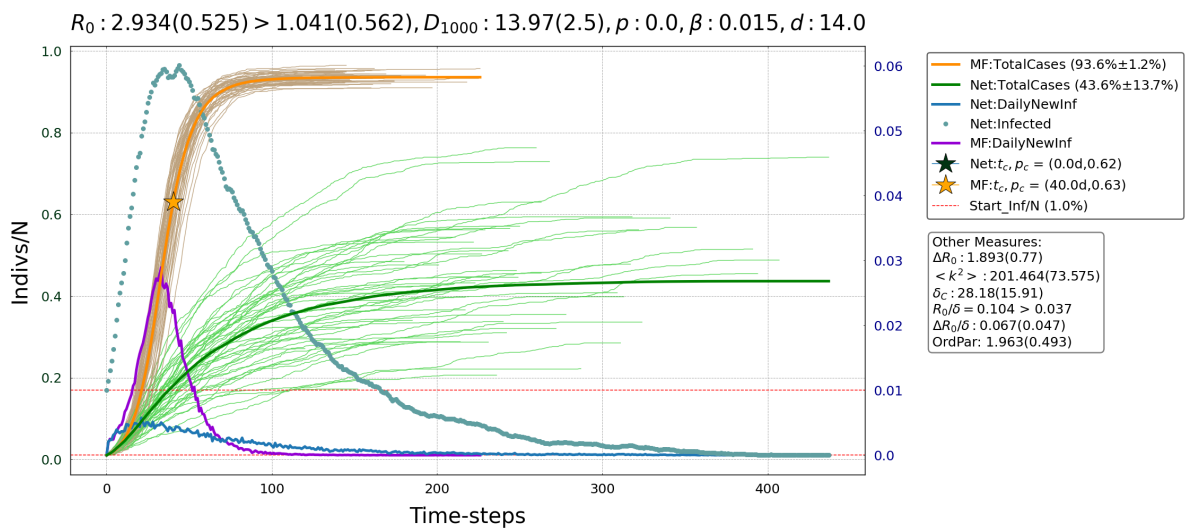
In [subsection 5.3.1](#) (cf. [section 5.1](#)), by varying  $D$  while fixing the *biological factor*  $\lambda := \frac{\beta}{\mu}$ , we will use the *epidemic severity*  $\Delta R_0(\delta)$  which better describes the diffusion of a pathogen in a network.

In [Figure 5.9a](#), we will underline how by increasing the transmissibility  $\beta$  also the  $\pi_{max}$  rises nearly to 14 times than the homologous plot for  $\beta = 0.015$  ([Figure 5.5a](#)). This could be expected since, as explained in [section 3.2](#), whenever  $\langle k^2 \rangle \neq \langle k \rangle^2$ ,  $\lambda_c < \lambda_{c-MF}$  produces an enhancement on the fraction of the fraction of total cases  $\pi(t)$ . For example,  $\lambda_c \rightarrow 0 < \lambda_{c-MF}$  for a “scale-free” network. Hence in this scenario, the fraction of total cases is bigger than the Watts-Strogatz one.

In [Figure 5.9b](#), we will display the evolution of a pathogen faced with medical interventions (higher  $\mu$ ) than the COVID-19 one. On the other hand, in [Figure 5.9a](#) we will display the spreading of a pathogen with higher transmissibility of the COVID-19. As expected,  $\pi_{max}$  will be higher than in the WS case [Figure 5.5b](#).

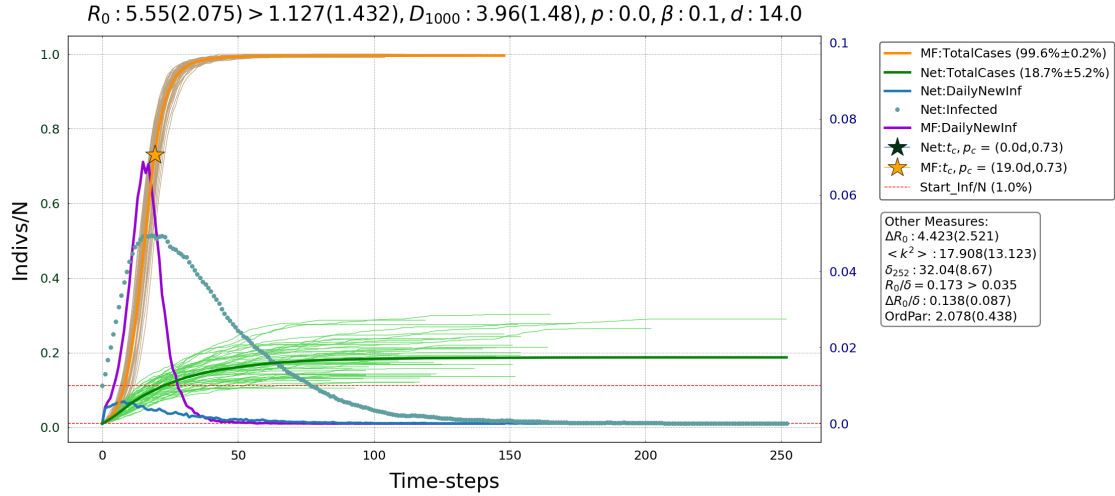


(a) SIR spreading for  $D = 8$  with COVID-19 parameters. Note that  $R_0 > R_{c-net}$  showing that the pathogen is naturally spreading. Moreover, there is no exponential growth, even at early times, where there is a big pool of susceptible. The  $\pi_{max}$  is higher than the one obtained for the Watts-Strogatz graph in Figure 5.5a as a sign that  $\lambda_{c-OPSW} < \lambda_{c-WS}$ .

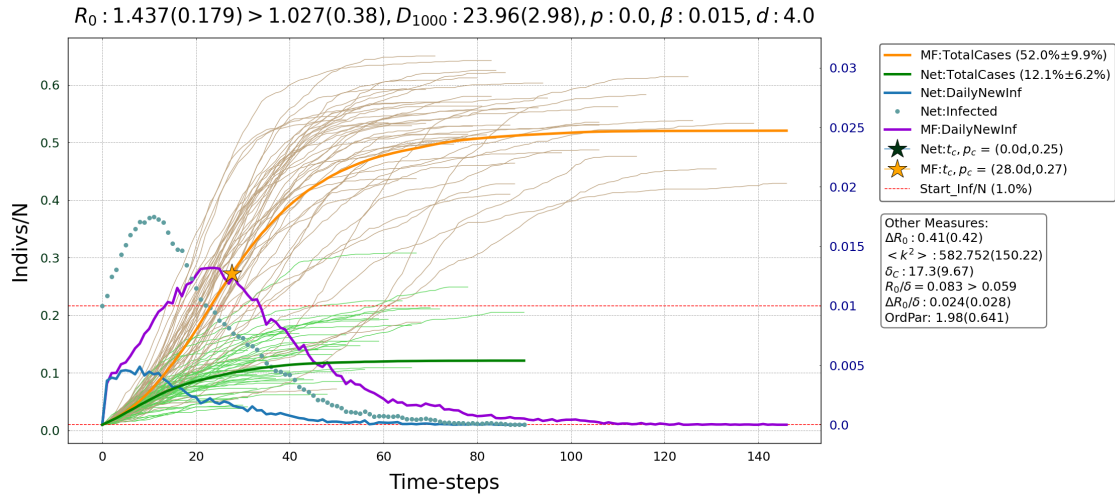


(b) SIR spreading for  $D = 14$ . The current topology ease the diffusion of the pathogen with respect to the regular Watts-Strogatz graph (cf. Figure 5.3b). By zooming into the onset of the outbreak, it could be seen an exponential increase of the total cases of the network curve (green curve). For  $D > 14$ , the epidemic curves on network develop a more defined exponential growth and start to resemble the mean-field ones.

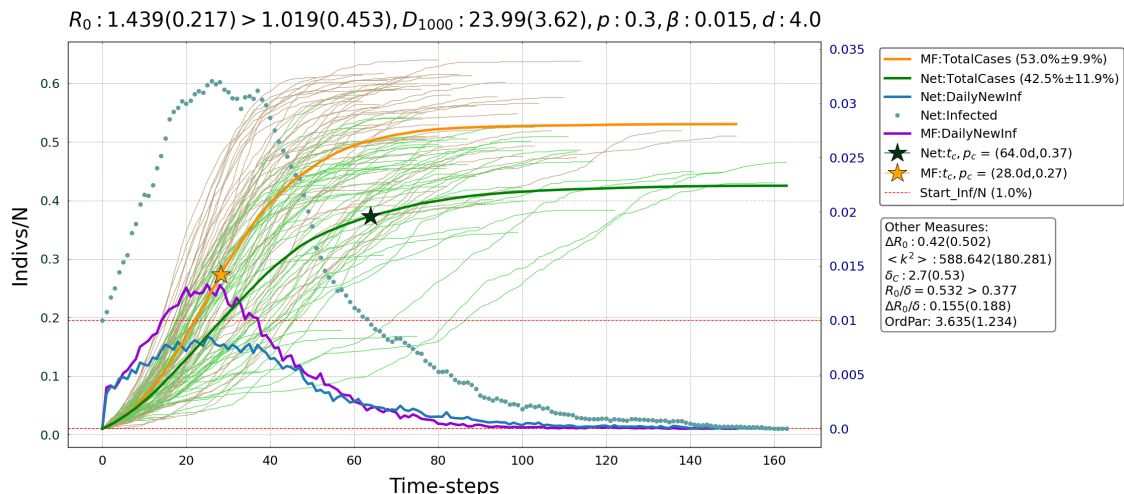
Figure 5.8: SIR spreading with COVID-19 parameters and a maximum  $D = 14$ .



(a) A pathogen with more transmissibility than COVID-19 and the other parameters drawn from Figure 5.8a. As before,  $\pi_{max}$  rises than the  $\beta = 0.1$  case even if  $D$  is halved (cf. Figure 5.8a).



(b) The evolution for COVID-19 faced with pharmaceutical interventions (PIs). They plays a relevant role since for  $D = 8, d = 14$  (Figure 5.8a) the final outbreak size overtakes the 40% of the population while, here, the final fraction of total cases  $\pi(t_{max}) \sim 13\%$  as  $D \sim 23, d = 4$ .

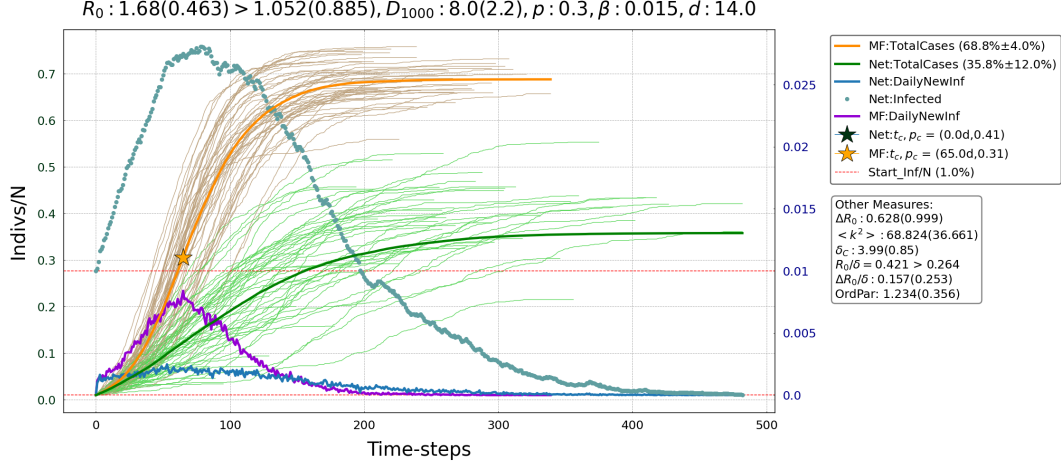


(c) The sub-exponential growth for a  $D$  slightly above  $D_c$  of Figure 5.12b and  $p = 0.3$ . It has been reported here for a direct comparison with the  $p = 0$  case. Indeed, the  $\pi_{max}$  is greater than the one reported for  $p = 0$  as the long-range nodes are present. For  $D < 24$ , the curves show trajectories which decay fast and are not smooth. Figure 5.8a shows how a pathogen could behave on the same network without Pharmaceutical Interventions. Lastly, by means of Equation 4.5, the estimated maximum of  $i(t)$  (green star) is overestimated; while the maximum for a mean-field is correct (yellow star). In addition, the former worsens as  $p = 0.3$ .

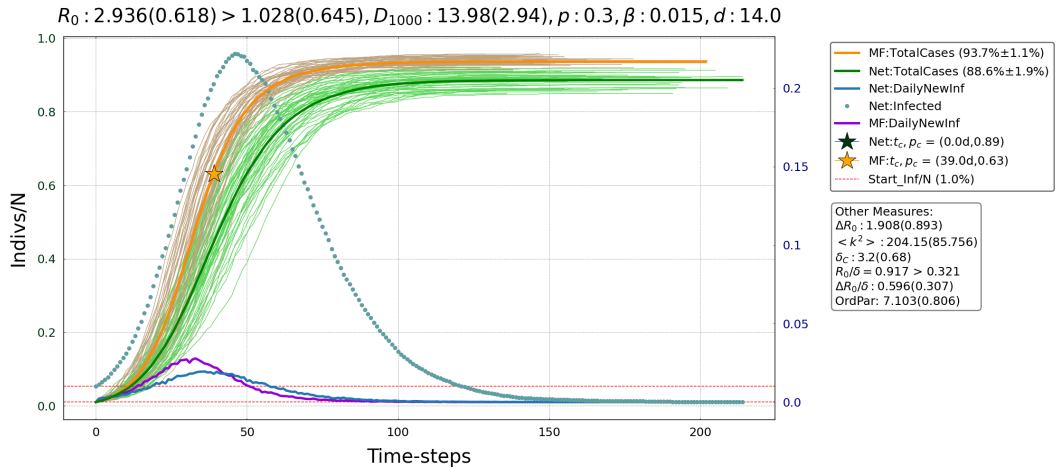
Figure 5.9: Spread for different epidemic parameters

## SIR on Long-Range O-PSW

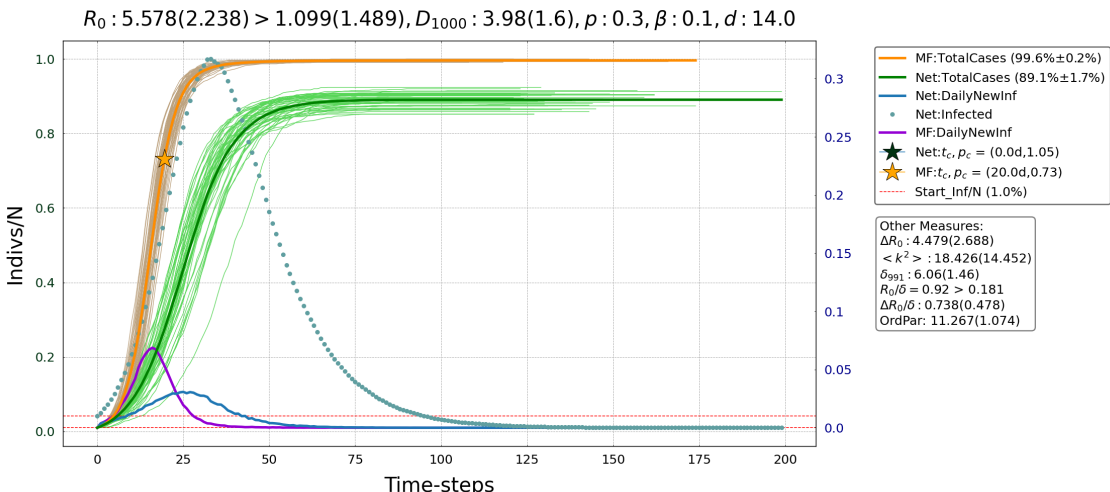
The diffusion of the pathogen for  $p = 0.3$  shares the overall shape with the  $p = 0$  case, but with an enhancement due to the possibility to jump into new pools of susceptible. In this way, an infected node may have more susceptible around and could spread easily.



(a) SIR spreading on OPSW with  $p = 0.3$ . The total cases  $\pi(t)$  are, roughly, linear in the first hundred days. Moreover, the *epidemic severity*  $\Delta R_0(\delta)$  accounts for the outbreak size  $\pi_{max}$ : the current evolution has  $\Delta R_0(\delta) \sim 0.147$  while the one in Figure 5.8b as  $\Delta R_0(\delta) \sim 0.013$ . On the other hand, the  $R_0 \sim 1.68$  and the difference  $R_0 - R_{c-net} \sim 0.6$  are similar to the these ones. Yet, the  $\pi_{max} \sim 36\%$  roughly twice as the  $\pi_{max} \sim 7\%$  obtained for  $p = 0$ .

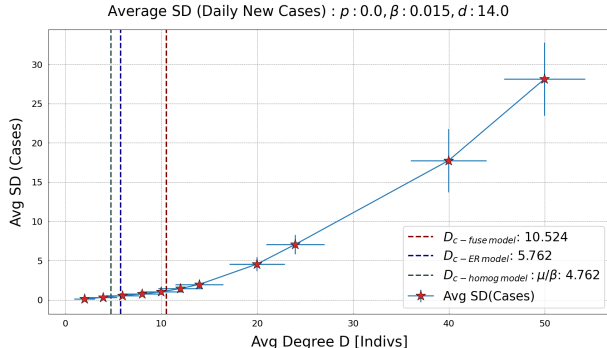


(b) SIR spreading for  $D = 14$  showing an enhancement in  $\pi_{max}$  with respect the Watts-Strogatz one in Figure 5.4c.

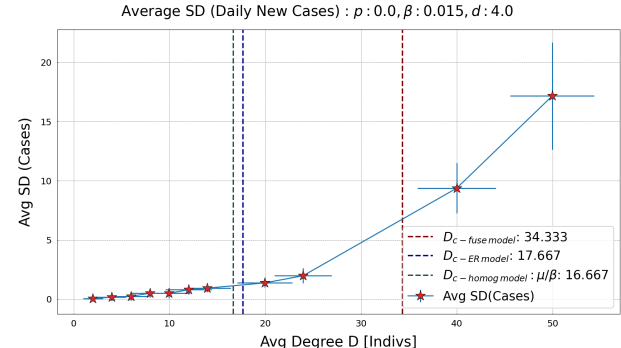


(c) SIR diffusion for  $D = 4$  but with higher  $\beta$ . As expected from the presence of long-range connections,  $\pi(t_{max})$  reach  $\sim 4$  times the total infected of the  $p = 0$  case. As in the previous cases, the WS model accounts for a lower enhancement as displayed in Figure 5.5b.

Figure 5.10: Overlapping PSW spread for COVID-19 parameters with  $p = 0.3$

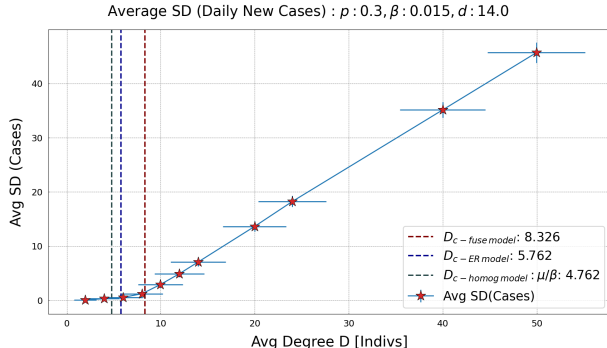


(a) Order Parameter with  $D_c \sim 10$  as shown by the small exponential phase at the early times of Figure 5.8. The  $D_c$ -fuse model properly estimates the real degree threshold.

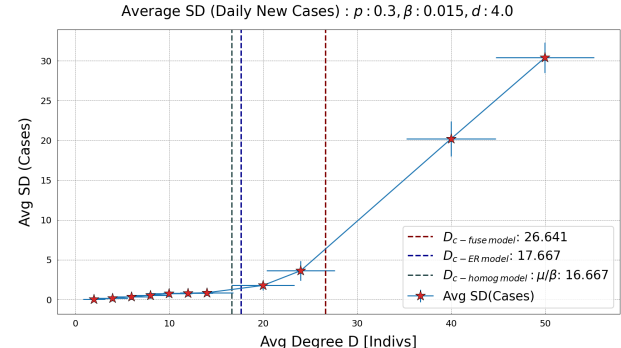


(b) Order Parameter with higher  $D_c$  since recovery rate is enhanced.  $D_c \sim 20$ . The fuse model deeply overestimates  $D_c$  as the Poissonian structure facilitates a faster growth of the standard deviation, i.e. the daily new cases, more than a fuse one. The transition is better described by the Erdős-Rényi  $D_c$ .

Figure 5.11: Order Parameter for Regular OPSW with different recovery rates at  $p = 0$ . Formally, the order parameter is an average of the standard deviations for each trajectory. Thus, the y-label “Avg(SD(C))”. We plotted both the order parameter and  $D$  with errorbars.



(a) Order Parameter dependence as in the upper plot, but  $p = 0.3$ . The fuse model approximation yields a proper estimate of  $D_c \sim 8.3$ . The introduction of distant node ease the exponential growth. Hence,  $D_c$  is lower than the one obtained in the  $p = 0$  case.



(b) Order Parameter for Regular OPSW with different recovery rates at  $p = 0.3$ . The critical degree of a fuse-model is corrected with the rewiring probability  $p$ . Thus, the estimates is more similar to the real change of regime.

Figure 5.12: Order Parameter ( $\text{AVG}(\text{SD}(\text{Cases}))$ ) for Long-Range OPSW of different pathogens and recovery rates. We plotted both the order parameter and  $D$  with errorbars.

## Order Parameters

### Regular O-PSW and Long-Range O-PSW Order Parameter

In this section, we will display how the order parameter (see section 3.3) changes as we vary the  $\mu$  and  $p$  parameters. Formally, the order parameter is the standard deviation of the daily cases  $SD(C)$  and we will consider it as a function of the average number of contacts  $D$ . Moreover, as  $D$  increases, it develops a kind of phase transition characterized by the critical degree  $D_c$ : as  $D < D_c$ ,  $SD(C) \sim 0$ ; while for  $D > D_c$ ,  $SD(C) \neq 0$ . In turn, the epidemics for  $D > D_c$  show an exponential grow at early times similar to the mean-field one. As a final result, we will obtained that in some cases the  $D_c$  is correctly estimated by a fuse-model (cf. Equation 3.25), while on the other the fuse overestimates it.

In Figure 5.11a, we exhibit the  $SD$  evolution for the COVID-19 epidemic parameters. The transition occurs for  $D_c \sim 10$  and it is well estimated by a fuse model. This is a desired result, since the *fuse* structure is similar to a *Poissonian* one. The second Figure 5.11b has an higher value of  $\mu$  as a result of the insertion of pharmaceutical

$$N_{22} : 990, D : 27.64(2.53), p : 0.3, \text{Inlinks} : 1, N_{3-out} : 0, SW_C : 0.387(0.204)$$

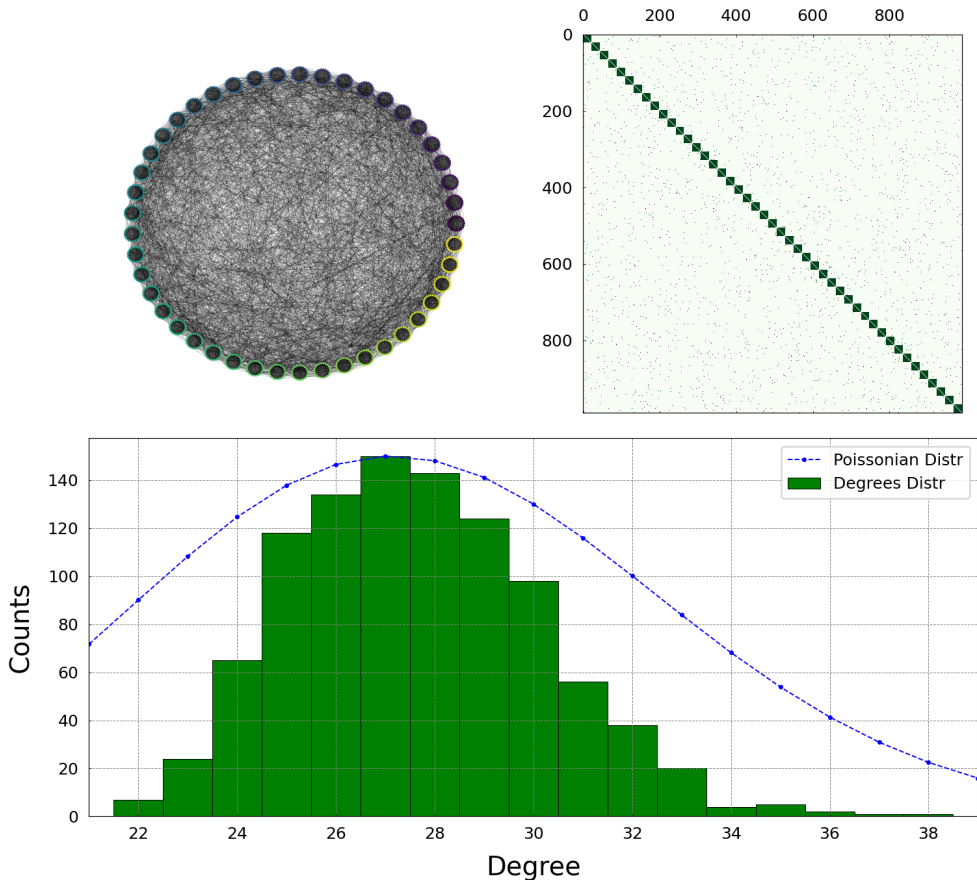


Figure 5.13: The visualization of a Caveman model properties: the graphical representation (upper right), where the colored dots represent a family; the adjacency matrix (upper right) and the degree distribution (lower figure). In particular, this realization is composed by 990 families of 22 components each and arranged on a circle. We connected each clique on the (two) nearest neighboring caves through 1 edge each. Then, we introduce a  $p = 0.3$  fraction of distant nodes. Thus, the [Equation 5.4](#) yields  $D \sim 27.3$ .

interventions, e.g. vaccines. By contrast to the previous case, this provides a higher  $D_c$ , since exponential growth of the total cases is more difficult:  $D_c$  of a fuse-model overestimates the simulated one, since a OPSW graph eases the spreading more than a fuse one. The Erdős-Rényi model provides a better measure of  $D_c$ .

Switching on the long-range interactions ( $p = 0.3$ ), the shape of  $SD(C)$  are similar to the previous ones. In [Figure 5.12](#), the most reliable prediction of  $D_c \sim 8.3$  comes from the *fuse model*, since the OPSW resembles a *fuse model*. In the [Figure 5.12b](#), we displayed the same scenario of [Figure 5.12b](#) but also the long-range interactions. The best estimate of  $D_c$  is provided by the Erdős-Rényi approximation. Nevertheless, as one finds in the legend, the fuse estimation is diminished since we actively considered the distant node  $D_{c-fuse\ model}$  as susceptible individuals in the analytical derivation (see [chapter 4](#)). As seen before, the epidemic curves are enhanced as we introduced the long-range interactions. Nevertheless, the order parameter does not display a perceiving reduction of  $D_c$  for  $p = 0.3$ .

## 5.4 Caveman Model

The most sensible lock-down measure was the household restriction. By limiting the individuals to have contacts only within families (or small communities), the pathogen was enclosed into small pools of susceptible and, hopefully, suppressed via the recovering of the nodes, e.g. [Figure 5.14a](#). As previously seen, forcing the nodes into overlapping neighborhoods with a sufficiently low  $D$ , diminishes the final outbreak size  $\pi_{max}$ . Therefore, we will arrange the individuals in cliques; while fewer connections will be left to wire to the other families either locally or distantly. As expected, this network will reduce the fraction of total cases  $\pi(t)$  with respect to the previous ones and, in particular, the Watts-Strogatz model.

Concretely, we used a “Caveman Model” (see [section 2.1](#)) and we connected the communities/caves to the nearest neighboring ones with 1 “on-ring link”: in the following plots, we reported the “OnRing” links quantity (see [chapter 4](#)). By introducing these “local” interactions, the assumption is that a family shares with two other ones only *one* “risky contact”, e.g. going to the *same* supermarket. This is the case whenever the families are distant or only a small fraction of the population is traced, e.g. by a voluntary usage of the mobile-application Immuni.

Moreover, we introduced the wiring probability  $p$  to the distant nodes to account for the leisure activities as expected for a light lockdown. Instead of rewire the existing links as done before, in the current model we added all the long-range edges to the previously existing connections not to destroy the family structures. Therefore, we calculated the average number of contacts  $D$  by using

$$D \sim \frac{2L_{tot}}{N_{tot}} = \frac{2}{N_{tot}} \left( (1+p) \frac{N_{cl}(N_{cl}-1)}{2} \cdot K + L_{nx}(K-1) \right) \quad (5.4)$$

where  $N_{cl}, L_{nx}, K$  are, respectively, the number of nodes composing a community, the number of links we used to reach the next community, the total number of cliques, namely

$K = \text{int}(1000/N_{cl})$ . For example, for [Figure 5.14a](#),  $N_{cl} = 4, L_{nx} = 1, K = 250$  yields  $D \sim 3.5$ .

As a brief outline, we will treat firstly the COVID-19 scenario ( $\beta = 0.015$  and  $d = 14$ ), then, we will modify the transmissibility  $\beta = 0.1$ , and the recovery days  $d = 4$ . More specifically, we considered  $\beta = 0.1$  to test how the network structure could respond to a stronger pathogen; while  $d = 4$  to capture the evolution of the COVID-19 when treated with the pharmaceutical interventions, such as a vaccines. Moreover, the evolution of the order parameter is not displayed since we simulated the epidemics for a limited number of average contacts  $D$ .

Lastly, we will obtain that the evolution of the Watts-Strogatz model will exhibit in every scenario an outbreak final size greater than the current topology. Thus, a Caveman Model enables to control more a diffusion of a pathogen. On the other hand, we will show that for a disease with high transmissibility  $\beta = 0.1$  another network should be considered [Figure 5.15a](#).

### SIR with Local Interactions

In this part, we will report the spreading of COVID-19 on a Caveman Model with 1 on ring link and  $p = 0.0^1$ . As seen previously, by fixing the epidemic parameters  $(\beta, \mu)$ , the epidemic grows faster as  $D$  increases.

In [Figure 5.14b](#), the final outbreak size  $\pi_{max}$  is smaller than the one of a Watt-Strogatz (WS) model for  $D = 2$  [Figure 5.2](#). Moreover, the average contacts for the caveman model are  $D \sim 3.5$ , bigger than the ones for the WS graph. Thus, the current topology shows a better control on the pathogen.

In [Figure 5.15a](#), we report a scenario for which the pathogen invade a considerable fraction of the population. This drives to the insight that with an higher transmission rate, namely  $\beta = 0.1$ , only drastic restrictions can limit the disease, e.g. forced quarantines.

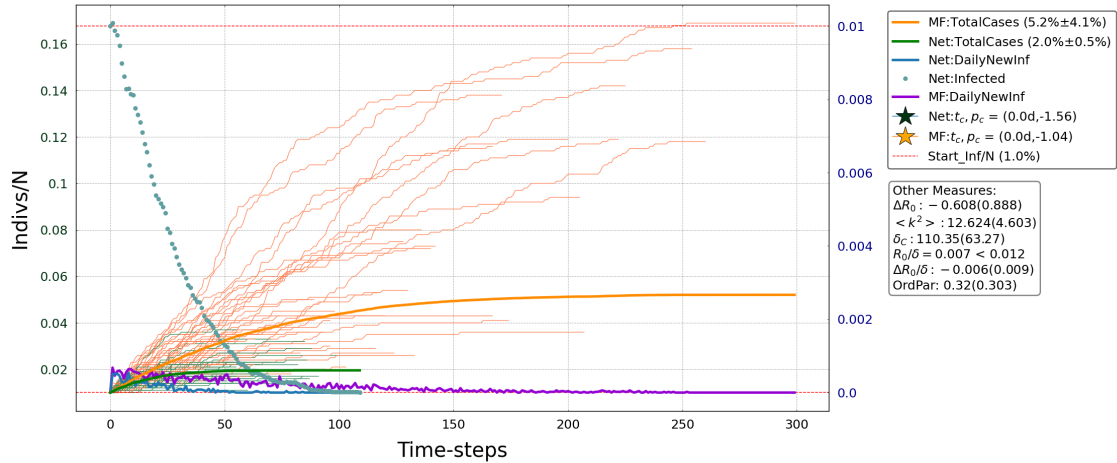
In [Figure 5.2](#) we showed a regular Watts-Strogatz model with the nodes disposed on a circle. In [Figure 5.14a](#), instead, we will display a similar structure: families (four individuals) are connected only locally on a ring. The latter structure will slow down the spreading as compared to the former one.

Ultimately, this topology is the best suited network in constraining a disease.

---

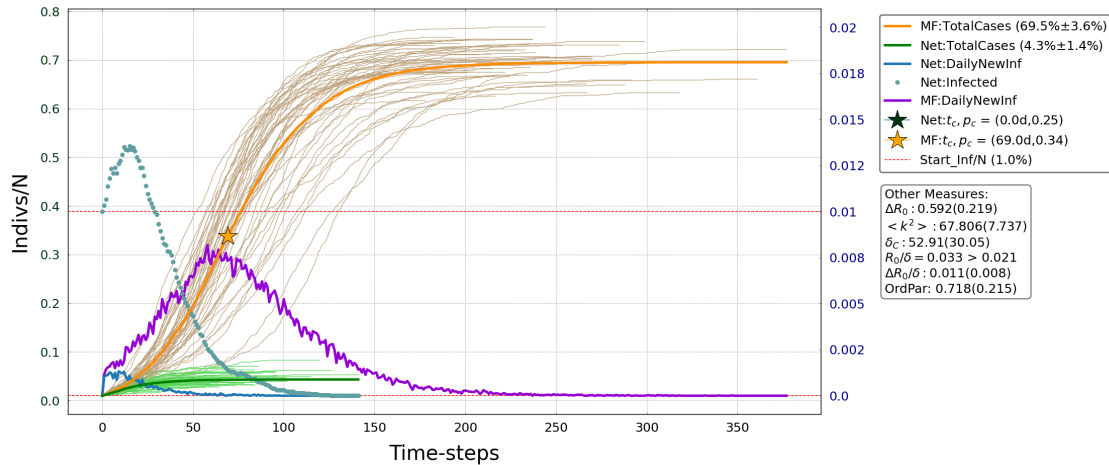
<sup>1</sup>In truth, we simulated the epidemic for both 1 and 3 on-ring-links, but we review only the *OnRing* = 1 case since *OnRing* = 3 have the same behavior but reaching a higher fraction of population.

$$R_0 : 0.735(0.128) < 1.343(0.878), D_{1000} : 3.5(0.61), \text{OnRing} : 1, p : 0.0, \beta : 0.015, d : 14.0$$



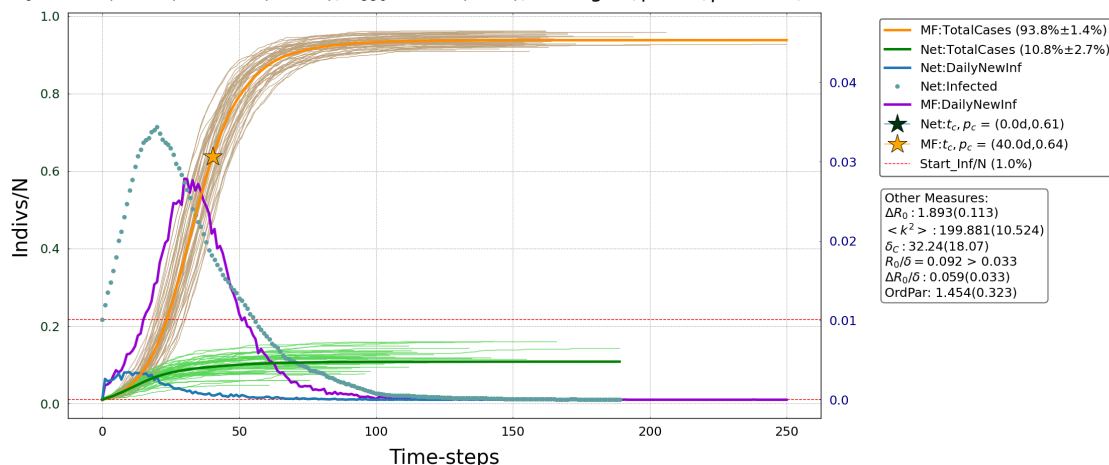
(a) A pathogen spreading on a Caveman Model with  $D \sim 3.5$ . Each clique/family is composed by four individuals and we wired each clique to the next one with 1 edge. In the Watts-Strogatz case  $\pi_{max} \sim 4.3\%$  for  $D = 2$ . Therefore, this topology exhibits more control in limiting the pathogen, since  $\pi_{max} \sim 2\%$ . Note that  $D = 3.5$  is comparable to household European size ([15]) or the USA one ([8]).

$$R_0 : 1.727(0.094) > 1.135(0.198), D_{999} : 8.22(0.45), \text{OnRing} : 1, p : 0.0, \beta : 0.015, d : 14.0$$



(b) A pathogen spreading on a Caveman Model with  $D \sim 8.22$ . Compared with Figure 5.8a, the caveman model diminishes the final total cases  $\pi_{max}$ .

$$R_0 : 2.968(0.076) > 1.075(0.083), D_{990} : 14.13(0.36), \text{OnRing} : 1, p : 0.0, \beta : 0.015, d : 14.0$$



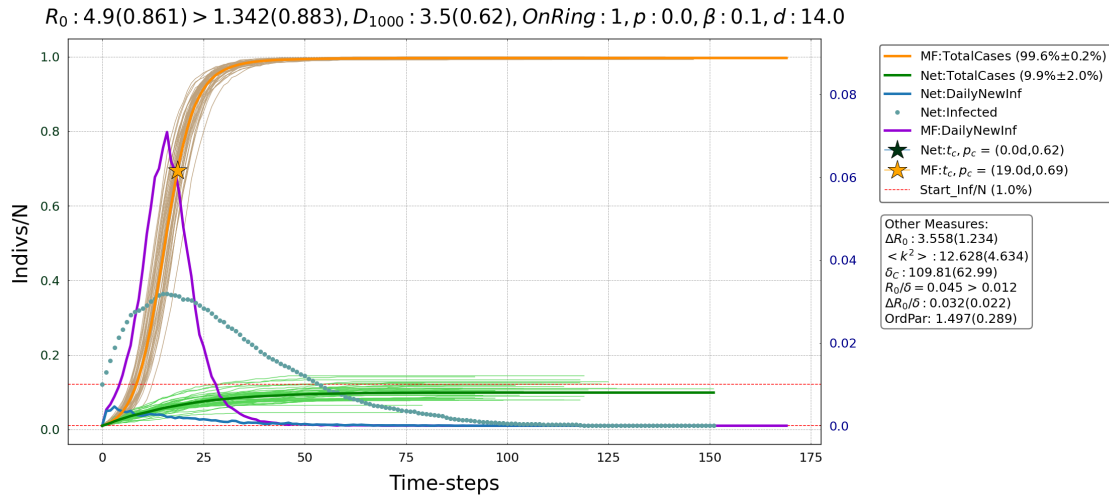
(c) A pathogen spreading on a Caveman Model with  $D = 14$

Figure 5.14: Last two spreading regarding an average degree  $D = 8$  and  $D = 14$ , as the previous networks, with “OnRing” = 1. These epidemic curves shows how cliques produce a drop in the  $\pi_{max}$  reached by the pathogen as in contrast with the percentages reported in Figure 5.8b, Figure 5.3b.

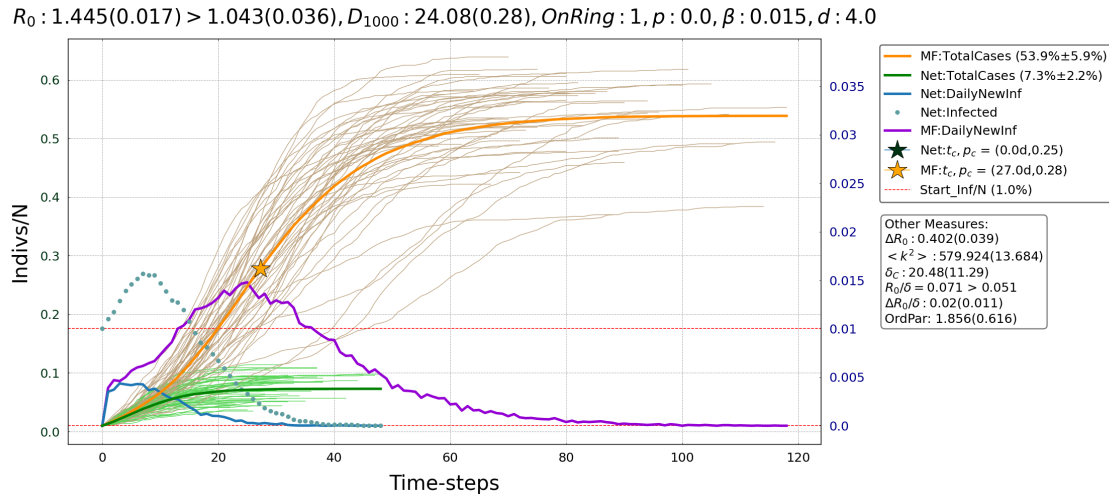
### Exploring SIR parameter on Caveman Model

The first figure of the next panel shows an epidemic curve with a transmission rate  $\beta = 0.1$  (Figure 5.15a) while the other parameters are drawn from Figure 5.14a, e.g. a new COVID-19 variant immune to the available vaccines. Nevertheless, since the network allows for a localized spread, the overall fraction of total cases stays small even if the pathogen has roughly 7 times the transmissibility of the COVID-19.

The second figure Figure 5.15b is characterized by a recovery rate of  $\mu = 1/4$  while other parameter are in accordance with the Figure 5.14c. This is a paradigmatic situation where pharmaceutical interventions are at work and the mean  $d = 4$  accounts for vaccinated and not-vaccinated individuals. Therefore, it is reported a reduction in the overall infected nodes.



(a) A pathogen stronger than COVID-19 keeping fixed the time to recover, e.g. a new variant immune to a vaccine for a different type of COVID-19. The current structure drives to  $\pi_{max} \sim 13\%$ ; while for a WS model we reported a greater fraction  $\pi_{max} \sim 44\%$  in Figure 5.5b.

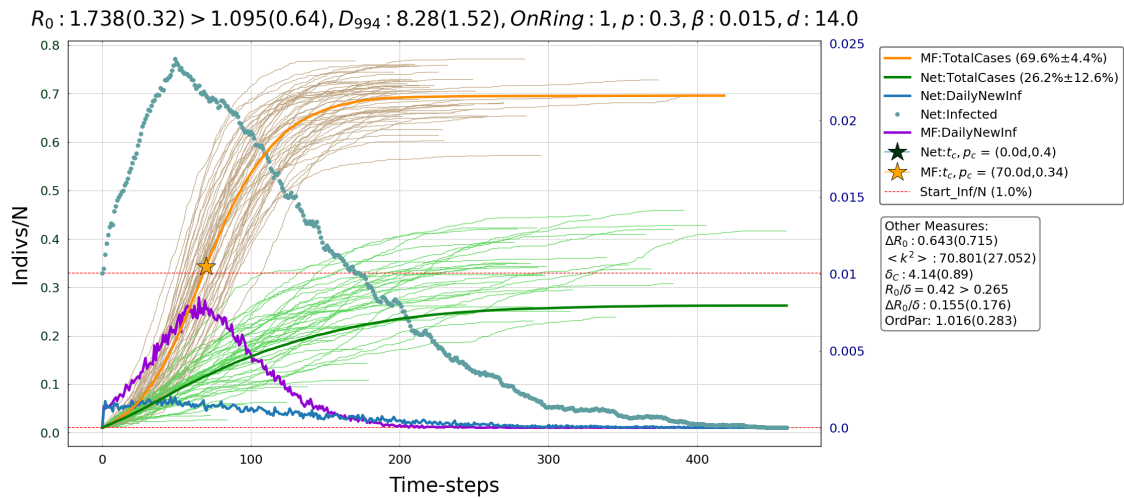


(b) Fixed the transmissibility coefficient to COVID-19, while decreasing the recovery to  $d = 4$ , the pathogen diffuses less than in a WS graph with the same parameters (cf. Figure 5.5c). This is also recovered by looking at the bump in the infected (azure dots) which is more contained than in the quoted figure.

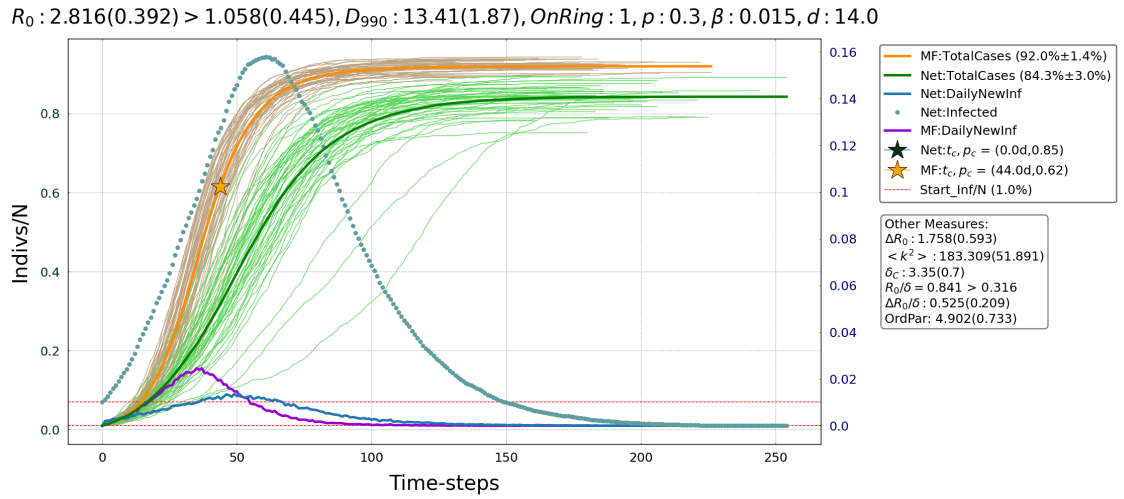
Figure 5.15: SIR evolution for  $D = 3.5, \beta = 0.1$  or  $D = 24, d = 4$ . The remaining parameters are drawn from the previous plots.

### 5.4.1 Long-Range Caveman model

In this section, we will analyzed the epidemic curves of a Caveman Model with both local (“On Ring Links”) and long-range interactions by switching on the wiring probability  $p = 0.3$ . By contrast with the other models, we will add the distant interactions on top of the pre-existing structures, e.g. families. Thus, the network has communities arranged on a circle, but also distant links due, for example, to work or leisure activities. As recovered in the previous cases, for  $p \neq 0$ , on finds an increase of the outbreak final size  $\pi_{max}$ . Nevertheless, the fraction of total cases  $\pi(t)$  will be smaller than the other models, namely the Overlapping Poissonian Small-World (O-PSW) and Watts-Strogatz (WS) graphs, even if we added distant interactions on top of the pre-existing families.



(a) A pathogen spreading in a Caveman Model with  $D = 8, p = 0.3$ . Final outbreak size is smaller than the WS model and the OPSW models [Figure 5.6a](#), [Figure 5.8a](#). In [Figure 5.8a](#) the overall value of  $\pi_{max}$  is nearly 3 times the present one. Hence, a “regular” Caveman Model constrains the most an epidemic.

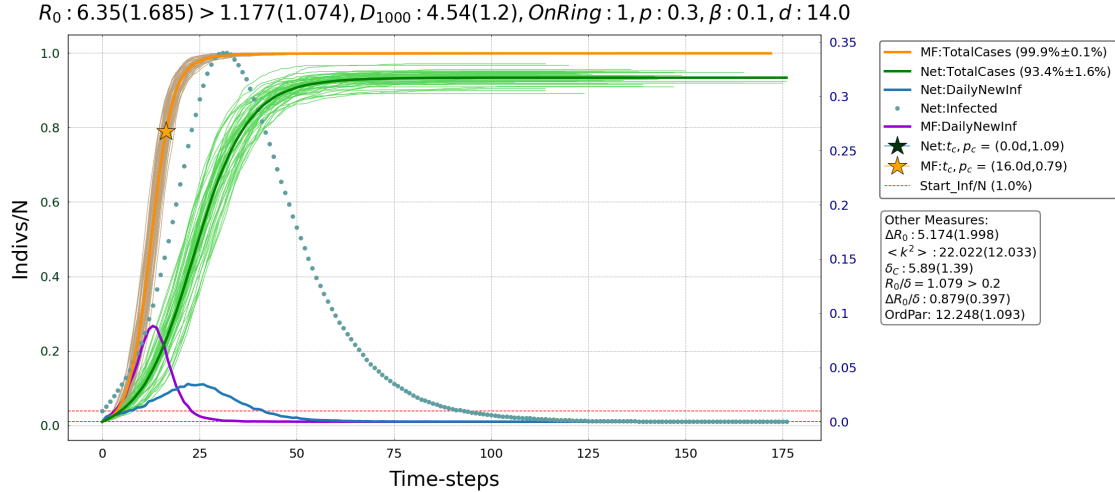


(b) A pathogen spreading in a Caveman model with  $D = 14, p = 0.3$ . The discussion is the same as the  $D = 8$  one.

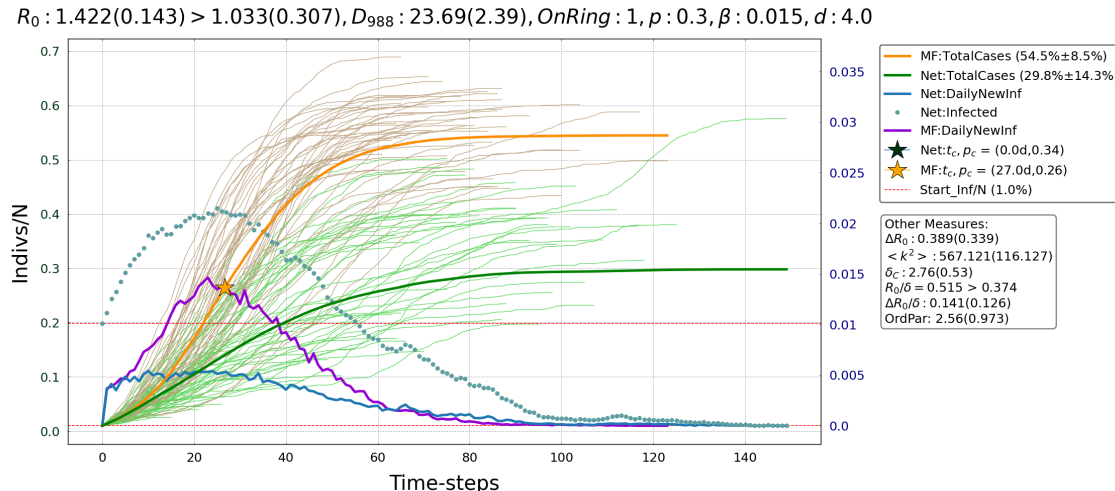
Figure 5.16: SIR model with COVID-19 parameters evolution for different average number contact per individuals.

## Exploring SIR parameters

On the way to understand more deeply how the network constraints the pathogen, we will consider a different epidemic and a diminishing recovery days due to insertion of the pharmaceutical interventions. The former would be analyzed by changing only  $\beta = 0.1$ ; while the latter by fixing  $d = 4$ .



- (a) A pathogen more contagious than COVID-19 but with same time of recovering, e.g. a new variant immune to a vaccine developed for a different COVID-19 strain. Weighted against a WS model (Figure 5.5b) the suppression is not so high since the pathogen is really strong. This is the effect of a strong epidemic agent, which could be nearly approximated by a “well-mixed” model. In fact, the long-range interactions drive the caveman model to be similar to an Annealed-Mean-Field Network. Moreover, we reported a bigger increase for a OPSW graph Figure 5.10c.



- (b) Fixed the transmissibility coefficient to COVID-19, while decreasing the recovery to  $d = 4$ , the pathogen diffuses less than in Figure 5.9c.

Figure 5.17: SIR evolution for  $D \sim 5, \beta = 0.1, p = 0.3$  and  $D = 23, d = 4, p = 0.3$ . We draw the remaining parameters from the previous plots.

$N : 1000, D : 27.61(22.85), p : 0.0, N_{3-out} : 40, USW_C : 1.224(0.389), k_{max} : 191$

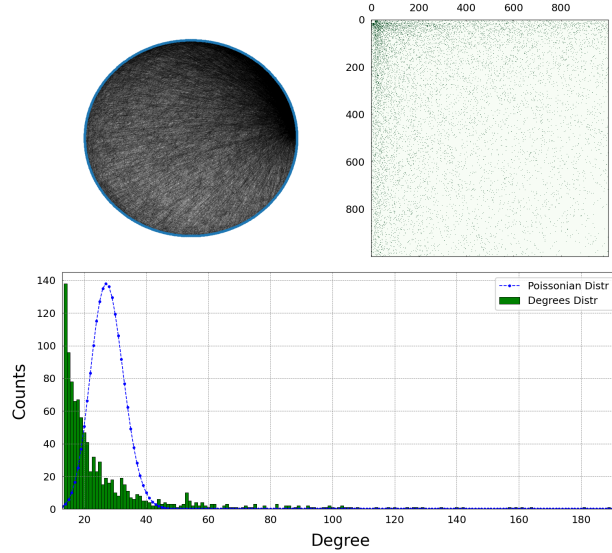


Figure 5.18: In the panel above, we reported the properties of a realization of the Barabási-Albert (BA) model. In particular, one finds the graphical representation (upper left), the contact matrix (upper right) and the degree distribution (lower band). In the latter, the BA degree distribution deviates from a poissonian one, since this model accounts for the presence of the hubs. In turn, this implies that the error of the average contacts  $D$  (value in rounded brackets near  $D$ ) is comparable to  $D$ . In addition to the previous graphs chapter 4, we reported in the title the *ultra small-world coefficient*, namely  $USW_C := \langle l \rangle / \ln(\ln(N))$  and the degree(s) of the maximum hub(s)  $k_{max}$ . This allow to understand the deviation of the hubs from the mean and their capabilities of spreading a pathogen. The white square on the top left of the adjacency matrix represents the starting point to build a BA model. Indeed, we chose to begin with a star graph of  $D/2$  nodes and, then, to add the newer nodes to it.

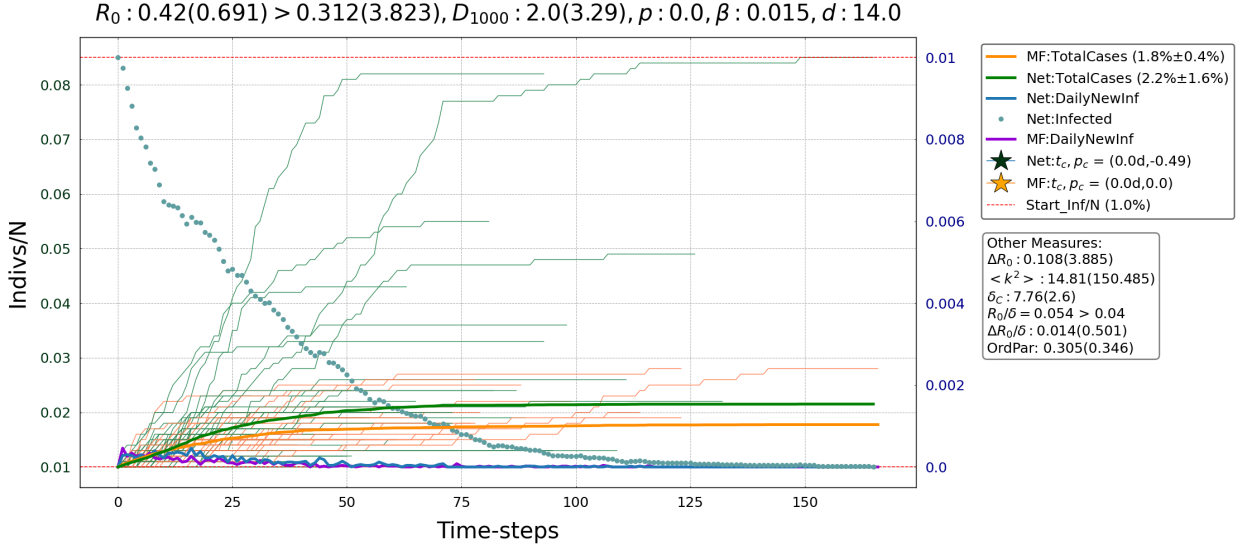
## 5.5 Barabási-Albert Model

As seen in Figure 2.4.2, this network topology allows to fit a variety of real networks, since it accounts for the presence of the hubs. Rather, the lockdown measures restricted the individual contacts. Nevertheless, we devote a section to it, in order to capture the novelties that hubs could provide with respect to the previous models. Ultimately, we will exhibit an increase fraction of the total cases  $\pi(t)$  with respect the Overlapping Poissonian Small-World (O-PSW) graph which provided the highest enhancement of  $\pi(t)$ . Hence, the Barabási-Albert (BA) model is better suited to describe other kinds of spreading, e.g. the diffusion of knowledge.

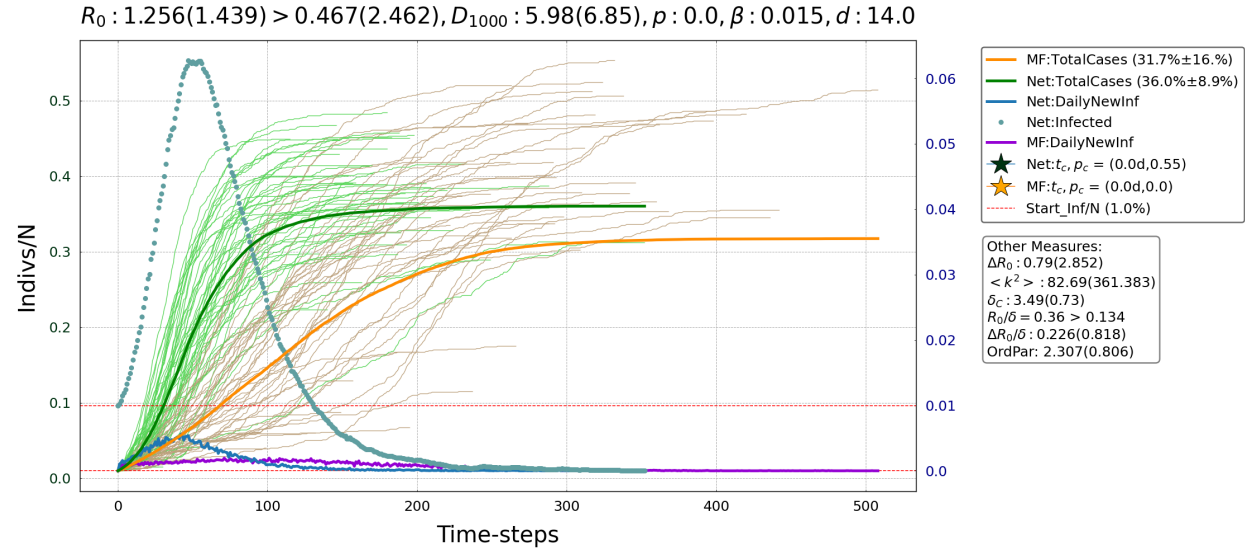
### SIR evolution

The panel Figure 5.19 displays different epidemic curves depending on the average number of contacts  $D$ . By contrast to the previous evolutions, for  $D = 6$  the scale-free topology shows a higher fraction of total cases  $\pi(t)$  than the mean-field one, as shown in Figure 5.19b and described in chapter 3. After that burst, starting from  $D = 10$  on, the “well-mixed” model retakes the lead in spreading the disease. As quoted before, the SIR spreading with the same parameters reached a lower value of  $\pi_{max}$  in the Overlapping Poissonian Small-World (O-PSW) model subsection 5.3.1.

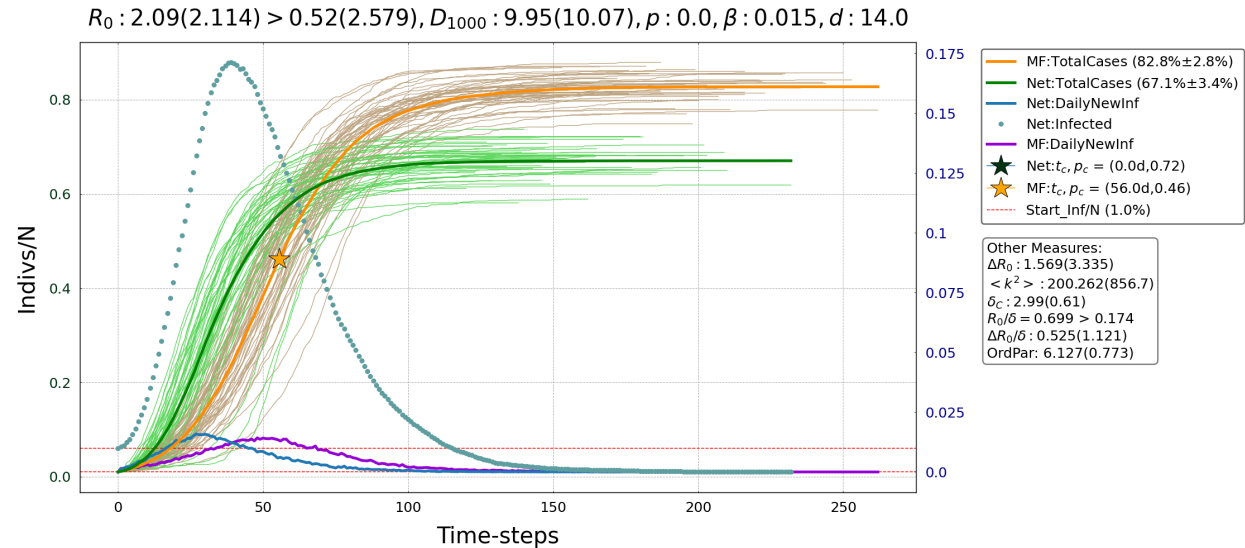
In Figure 5.20a, we plotted the evolution of a “stronger” pathogen than the COVID-19. Compared with Figure 5.9a, the  $\pi_{max}$  reaches a larger fraction of the population, nearly 2 times the OPSW one. Moreover, in Figure 5.20b, despite the fast healing of nodes and especially of the hubs, the total fraction of infected remains high. This drives to the idea that only a vaccination campaign targeting the hubs (e.g. doctors, nurses, ...) could limit a pathogen. Another effective procedure could be to close the “infrastructural hubs” such as airports, stores, gyms, ...



(a) A pathogen spreading in a BA model with  $D = 2$ . Note that for  $R_0 < R_{c-net}$ , the number of infected  $i(t)$  (azure dots) is always decreasing. For  $R_0 < R_{c-net}$ , we displayed the typical increase of  $i(t)$ .



(b) A pathogen spreading in a BA model with  $D = 6$ . The final outbreak size is far higher than the previous models (see Figure 5.8a)

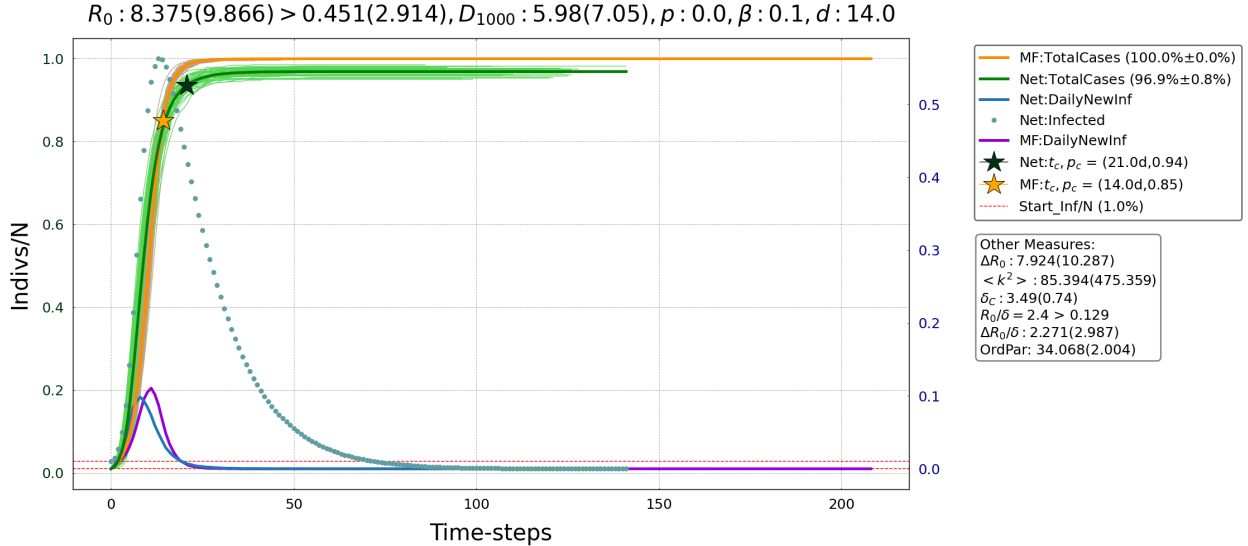


(c) A pathogen spreading in a BA model with  $D = 10$ . The Barabási-Albert model has retaken the lead over the mean-field represented by the Annealed-Mean-Field Network. The overall fraction of cases is enhanced Figure 5.8b even though the quoted figure has  $D = 14$ .

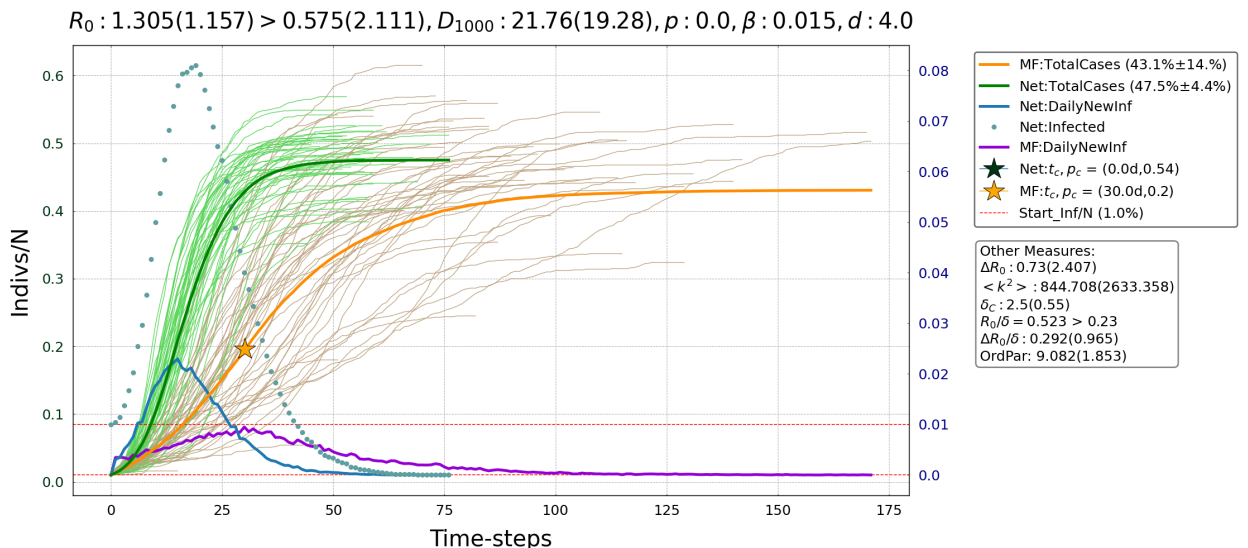
Figure 5.19: SIR evolution on a Barabási-Albert Model

### Changing epidemic parameters

Here, we report the most peculiar curve obtained by increasing the transmission rate  $\beta = 0.1$  and the days to recover  $d = 4$ .

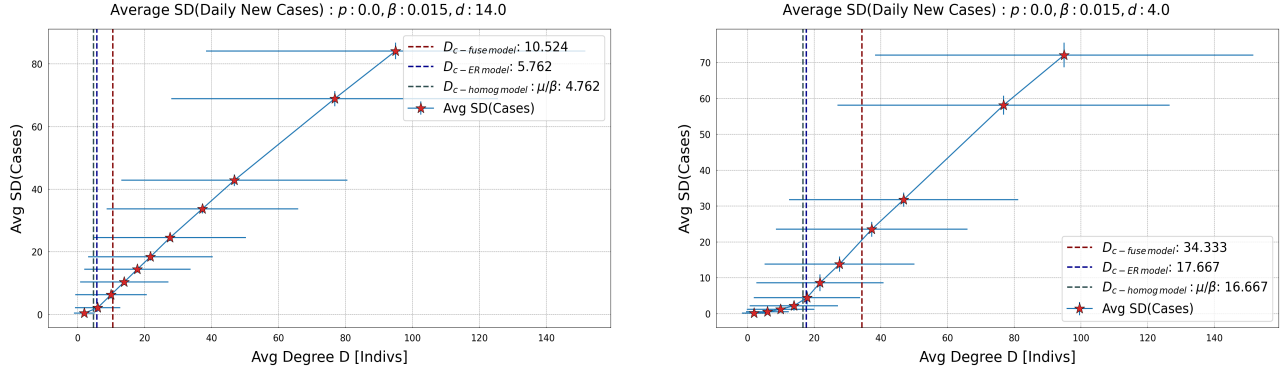


(a) Diffusion on a BA model with  $\beta = 0.1$ . A direct comparison with the Figure 5.9c shows how the BA model enhances the final outbreak size  $\pi_{max}$ . The estimated maximum of  $i(t)$  (green star) is *slightly* overestimated, since the pathogen is “strong” enough to resemble a mean-field. The maximum for a mean-field is correct (yellow star).



(b) Despite the fast healing of the infected individuals, the network enables a diffusion on a larger fraction of population than “free” previous spreading. Only a vaccination campaign addressed to the hubs could produce a relevant drop in the number of cases.

Figure 5.20: SIR model with enhanced parameters



(a) Linear growth in the  $SD(C)$  for COVID-19 parameters with no critical degree.

(b) Order Parameter for a fast recovery rate  $d = 4$ . The better estimate of the  $D_c$  comes from the homogeneous mean-field  $D_c \sim 16.667$ .

Figure 5.21: Order Parameter ( $\text{Avg}(\text{SD}(\text{Cases}))$ ) as a function of the average number of contacts  $D$  for the Barabási-Albert Model. We plotted both the order parameter and  $D$  with errorbars.

### Order Parameters

As the network enhances the possibility of a pathogen to diffuse, for the COVID-19 parameters a clear  $D_c$  does not exists; meanwhile, taking advantage of the (possible) Pharmaceutical Interventions (PIs), the  $d = 4$  case is characterized by a sharper transition among the linear and exponential growth. Only the “mean-field” approximation could capture the behavior of the  $D_c$  due to the hubs. The “fuse model” clearly deviates from the  $D_c$  estimate.

# Conclusions

The main purpose of this thesis was to study the evolution of an pathogen over different (social) networks. The rationale was to simulate the lockdown restrictions either through a drop of the average number of contacts  $D$ , as reported by [21]; and changing the network structure. Moreover, we introduce the *epidemic severity* (chapter 4)  $\Delta R_0(\delta)$  to capture the final outbreak size of different graphs and epidemic parameters. By contrast, we showed that the *basic reproduction number*  $R_0$  is informative only at early times. Finally, we used the standard deviation of the daily cases to underline the presence of a transition among the linear and the exponential regimes. The point, where this transition occurred, is called *critical degree*  $D_c$ .

In section 5.1 we used a Watts-Strogatz model to analyze  $R_0$  and  $\Delta R_0(\delta)$ . We obtained that the *epidemic severity* accounts for a variety of different final outbreak size.

In section 5.3, we exploited a Poissonian Small-World network to capture the heterogeneity of a social network without the presence of the hubs. Hence, for the same  $D$ , this topology enhanced the fraction of total cases with respect to the Watts-Strogatz model as described in section 3.2. Considering also the relink to distant nodes  $p = 0.3$ , the result does not change. In addition, we recovered that the fuse-model better estimates the (simulated)  $D_c$  for the  $d = 14$  cases. For  $d = 4$ , the fuse-model overestimates the critical degree, since the fuse model constrains the epidemic in a more suited way than the Poissonian models. Thus, the *critical degree* is lower for a Poissonian model. For  $p = 0.3$ , the estimates is marginally cured, due to the removal of distant nodes.

In section 5.4, we aggregated the individuals into families and locally connected them. As the Caveman model is the most constrained graph, we observed a lower final outbreak size than the Poissonian Small-World and the Watts-Strogatz graphs.

In section 5.5, we considered a Barabási-Albert network which accounts for the hubs. As reported in section 3.2, this “scale-free” networks enhanced the total cases more than the other models. Moreover, we obtained that a clear *critical degree* does not exists for the COVID-19 parameters; while, taking advantage of the Pharmaceutical Interventions (PIs), the  $d = 4$  case is characterized by a sharper transition. This suggest that a pathogen could be limited by vaccinating the hubs at first. The fuse-model does not provide a fair estimate to the *critical degree* due to the presence of the hubs. The  $D_c$  is better estimated by the *homogeneous critical degree*.

The final ordering of the best network constraining a disease is the following: the Caveman model, the Watts-Strogatz graph, the Poissonian Small-World network and the Barabási-Albert topology. As expected, by aggregating the infected as in the Caveman model the spreading is suppressed. Subsequently, the Poissonian topology provides an enhancement of the epidemic diffusion as a result of  $\langle k^2 \rangle > D^2$  as seen in section 3.2. Accounting for the hubs, we derived that the Barabási-Albert topology provides the worst topology in limiting the pathogen diffusion.

In most of the cases, we recovered that many networks account for a “sub-exponential” regime differently to the exponential one yielded by the homogeneous mean-field approximation e.g. Figure 5.2. Yet, we reported also a linear growth at early times for the mean-field as  $D$  is small Figure 5.14b. Nevertheless, a “scale-free” network could enhance the spreading over the mean-field approximation.

## 6.1 Future Developments

The real social networks are highly non trivial structure, by including a multilevel organization; weak ties between communities; and temporal aspects that suggest a degree of fluidity with stable social cores [35]. Therefore, in this thesis, we grasped the relevant feature of the contact networks but our study leaves room for future developments. For example, the Caveman model could be generalized to account for a variable number of individuals inside a family. In addition, we classified the individuals as “susceptible”(S), “infected”(I) or “recovered”(R). As said in [chapter 3](#), one can add other compartments, such as the quarantined individuals (Q) or asymptomatic person (A). This extension will be effortless, since the implementation of the new classes will be the same as for the older ones (S,I,R). Moreover, we introduced the *epidemic severity* as an experimental value to account for the total outbreak size, while a theoretical explanation still misses. Furthermore, we tried to predict the maximum of the infected  $i(t)$ <sup>1</sup> but more work has to be done to estimate its value. Another improvement could be to plot the total outbreak sizes as a function of  $D$ , since we expect that it will exhibit a phase transition similar to the the one of the epidemic threshold [Figure 3.3](#). On the other hand, the prediction of the *critical degree* is a hard problem since it is related to the number of infected as seen in [chapter 4](#).

Lastly, the COVID-19 pandemic was characterized both by an initial uncertainty on how to trace the infected and by the changing of restriction measures. Thus, the social network could rapidly change driving to a new behavior of the pathogen. A way of tackling this problem is by mean of “Deep Learning for Graphs” [3]. Specifically, by generating a “functional network” of the United States of America, one may capture the relationship among the states and use this information to predict the *instantaneous reproduction number*  $R(t)$  [11].

In conclusion, this thesis was a starting point, devoted to the study of a SIR model diffusing on networks. According to the theory and our perception of the phenomenon, we obtained some important results while there is a lot of room for future studies.

---

<sup>1</sup>As reported in [chapter 4](#) they differ from the new daily cases  $C(t)$ , since  $i(t)$  embodies the total infected at a fixed time  $t$ .

# Appendix

## A.1 Scale-Free Distributions Details

In the following part, the discrete approach, assuming  $k = 0, 1, 2 \dots$ , is going to be developed; while only the continuum result would be reported. In fact, the discrete approach provides the ready-to-use formulas handle by a calculator which, by construction, performs discrete operations. On the other hand, the continuum approach is useful for analytically support the calculations and could be obtained similarly to the discrete case. Formally, by exploiting the constraint on probabilities  $p_k = C \cdot k^{-\gamma}$

$$\sum_{k=1}^{\infty} p_k = 1,$$

it is possible to recover the closed form [6]

$$p_k = \frac{1 - p_0}{\zeta(\gamma)} k^{-\gamma}. \quad (\text{A.1})$$

where  $p_0 = p_{k=0}$  has been separated, since the power-law diverges for  $k = 0$ .

On the another hand, the continuum formalism drives to

$$p(k) = (\gamma - 1) k_{min}^{\gamma-1} k^{-\gamma},$$

since the the smallest value for the power law to hold is not 1, as in the discrete approach, but the minimum degree for a node  $k_{min}$ .

Formally,  $k_{min}$  is the degree for which

$$\int_0^{k_{min}-1} p(k) dk \stackrel{!}{=} 1/N \quad \text{or} \quad P(k_{min} - 1) \stackrel{!}{=} 1/N. \quad (\text{A.2})$$

In the next part, the allowed maximum degree  $k_{max}$  would be obtained both for an exponential bounded and a power-law distributions. Through this quantitative insight, it would be shown the dependence of  $k_{max}$  on  $N$ , i.e. the size of the network.

In particular, the exponential distribution for which  $\int_{k_{min}}^{\infty} p(k) dk = 1$  holds, is

$$p_k = \lambda e^{\lambda k_{min}} e^{-\lambda k}$$

where, using Equation A.2,  $k_{min} = 1$ . Furthermore,  $k_{max}$  (or the “natural cutoff”) is defined to be such that the at most one node  $i$  could have a degree  $k_i$  larger than  $k_{max}$ .

In other words, the cumulative distribution for degrees greater than  $k_{max}$  is  $1/N$ ; and, hence,  $k_{max}$  is expected to be the size of the bigger hub.

In formulas,

$$\int_{k_{max}}^{\infty} p(k) dk = 1/N \implies k_{max} = k_{min} + \frac{\ln(N)}{\lambda}. \quad (\text{A.3})$$

Hence,  $k_{max}$  would not differ much with respect to  $k_{min}$  since  $\ln(N)$  strongly reduces contribution due to the size of the graph  $N$ . For a Poisson distribution, more effort is needed but the same interpretation holds.

On the other hand, applying the same rationale to a scale-free network,

$$k_{max} = k_{min} N^{\frac{1}{\gamma-1}}. \quad (\text{A.4})$$

In this case,  $k_{max}$  can differ many order of magnitude from  $k_{min}$ . Indeed, as a simple example, WWW forms a graph of on  $N \sim 10^5$  documents with  $\langle k \rangle \simeq 4.6$  and  $\gamma = 2.1$  [6]. By assuming  $\lambda = 1$  and recovering that,  $k_{min} = 1$  using [Equation A.2](#),  $k_{max} \sim 14$ ; while  $k_{max} = 95.000$  for a scale-free network with  $\gamma = 2.1$ , e.g. WWW network. This short result reinforces the quoted insight that for the class of “exponentially bounded distributions” the hubs are strongly forbidden since the nodes have comparably the same degree. Instead, the highly connected nodes are naturally arising by increasing  $N$  with an underlying power-law distribution.

Not all the network are scale-free since the hubs are present only if nodes have unlimited degree capacities. In fact, there could be constraints, such as cost-benefit problem, which limit  $k_{max}$  of the bigger node. In this overview, random network may be the best fit, e.g. national highways network, power grid of generators and switches, ...

With all the previous effort a more quantitative approach to the explanation on the “scale-free” etymology could be ultimate. More precisely, defining the statistics momentums as

$$\langle k^n \rangle := \int_{k_{min}}^{k_{max}} k^n p(k) dk \quad (\text{A.5})$$

it is possible to recover the the mean and the variance for  $n = 1, 2$ . Thus, for a Poissonian distribution, the nodes degree  $k$  belong to  $\langle k \rangle \pm \langle k \rangle^{1/2}$  interval, which drives to the desired  $\langle k \rangle$  scale. At the same time, for a power-law distribution holds

$$\langle k^n \rangle \sim \frac{k_{max}^{n-\gamma+1} - k_{min}^{n-\gamma+1}}{n - \gamma + 1}. \quad (\text{A.6})$$

Therefore, knowing that real networks have typically  $\gamma \in (2, 3)$ , e.g. WWW has  $\gamma = 2.1$  [6]

$$k \in \langle k \rangle \pm \lim_{N \rightarrow \infty} \langle k^2 \rangle = \infty. \quad (\text{A.7})$$

where the hidden limit of  $k_{max} \rightarrow \infty$  is understood, since  $k_{max}$  increases with the system size. Hence, no scale naturally arises.

The result rapidly quoted before is surrounded by three other regimes [10]:

$$\langle d \rangle = \begin{cases} \text{constant} & \gamma = 2 \\ \ln(\ln(N)) & \gamma \in (2, 3) \\ \frac{\ln(N)}{\ln(\ln(N))} & \gamma = 3 \\ \ln(N) & \gamma > 3 \end{cases} \quad (\text{A.8})$$

**Anomalous Regime ( $\gamma = 2$ ):** Due to  $k_{max} \sim N$ , the network is forced into a “wheel rim configuration”, a central hub with spoke nodes. In this regime, the average path length is independent on the size of the graph.

**Ultra-Small World Regime ( $2 < \gamma < 3$ ):** By predicting a  $\ln(\ln(N))$  trend of the average distance, [Equation A.8](#) guides to the concept of “ultra-small world phenomenon” as a slower growth than random network. Indeed, recalling the worldwide social network,  $\ln \ln(N) \sim 3$  while  $\ln(N) \sim 22$  more than few times higher than the expected “six degrees of separation”.

**Critical Point ( $\gamma = 3$ ):** Looking back on the [Equation 2.7](#), the variance ( $n = 2$ ) is finite, marking the passage between the small-world ( $\sim \ln(N)$ ) and the ultra-small world ( $\sim \ln(\ln(N))$ ) classes of graphs.

**Small World ( $\gamma > 3$ ):** In this regime, the finiteness of the variance is understood, due to the light aggregation that the high-degree nodes could perform in these kind of networks.

Moreover, recalling the root of “ultra-small world” [Equation A.4](#), for  $N \lesssim 10^2$  the path length distributions overlap in all the reported regimes and, so, converges to a Poisson distribution ( $\gamma > 3$ ) whose hubs are small to produce the “ultra-small world” phenomenon. In fact, to validate the power-law nature of a distribution, the nodes degree should be separated by 2-3 orders of magnitude. Hence, reverting the [Equation A.4](#),

$$N = \left( \frac{k_{max}}{k_{min}} \right)^{\frac{1}{\gamma-1}},$$

which lucidly reproduce  $N \sim 10^2$  for  $\gamma = 2.1$  (WWW network).

Thus,  $\langle d \rangle$  is changing with  $\gamma$ , as the smaller it is, the shorter would be the average distance; but also with  $N$ , as it is the “ab ovo” hypothesis for having big hubs.

A sociological fact has to be remarked when trying to map the “ultra-small” world over social interactions. Indeed, an online experiment which aimed to replicate the “six degrees” concept find that individuals involved in complete chains, reaching their target, were less likely to send a message to a hub than individuals involved in incomplete chains [12]. The reason may be self-imposed, since hubs are perceived as being busy, so contacted only in real need and avoid to concretely complete an “online experiment” challenge. Thus, network is not everything since actual success depends sensitively on individual incentives.

## A.2 Recovering Power-Law Distribution

Due to a new  $m$ -stubs node, the degree of an existing node  $i$  changes at a rate

$$\frac{dk_i}{dt} = m\Pi(k_i) = m \frac{k_i}{\sum_j k_j}. \quad (\text{A.9})$$

Hence, for  $t \gg 1$ ,

$$k_i(t) = m \left( \frac{t}{t_i} \right)^\beta \quad (\text{A.10})$$

where  $\beta$ , alias “dynamical exponent”, has the value  $\beta = 1/2$  [6] and  $t_i$  is the entering time for the node  $i$ .

The remarks, coming from the [Equation A.10](#), are multiple:

- all the nodes follow the same power law, since  $\beta$  is independent on the node label  $i$ . Furthermore, it is independent on  $m$  and  $m_0$  constructing parameters;
- the inverse dependence of  $k_i \sim 1/t_i$  is a clear signal of the fact that old nodes are supposed to be larger, also called “first-mover advantage” in business;
- both  $\beta = 1/2 < 1$  (sublinear growth) and the rate  $dk_i/dt \sim 1/\sqrt{tt_i}$  underly a competing scenarios: the existing nodes compete for the  $m$ -new stubs with a growing bunch of nodes, resulting in a sublinear growth, which drives to a decreasing rate of acquaintances.

To validate the power-law nature of the probability of having a certain node degree, by exploiting [Equation A.10](#) it is possible note that the nodes  $i$  with a degree higher than  $k$  are such that

$$t_i < t \left( \frac{m}{k} \right)^{1/\beta}.$$

Thus, for  $t \gg m_0$ , the (cumulative) probability of having a degree less than  $k$  is

$$P(k) = 1 - \left( \frac{m}{k} \right)^{1/\beta},$$

from which the probability of having a degree  $k$  could be recovered, by differentiating  $P(k)$  and substituting  $\beta = 1/2$ ,  $p_k = 2m^2k^{-3}$  [6]. As desired, the distribution exhibits a long-tail nature with  $\gamma = 1/\beta + 1 = 3$ . Alongside with the BA model simulations, the dependence between  $\gamma$  and  $\beta$  demonstrate the deep relationship among the graph topology and the temporal degree evolution, respectively contained in  $\gamma$  and  $\beta$  parameters.

Another feature present in [Equation A.10](#) is that the degree distribution is independent on  $t$  and  $N$  or a “stationary distribution”. This result is the one expected, since the model aims at describing the real networks in general; thus, of rather different age and size.

## A.3 The Origins of Preferential Attachment

Since preferential attachment plays a relevant role in guiding the dynamics of a real network, the goal is to recover the same  $\Pi(k)$  as the one assumed in the Barabási-Albert model. It worths to introduce two classes of microscopic processes that generate it naturally [6]: “*local (or random) mechanisms*” representing the interplay between random events and some structural properties of the network; and “*global (or optimized) mechanisms*” which take advantages of a cost-benefit analysis on the whole graph. In the following, it would be reviewed the “Link Selection” and “Copying” Models which belongs to the random class; and, finally, the “Optimization” Model of the second one.

### A.3.1 Local Mechanisms

#### Link Selection

Assuming growth is at work, i.e. at each event time a new node is added, select randomly an edge and connect the new node to a vertex belonging to that edge. Thus, the probability  $q_k$  that the selected node, already present in the graph, has degree  $k$  is

$$q_k = \frac{1}{\langle k \rangle} \cdot kp_k \quad (\text{A.11})$$

where the first factor exploiting the normalization constraint  $\sum_k q_k = 1$ . Hence, it has the hoped form, being linear in the number of stubs ( $k$ ) and in the frequency of the degree- $k$  nodes ( $p_k$ ). This displays an increasing of the chance of wiring to a degree  $k$  node, by enhancing either the number of degrees or the presence of degree- $k$  nodes themselves.

#### Copying Model

The idea is compute the probability of obtaining a connection of a degree- $k$  node by mimicking the phenomenon of authors of a new webpage which copy links from existing webpages on the related topic [13].

By introducing a new node  $n$  in the network, as before, the difference stands in the link selection. More in detail, selecting an existing node  $u$  regardless of its degree, e.g. picking an arbitrary web document which topic is related to  $n$ , there are two possible way of connections:

- Random (direct) connection: with a probability  $p$ , link  $n$  to  $u$ ;
- Copying (undirect) connection: with likelihood  $1 - p$ , wire  $n$  to an neighboring node  $v$  of  $u$ . Reprising the web example, the new webpage  $n$ , copying the link of  $u$ , connects with its target  $v$ .

As a constraint to recover a dependence on  $k$  of  $\Pi(k)$ , fix that  $v$  should have degree  $k$ , by considering  $p_v = k/2L$ . Hence,

$$\Pi(k) = \frac{p}{N} + \frac{k}{2L}(1 - p) \quad (\text{A.12})$$

which is linear in  $k$ , yielding the desired preferential attachment. The power of this approach is its “empirical” root which could be detected from citation networks to the social network of acquaintances.

### A.3.2 Global Mechanisms

#### A.3.3 Optimization Mechanism

The principle of minimization of cost-benefits analysis in an economic market [29] can lead to preferential attachment whether a proper cost function is considered.

For simplicity assume that the vertexes are laying in an unit square, e.g. routers in a square continent. As before, at each event time a new router  $i$  is added, while an edge with an existing node  $j$  is created according to the cost function [6]

$$C_i = \min_{j \in G(V, E)} (\delta d_{ij} + h_j).$$

where  $d_{ij}$  is the euclidean distance between the vertex  $i$  and  $j$ ; while  $h_j$  is the number of hops from  $j$  to a pre-defined “center” which embodies the best network performance, e.g. net distribution hub. More clearly,  $d_{ij}$

and  $h_j$  represent the physical distance and “network-based” distance. Their summation describes the cost to be minimized for real results.

Depending on  $\delta$  and  $N$ , there are 3 network topologies:

- **Star Network** ( $\delta < (1/2)^{1/2}$ ): only  $\delta d_{ij}$  drives the growth, thus, the new nodes connects with the central one forming a star;
- **Random Network** ( $\delta \geq N^{1/2}$ ):  $h_j$  is the minimum quantity to be minimized. Hence, the new nodes connect to the nearest node;
- **Scale-free Network** ( $4 \leq \delta \leq N^{1/2}$ ): in this intermediate regime scale-free topologies may be recovered as a result of optimization and randomness. In particular, optimization creates a basin of attraction with size  $s \sim k_j$  and centered in  $j$ , within all the appearing nodes  $i$  wire with  $j$ . On the other hand, Randomness is the chance of choosing a specific basin.

Thus, linear preferential attachment can come from both rational choice and random actions. Yet, most complex systems are driven by processes that have a bit of both luck or reason.

## A.4 Error Propagation and recovery time table

Using the *propagation of errors*, we have obtained the errors of  $R_0, R_{c-net}, \Delta R_0, \Delta R_0(\delta)$  displayed inside the rounded brackets of [chapter 5](#).

Error propagation for  $R_0 := \beta D / \mu$ :

$$\sigma_{R_0} = \sqrt{\beta/\mu} \cdot \sigma_D \quad (\text{A.13})$$

Error propagation for  $R_{c-net} := \frac{\langle k \rangle^2}{\langle k^2 \rangle - \langle k \rangle}$  where  $D := \langle k \rangle^2$  :

$$\begin{aligned} \sigma_{R_{c-net}}^2 &= \left[ \frac{2D\langle k^2 \rangle - D^2}{(\langle k^2 \rangle - D)^2} \right]^2 \cdot \sigma_D^2 + \left[ \frac{D^2}{(\langle k^2 \rangle - D)^2} \right]^2 \cdot \sigma_{\langle k^2 \rangle}^2 \\ &= \left[ \frac{R_{c-net}}{D} \right]^4 \cdot \left[ \left( \frac{2\langle k^2 \rangle}{D} - 1 \right)^2 \sigma_D^2 + \sigma_{\langle k^2 \rangle}^2 \right] \end{aligned} \quad (\text{A.14})$$

Error propagation for  $\Delta R_0 := R_0 - R_{c-net}$ :

$$\sigma_{\Delta R_0}^2 = \sigma_{R_0}^2 + \sigma_{R_{c-net}}^2 \quad (\text{A.15})$$

Error Propagation for  $\Delta R_0(\delta) := \Delta R_0 / \delta$ :

$$\begin{cases} A_1 := \frac{\Delta R_0(\delta)}{\delta} \sigma_\delta \\ A_2 := \frac{\sigma_{\Delta R_0}}{\delta} \end{cases} \implies \sigma_{\Delta R_0(\delta)} = \sqrt{A_1^2 + A_2^2} \quad (\text{A.16})$$

The following table displays the conversion among the recovery rate  $\mu$  and the *days* of recovery, which is the terminology used in medical articles.

Recovery Measures	
$\mu$ [1/time-step(s)]	days [time-step(s)]
0.071	14
0.111	9
0.167	6
0.25	4
1	1

# Ringraziamenti



Figure B.1: Portami via con te!

*Il primo pensiero va a voi come gruppo, come squadra che mi è stata vicino anche quando volevo stare da solo. Ognuno a suo modo nonostante le difficoltà, cosicchè se non ci siamo persi, il legame deve sì essere più solido di quello che percepiamo.*

Involutivi costrutti sintattici a parte, parto.

Ringrazio i miei genitori per aver dato grande importanza alle mie attitudini e a quelle di Anthea, volendoci dimostrare che nella vita la positività è giusto poco più in là della delusione.

Ringrazio la mia *famiglia*: il babbo *Eros* per tutti i sinceri aiuti che non sono sempre stato in grado di accogliere, la mamma *GRabri* per lo spirito di condivisione e coraggio che avrei voluto avere in diverse situazioni, la mia Crossfitter preferita *AntHea* per non aver detto alla mamma che l'avevo fatta cadere io dalle scale e procurato dei punti sotto il mento; per aver lavato le stoviglie quando io volevo solo suonare; per gli abbracci di Natale; i letti spostati; i pomeriggi di luglio a vedere “*The Hills*”; aver distrutto le costruzioni di LEGO così ho potuto ricreare più volte quello che mi sembrava già concluso; e che dimostra ogni giorno una capacità di scelte oculate che mi ispirerà nel futuro. Ringrazio di nuovo mio papà per una recente frase che mi ha dato sicurezza nei diversi bivi di quest’anno: *La vita va vissuta, ma anche saputa raccontare*.

*Marco R.* è con stima che lo ricordo per avermi fatto realizzare che l’età non conta quando si vuole essere (giovani) adulti.

Ringrazio *Sara* con cui condivido il sentimento più astratto, ma che per me è il più concreto di tutti. Di avermi preso la mano e portato a raggiungere *quella piccola poesia anche per me*. Di avermi fatto vedere il buono della condivisione e della leggerezza anche quando per me lo studio era tutto. Ci sarà altro tempo per insegnarci dell’altro.

Rendo grazie alla *Zia Rita* per incoronarmi “el più bel de Maran”: compito impegnativo, ma anche decoroso. A parte gli scherzi, ringrazio *te, Giulia e Laura*, per averci aiutato a sentirsi parte di una famiglia anche a distanza. Colgo l’occasione per estendere il merito anche ad *Ale e Rico* che fino a questo punto credevano non sarebbero stati citati invece anche la loro importanza è rilevante. Non ultimi i cuginetti *Giada, Sveva, Ambra, Niccolò, Marialuce, Fiona e Cosmo* (in ordine di apparizione) per avermi insegnato che ho già un ruolo nelle loro vite e tanto vale non sprecarlo.

Rilevante è la parte di famiglia di Maran con *Nonna Ina, Zio Ivano, Zia Nuccia, Elisa e Marco* per una crescente vicinanza condivisa. Mi avete insegnato lo spirito dei Milocco che mai sarà dimenticato: risate, cantate, ma anche spirito di sacrificio e perseveranza.

Ringrazio l’altra *famigghia* che mi ha accolto con simpatia e inclusione al momento più opportuno. *Marco S.* per il coraggioso ritorno dalla carriera militare per dedicarsi alla famiglia e *Luciana* per la ricercata unione familiare.

*Marta* per sfatare il preconcetto che un’artista deve essere libero, perché è nei vincoli che si ritrova il *genio*. *Giovanni* per non aver paura di piantare e stabilizzare le sue radici in ogni posto in cui si trovi.

Ringrazio ora l’ UniPD...ahah...no tocca a voi amisci.

[Treccani] *L'amicizia è un rapporto fatto di fiducia, simpatia, affetto e reciproca scelta, che si riscontra in ogni tempo e in ogni luogo, ma che nessuna teoria può spiegare del tutto.*

Ricordo con valore *Alessandro* per la logica con cui anche le costruzioni più astruse diventano plausibili e la passione per la vita edonista tra birrette e buon cibo.

Sono grato ad *Andrea* per avermi ascoltato sempre nei momenti del bisogno e aver condiviso quell' instabilità nella ricerca di se stessi che sprona ad andare avanti ed andare meglio. Sento che non siamo ancora arrivati, ma la conoscenza è ampia per saper intuire dove andare.

Rimembro *Aldo* per essere stata l'interfaccia tra *noi poeti "elementari"* e il mondo là fuori. Un riferimento severo, ma vero. Ringrazio *Giulia* per la luce che diffonde sempre. Ora doppiamente...

Rendo grazie a *Marco B.* per le focose discussioni di Fisica che, in molti frangenti, hanno creato la giusta motivazione per approfondire un argomento.

Ringrazio *Luca* per non aver mai mollato ed essere arrivato fino in fondo insieme a noi.

Avvaloro *Dario e Giuseppe* che, emersi da poco, mi hanno dimostrato quanto un partecipato confronto possa generare delle soluzioni esatte. D'altra parte, che l'indipendenza nelle scelte è parte fondamentale della vita.

Avvaloro il ruolo dei miei coinquilini *Filippo e Matteo*: *Filippo* per aver ascoltato i monologhi sulla tesi e *Matteo* che ancor oggi non mi ha denunciato.

Ringrazio *Giancarlo* per una spalla che a Milano, e oltre, con cui ho sempre scambiato delle importanti riflessioni.

Volevo dare spazio a tutti e spero di esserci riuscito, non lasciando nessuna parola a me★★..Ops.

### **Latinismi Sparsi**

Siccome volevo ci fosse “nu poco ’e vvoi”, ho chiesto di darmi delle frasi latine da inserire “n copp’ a’ tesi”. Dunque, ringrazio gli “alias” di *Sara Sagone* ([page 19](#)) , “Est modus in rebus” di *Giuseppe Meneghini* ([page 2](#)) , “Rebus sic stantibus” di *Dario Massa* ([page 18](#)) , e il “Ça va sans dire” di *Andrea Marzo* ([page 18](#)).

# Bibliography

- [1] P. W. Anderson. More is different. *Science*, 177(4047):393–396, 1972.
- [2] Christie Aschwanden. Five reasons why covid herd immunity is probably impossible, 2021.01.07. <https://www.nature.com/articles/d41586-021-00728-2>.
- [3] Davide Bacciu, Federico Errica, Alessio Micheli, and Marco Podda. A gentle introduction to deep learning for graphs. *Neural Networks*, 129:203–221, 2020.
- [4] Scott Baier and Samuel Standaert. Gravity models and empirical trade, 03 2020.
- [5] Albert-László Barabási and Réka Albert. Emergence of scaling in random networks. *Science*, 286(5439):509–512, 1999.
- [6] Albert-László Barabási and Márton Pósfai. *Network science*. Cambridge University Press, 2016.
- [7] George E. P Box. *Statistics for experimenters : design, innovation and discovery*. Wiley-Interscience, Hoboken, N.J., 2nd ed. edition, 2005.
- [8] United States Census Bureau. Historical households tables. Technical report, USCB, 2020. Consulted sites at 30/09/2021.
- [9] Kimberly Chriscaden. Impact of covid-19 on people's livelihoods, their health and our food systems, 2021.07.01. [site](#).
- [10] Reuven Cohen and Shlomo Havlin. Scale-free networks are ultrasmall. *Physical Review Letters*, 90(5), Feb 2003.
- [11] Mohammad Reza Davahli, Krzysztof Fiok, Waldemar Karwowski, Awad M. Aljuaid, and Redha Taiar. Predicting the dynamics of the covid-19 pandemic in the united states using graph theory-based neural networks. *International Journal of Environmental Research and Public Health*, 18(7), 2021.
- [12] Peter Sheridan Dodds, Roby Muhamad, and Duncan J. Watts. An experimental study of search in global social networks. *Science*, 301(5634):827–829, 2003.
- [13] Kleinberg et al. The web as a graph: Measurements, models, and methods. In *Computing and Combinatorics*, pages 1–17, Berlin, Heidelberg, 1999. Springer Berlin Heidelberg.
- [14] S.A. Laurer et Al. The incubation period of coronavirus disease 2019 (covid-19) from publicly reported confirmed cases: Estimation and application. *Annals of Internal Medicine*, 172(9):577–582, 2020. PMID: 32150748.
- [15] EuroStat Statistics Explained. Household composition statistics. Technical report, Eurostat, 2020. Consulted sites at 30/09/2021.
- [16] Murray Gell-Mann. Simplicity and complexity in the description of nature. *Caltech Magazine*, 1987. <http://caltech.library.caltech.edu/3579/>.
- [17] Youyang Gu. Path to normality website, 2021.01.07. <https://COVID19-projections.com/>.
- [18] Our World in Data. Merged dataset from jhu csse covid-19 data. Technical report, Our World In Data, 2020. Consulted sites at 30/09/2021.
- [19] Istvan Z Kiss, Joel C Miller, and Peter Simon. *Mathematics of epidemics on networks: from exact to approximate models*. Springer, 2017.
- [20] K. Leung, M. Jit, E. Lau, and Joseph T. Wu. Social contact patterns relevant to the spread of respiratory infectious diseases in hong kong. *Scientific Reports*, 7, 2017.

- [21] Carol Y. Liu, Juliette Berlin, Moses C. Kiti, Emanuele Del Fava, André Grow, Emilio Zagheni, Alessia Melegaro, Samuel M. Jenness, Saad Omer, Benjamin Lopman, and Kristin Nelson. Rapid review of social contact patterns during the covid-19 pandemic. *medRxiv*, 2021.
- [22] Google LLC. Hardware service for data science. site, 2021. Consulted sites at 30/09/2021 <https://colab.research.google.com/>.
- [23] Filippo Menczer, Santo Fortunato, and Clayton A. Davis. *A First Course in Network Science*. Cambridge University Press, 2020.
- [24] Joël et al. Mossong. Social contacts and mixing patterns relevant to the spread of infectious diseases. *PLoS Medicine*, 5(3):e74, 03 2008.
- [25] M. E. J. Newman. *Networks: an introduction*. Oxford University Press, Oxford; New York, 2010.
- [26] NBC news. Initial dates of the stay-at-home restrictions, imposed by the usa states. Technical report, NBC news, 2020. Consulted sites at 30/09/2021.
- [27] Romualdo Pastor-Satorras and Alessandro Vespignani. Epidemic Spreading in Scale-Free Networks. *Physical Review Letters*, 86(14):3200–3203, April 2001.
- [28] Clara Pizzuti, Annalisa Socievole, Bastian Prasse, and Piet Van Mieghem. Network-based prediction of covid-19 epidemic spreading in italy. *arXiv*, 2020.
- [29] Gerald Shively. An overview of benefit-cost analysis, 01 2012.
- [30] Demographic Online Sites. Population estimates, 30/09/2021.  
*United States:* <https://www.census.gov/popclock/>,  
*Italy:* <https://www.istat.it/en/archivio/253831>,  
*Austria:* <https://www.austria.org/population,>
- [31] Complex System Society. Site, 2021.01.07. <https://cssociety.org/about-us/what-are-cs>.
- [32] Olaf Sporns. The non-random brain: Efficiency, economy, and complex dynamics. *Frontiers in Computational Neuroscience*, 5:5, 2011. Open Access policy: <https://www.frontiersin.org/about/open-access>.
- [33] Johannes Stübinger and Lucas Schneider. Epidemiology of coronavirus covid-19: Forecasting the future incidence in different countries. *Healthcare*, 8(2), 2020.
- [34] Stefan Thurner, Peter Klimek, and Rudolf Hanel. Appendix: A network-based explanation of why most covid-19 infection curves are linear. *Proceedings of the National Academy of Sciences*, 117(37):22684–22689, 2020.
- [35] Stefan Thurner, Peter Klimek, and Rudolf Hanel. A network-based explanation of why most covid-19 infection curves are linear. *Proceedings of the National Academy of Sciences*, 117(37):22684–22689, 2020.
- [36] Ze Ye, Kin Sum Liu, Tengfei Ma, Jie Gao, and Chao Chen. Curvature graph network. In *International Conference on Learning Representations*, 2020.
- [37] Daniel Zelazo and Mehran Mesbahi. Graph-theoretic analysis and synthesis of relative sensing networks. *Automatic Control, IEEE Transactions on*, 56:971 – 982, 06 2011.
- [38] Abdelhafid Zeroual, Fouzi Harrou, Abdelkader Dairi, and Ying Sun. Deep learning methods for forecasting covid-19 time-series data: A comparative study. *Chaos, Solitons & Fractals*, 140:110121, 2020.
- [39] Janaina P. Zingano, Paulo R. Zingano, Alessandra M. Silva, and Carolina P. Zingano. Herd immunity for covid-19 in homogeneous populations, 2021.